Dissertation Thesis

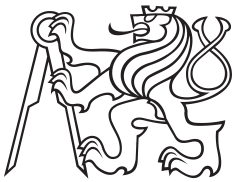

Czech Technical University in Prague

F3

Faculty of Electrical Engineering
Department of Measurement

Local navigation methods for metal detectors

Ing. Petr Nováček

Supervisor: Prof. Pavel Ripka, CSc.
Supervisor–specialist: Doc. Jan Roháč, Ph.D.
Field of study: Electrical Engineering and Information Technology
Subfield: Air Traffic Control
February 2017

Acknowledgements

I would like to take this opportunity to express my gratitude to my supervisor Pavel Ripka and my supervisor-specialist Jan Roháč for their scientific guidance, invaluable comments and patience during my studies.

Secondly, I would like to thank my colleagues Martin Šipos, Jan Popelka, Jakub Šimánek and Mushfiqul Alam for their encouragement, friendship and participation within our great working environment.

Finally, yet importantly, I would like to thank my family for their support and patience through some difficult times. My research would not have been possible without their support.

Declaration

I declare that this work is all my own work and I have cited all sources I have used in the bibliography.

Prague, February 23, 2017

Prohlašuji, že jsem předloženou práci vypracoval samostatně, a že jsem uvedl veškerou použitou literaturu.

V Praze, 23. února 2017

Abstract

This dissertation addresses the implementation of navigation capabilities for metal detection, in particular landmines. The precise aim of this thesis is to find a professional handheld metal detector search head position. This allows the creation of a magnetic image of the area searched, which opens a new prospective to increase the discrimination ability of metal detection between conductive scrap and the surveillance of unexploded ordnance.

This thesis has two parts. The first and main part focuses on the enhancement of professional handheld metal detector discrimination functionality. This was the main stream of my research work. The second part deals with position estimation as a tool to reach the objectives of the first part. The navigation is based on low-cost MEMS inertial sensors of angular rate and acceleration, which have minimum metal content. The required precision, in centimetres, can only be achieved by using calibration and signal enhancement procedures. The utilization of the magnetic position markers directly detected by a metal detector itself is my main original scientific contribution to the knowledge in the scientific area of aiding navigation.

Position markers with specific characteristics are placed in a known location and are recognised by a metal detector during its overhead movement.

The metal position markers described are a connection link between the navigation part and the part dealing with metal detector enhancement. Their usage is only enabled due to previous research made on the signal dependency of the metal detector's output on a detected object's material, size and distance from the detector's search head. Metal position markers are a by-product of this research, which focuses in particularly on the improvement of metal detector discrimination abilities.

The ability of metal detector discrimination can also be increased by using several excitation signal frequencies. The methods published up to now use multitone signals composed of sinewaves with two to four frequencies. In the presented papers we show that using $sin(x)/x$ excitation signal brings new possibilities in this area.

Keywords: Metal Detectors, Inertial Sensors, Unexploded Ordnance

Supervisor: Prof. Pavel Ripka, CSc.

Abstrakt

Tato dizertační práce se zabývá implementací navigačních schopností na detektory kovových předmětů a zejména min. Určení pozice detekční hlavy profesionálního detektorů kovu je přesný cíl této dizertační práce. Známá pozice umožní vytvoření magnetického obrazu zkoumané oblasti a tím zvýší diskriminační schopnost detektoru kovů odlišit nevybuchlou munici od vodivého odpadu.

Dizertační práce má dvě částí. První, hlavní část, je zaměřena na zvýšení diskriminačních schopností profesionálního ručního detektoru kovů. Toto byl hlavní směr mé výzkumné činnosti. Druhá část se zabývá odhadem pozice detektoru jako nástroje k dosažení cíle první části práce. Navigační schopnost je založena na využití levných inerciálních senzorů typu MEMS měřících zrychlení a úhlovou rychlost, u kterých byl kladen důraz na minimální obsah kovů. Vyžadované přesnosti jednoho centimetru je možné dosáhnout pouze za pomoci kalibrace a zpřesňujících postupů. Využití magnetických pozičních značek přímo detekovaných detektorem kovů je mým vlastním vědeckým přínosem vědecké znalosti v oblasti navigačního zpřesňování.

Popisované kovové poziční značky jsou pojítkem mezi navigační částí a částí zabývající se vylepšením detektorů kovů. Jejich využití je umožněno pouze díky předchozímu výzkumu prováděného na závislosti výstupního signálu detektoru kovů na materiálu detekovaného objektu, jeho velikosti a vzdálenosti od detekční hlavy detektoru kovů. Kovové poziční značky jsou vedlejším produktem tohoto výzkumu, který cílil především na zvýšení diskriminačních schopností detektoru kovů.

Zvýšení diskriminačních schopností detektoru kovů může být dále docíleno i za pomoci využití více frekvencí použitých v budícím signálu. Publikované metody využívají více tónového signálu vytvořeného ze sinusoid o dvou až čtyřech frekvencích. V prezentovaných výsledcích jsme ukázali, že využití $sin\ (x)/x$ budicího signálu přináší nové možnosti v této oblasti.

Klíčová slova: Detektory kovů, Inerciální senzory, Nevybuchlá munice

Překlad názvu: Metody lokání navigace pro detektory kovů

Contents

Figures

Chapter 1

Introduction

Although the last war in Europe was in the nineties, we still need to address Unexploded Ordnance (UXO). It is still quite common to find bombs in residential districts of Czech cities, which were affected by carpet-bombing during the Second World War. The UXO detection and clearance is still an important task for humanitarian missions in regions affected by recent military conflicts. Nowadays, personal security plays a very important role in such missions which generates many interesting scientific tasks in the field of metal detection improvements. A similar problem is found with landmines; both Anti-Tank (AT) and Anti-Personnel (AP) mines.

Mine clearance, or demining, is the process of clearing affected areas from mines in general. AP mines represent an especially high injury risk to civilians after war conflicts all round the world. More than 100 million mines are expected to have been placed across the world. Modern mines are made with a low metal content. The case is constructed from non-metallic material like wood or plastic, which further decreases the possibility of detection. In addition, the size of modern landmines plays a role. A landmine could be constructed with a $10cm$ diameter and is still able to stay functional for a long period. In these cases, UXO means not only AP and AT mines, but also artillery blast and the remains of used and unused munition etc. UXO, mines, and abandoned ordnance are usually called Explosive Remnants of War (ERW).

Demining is also quite an expensive process. Single mine clearance costs vary from 300 to 1000 US$ depending on the area. However, the price of a mine is between 3 and 30 US$ (Habib 2011). This enormous clearance cost is accrued by false alarms; less than 1% of objects detected represent real ERW.

This thesis illustrates possible approaches of false alarms reduction and UXO discrimination utilized in landmine detection. A professional metal detector as a key demining instrument is used. Metal detector will be complemented with additional electronics to add position estimation functionality. This implementation will be discussed as one option, and the use of the com-

plex excitation signal will be described. Both approaches will be referenced in the results published.

Chapter 2

Current State of the Art

Many principles have been tested for the detection of various types of ERW. The usage of a specific type of a measurement device is also influenced by specific soil background and in addition, it depends on the prior use of the area and is contamination.

Direct Current (DC) magnetic methods are most effective for finding bombs and large mines, which are often buried deep in the ground (Butler 2003).

Methods employing chemical sensors detect volatile particles in the air. Up to now, the most effective sensor of this kind are dogs. Dog training is time consuming and its usage in the field is hazardous for the animal and dog handlers. It is also impossible to identify what dog sniffing is exactly. This leads to the effort of distance sensor development (Miles, Dogariu & Michael 2012), with the capability of ERW fingerprints detection in air. The use of dogs is not the only option. It is known that UXO can be detected by rats and insects (King, Horine, Daly & Smith 2004).

Ground Penetrating Radar (GPR) (Smitha & Singh 2016) is effective in detecting plastic explosives due to a contrast in electric susceptibility. However, still the most common principle is an eddy-current metal detector (Yamazaki, Nakane & Tanaka 2002), which is able to detect electrically conducting objects, in particular metal.

2.1 Unexploded ordnance and AP mines discrimination

Many scientific groups, throughout the world, are trying to create new procedures to decrease injury risk for metal detectors operators and false alarms count during explosives remnants of wars ERW localization (Hyland & Smith 2009). Special semi-autonomous constructions are also possible (Trevelyan 1996), but they are suitable only in laboratory or testing conditions.

Today, the age of UXO comes to play a role too (Taylor, Bigl & Packer 2015). The corrosion of explosives and soil contamination complicates the disposal part of the demining process. The aforementioned paper describes the inspection of military testing areas in detail. Several types of UXO and their damage caused by detonation or by malfunction and ageing are discussed.

Although many AP mines are called non-metallic or low-metal content mines, they contain small metallic parts such as springs. Advanced eddy-current metal detectors are still able to detect and localize them, and they are still the most effective devices for this purpose. In order to detect low metal content mines, the sensitivity of the metal detectors should be significantly increased. This brings the problem previously mentioned to an increased number of false alarms (Theera-Umpon & Auephanwiriyakul 2004) caused by small pieces of metal debris. Present demining campaigns are characterized by a large false alarm rate, which leads to the decrease of operator awareness – causing a serious increase of injuries.

The first approach is to register the magnetic signature of the localized object and employ imaging and image processing methods to discriminate between different types of targets (Kruger & Ewald 2008). This requires measuring the precise position of the sensing head together with the detector signal during the scanning process. A magnetic map can be constructed and an image processing technique may be used to classify the detected object (Suganthi & Hanumanthappa 2016).

Another modern approach is to use complex excitation signals, which bring more rich information about the object examined (Svatos, Vedral & Fexa 2011).

Multiple types of sensors are an alternative way for landmine detection. A combination of ElectroMagnetic (EM) induction and GPR may be a good option (Sato 2008). Multiple sensor combination improves not only the precision of target localization, but also the possibility to distinguish UXO from metal clutter.

The possibility of known target modelling relying on a single induced magnetic dipole is considered (Ambrus, Vasic & Bilas 2016). Object discrimination is, in this case, possible by the comparison of a magnetic map and model output detection.

The paper (Zhao, Yin, Ktistis, Butterworth & Peyton 2016) also presents a specific approach to metal content detection and investigates multi-position measurement and the use of EM polarizability tensor.

2.2 Unmanned detection

One of the most popular approaches is the utilization of autonomous or remotely controlled vehicles (Hussain 2007, Heußlein, Patullo & Macmillan 2009). For this case, low cost robots appear to provide the most suitable solution (Fracchia, Benson, Kennedy, Convery, Poultney, Anderson, Tan, Wright, Ermilio & Clayton 2015). Low cost devices could be used as the UXO disposal device.

Apart from a wheeled or belted solution, there is also an effort to involve robots with legs (Estremera, Cobano & de Santos 2010). This solution is suitable for climbing stairs or rock-like surfaces and steep terrains.

An unconventional solution is described (Jin, Ko, Seok, Lee & Kang 2013), where an ordinary tracked robot is suggested. Instead of searching an area in the direction of movement, the paper presents side detection. This solution to decrease the possibility of damaging a robot also allows the simultaneous excavation of a detected object.

During humanitarian demining missions, cost plays one of the highest priorities, particularly if there is a necessity to clear large areas, and airborne demining might be one of the cheapest solutions (Habib 2001). Airborne minefield identification helps at the beginning of a demining procedure and later multispectral image processing assists additionally.

Although remotely controlled vehicles are already playing significant roles, there are still areas where their use would be inefficient, expensive or impossible, e.g. moisty soils, bushes, and steep terrain. In such locations, handheld metal detectors are the only choice during demining missions (Lewis, Bloodworth, Guelle & Smith 2003).

Navigation ability is suitable also for a handheld metal detector (Krüger 2010), which would allow the possibility for in-situ detected object classification.

Handheld metal detectors are chosen especially because of the costs. A comparison between handheld and autonomous metal detection shows that cost of the autonomous devices would still be multiplicatively higher. The main disadvantage of handheld metal detectors is the risk of severe injury to the operator.

2.3 Inertial sensors

Local navigation leads towards the use of inertial sensors, namely accelerometers and angular rate sensors. Microelectromechanical Systems (MEMS) are

the only applicable solution in terms of cost (Reinstein, Rohac & Sipos 2008). During the last two decades, the MEMS system has been through intensive evolution and nowadays it is common to integrate them in cellular phones. Therefore, it is possible to use these microchips in other battery-powered devices. There is still a necessity for a supplementary source of position information (so called position aiding) (Kong, Li, Yu & Wu 2014, Sahawneh & Jarrah 2008), which will be discussed later in the text.

Chapter 3

The Aim of Disertaion

This thesis aims to introduce a novel approach in metal object detection, localization and identification. This wide range of interest is specified by two main objectives. Firstly, adding a navigation ability to metal detectors, and secondly, with the metal detector itself and its improvements to decrease injury risks together with reducing the number of false alarms.

3.1 Local navigation

The first objective is the development and implementation of semi-autonomous navigation methods for an advanced professional metal detector. The main challenge is to find methods and algorithms to reduce position sensor errors to a level acceptable for a small-area mapping system that would also be able to create a magnetic image of the localized target. The collected images can then be processed by software recognition and discrimination packages. This also includes calibration tasks for such a system. The use of low-cost sensors is recommended and the discovery of supplementary position information would be an important part of the development.

3.2 Improved metal detection

The second objective is the improvement of the typical use of a metal detector. One of the solutions is the use of several excitation signals. This solution would increase resolution and the precision of measurements. Usage of improved metal detection sensors allows the increased request on signal post processing, but it improves potential detector discrimination ability.

Chapter 4

Initial analysis

The first part of this thesis is not devoted to the development of metal detectors themselves, but rather to the further enhancement of existing ones – All Terrain Mine Detector (ATMID) (Schiebel 2003, Siegenfeld 2003). Handheld metal detectors were used as the basic device during navigation methods development.

4.1 Eddy current metal detection

This section briefly describes the metal detectors used. Continuous Wave (CW) metal detectors, which work at *kHz* frequencies, are discussed. These detectors are also called eddy current metal detector and they are based on precisely arranged Transmitting (TX) and Receiving (RX) coils (in the sense of shape and position) to obtain as low as possible mutual inductance M between them. TX coil voltage is defined by $V_T = I_T e^{j\omega t}$, where I_T is TX coil current, ω is angular frequency ($\omega = 2\pi f$), and t is time. The RX coil voltage depends on mutual inductance by $V_R = -j\omega M I_T e^{j\omega t}$, where M is mutual inductance.

RX coil output voltage is close to zero for a correct arrangement. However, if the detectors pass above a conductive object the amplitude and phase of output voltage changes. This is caused by a secondary EM field generated by the object passing below the detectors head. This secondary EM field is caused by eddy currents induced by a primary EM field generated by the TX coil. The secondary EM field unbalance coils and change mutual inductance between the RX and TX coils.

Eddy current problems and soil influence, together with penetration depth is widely discussed by (Bruschini, Marinella & Sorpresa 2002).

Figure 4.1 shows the X-ray image of the ATMID detector, and a CW search head with a double D coil setup. The excitation signal used in the ATMID

detector has a frequency of $8.17kHz$ and amplitude of $10V_{pp}$. The TX coil (upper left part) consists of 17 turns and the RX (bottom right part) coil has approximately 190 turns (Svatos 2015).

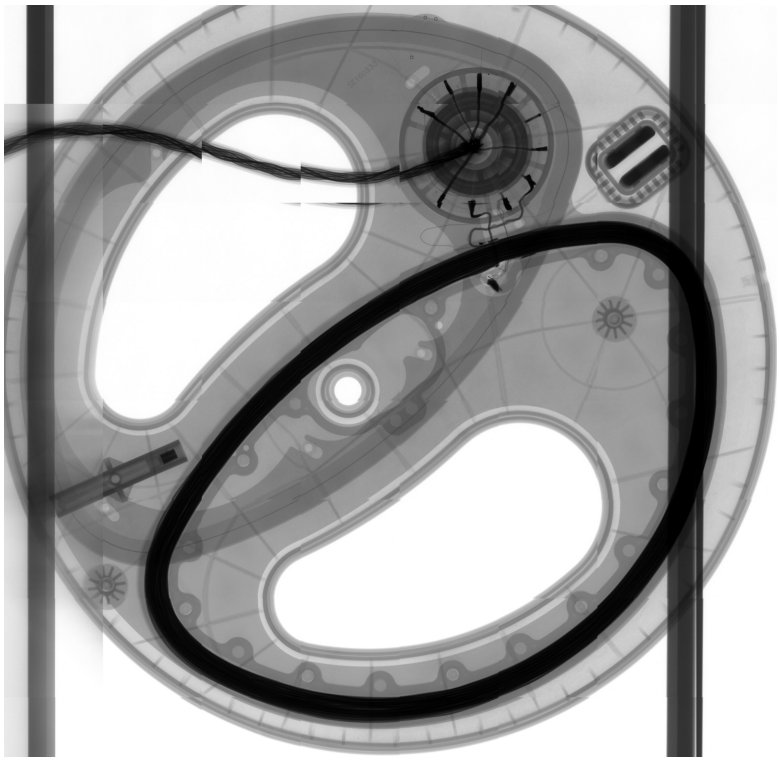

Figure 4.1: ATMID CW search head X-ray photo.

4.2 Evaluated principles

The main thoughts during the commencement of this work should be divided into the following steps of research:

- Inertial Navigation System (INS)

  Immediately after focusing on metal object localization, the implementation of the INS, and a tested solution was considered. At this point, Accelerometers (ACCs) and an Angular Rate Sensors (ARSs) are utilized especially in the MEMS versions used in Inertial Measurement Unit (IMU), further supplemented with additional sensors (Reinstein, Rohac & Sipos 2010). It seems a simple and accurate approach, but only after the analysis of the long-term precision was made - presented in (Ripka, Novacek, Reinstein & Rohac 2010). We concluded that using inertial sensors might be possible only together with the further enhancement

(aiding) of the sensors. Such an enhancement will periodically correct MEMS sensors to compensate for their inaccuracies.

- Global Navigation Satellite System (GNSS) enhancement

  Using GNSS appears to be a good option for INS enhancement (Hussain 2005), but systems offering centimetre accuracy are still very expensive and bulky. Metal detector improvement is discussed here and its usage is often performed in areas with low access such as forests, jungles, and steep valleys etc., which are areas with an insufficient precise GNSS signal. So finally, this option was also discounted.

- Optical Flow (OF)

  Using OF as a velocity information input into the position estimation system would seem a good option (Beauchemin & Barron 1995, Aires, Santana & Medeiros 2008). However, the camera required and electronics mounted on the detector head would strongly decrease the detection sensitivity. A second reason not to evaluate OF is that the ground surface is often very complex. Demining procedures are done over grass or leaves with variable ground distance.

- Signal height profile

  A metal detector's output signal profiles measured at different distances between the detector search head and the object tested show significant characteristics about a detected object (Bruschini et al. 2002). Profiles measured lead to an estimation of object material type and object size.

- Position marks

  The final approach evaluated for the aiding system for IMU inertial sensors is the use of absolute position marks. Usage of the metal detector itself to detect the position mark is therefore one of the aims of this dissertation.

After the aforementioned initial analysis of the local navigation problem for metal detectors, which was supported by numerous experiments, I have chosen an approach based on the usage of inertial sensors packed in IMU and position markers. Position markers aid IMU sensors inaccuracies and are possible to correct errors accumulated in the estimation of position.

The second part of this thesis addresses the implementation of complex excitation signals for metal detection, which also assists in position marks detection.

Chapter 5

Published Results

The following sections contain logically ordered authors' publications in impacted journals related to the topic of this doctoral thesis.

The publications commented on are divided into two parts.

5.1 Metal detection

The first part of the publications addresses metal detection, focused on mine detection. As previously mentioned, ATMID is used for testing purposes. This detector was equipped with additional sensors and electronics suitable for testing purposes with no influence on the eddy-current sensor. Publications follow each other chronologically with each new publication using results from the previous publication. Metal spheres, with a different size, are used in our experiments and are standard objects for the testing and calibration of metal detectors.

5.1.1 Mine Detector with Discrimination Ability

The first publication (Novacek, Ripka, Pribula & Fischer 2010) describes equipment attached to an ATMID detector together with the testing platform. The equipment involved consists of ultrasonic distance sensors measuring the height of the detector's sensing head movements above the ground and a measuring platform allows precise height adjustment for testing purposes. The results of ATMID signal output dependent on height, size and material of the object detected, were investigated and presented.

Initially, the height profiles measured from the signal output dependency of the metal detector on localized object is shown. The target three spheres are used, each made of a different type of material, but all of them with the same $10mm$ diameter.

Figure 5.1 shows the INOX metal sphere height profile. The INOX AISI 420 is used in measurement and represents ferromagnetic material with small permeability.

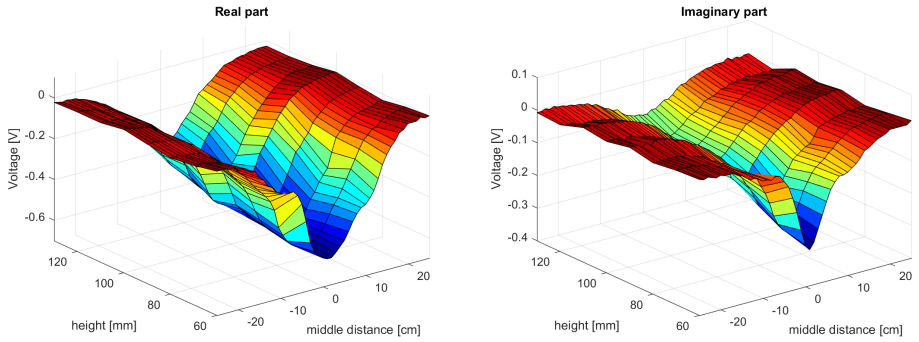

Figure 5.1: Signal height profile of INOX AISI 420 sphere ($10mm$ diameter).

Figure 5.2 illustrates height signal dependency for an aluminium sphere of $10mm$ diameter. Aluminium represents the non-magnetic type of material. As it can be seen from figure, the measurement consists of both real and imaginary parts of the signal.

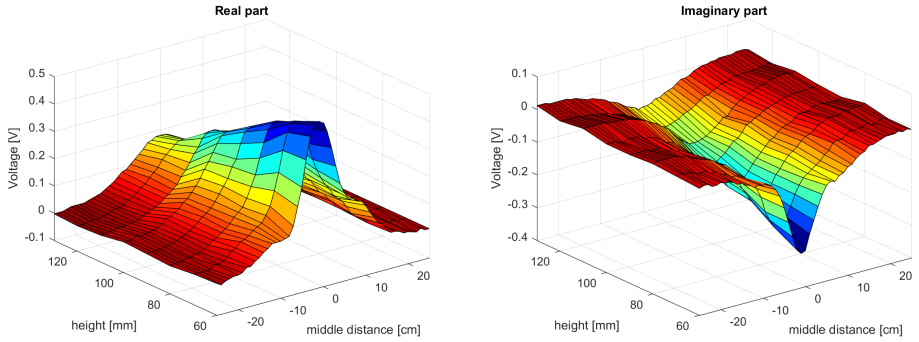

Figure 5.2: Real and imaginary parts of the metal detector signal dependency on height over an aluminium sphere (10mm).

Figure 5.3 shows a bronze sphere, which has a similar signal output in case of voltage polarity as aluminium, but lower amplitude in the real signal part and higher in the imaginary part.

Figures 5.1 to 5.3 show an obvious signal output dependency on the target measured. The difference between the ferromagnetic and nonmagnetic material is the key output of the profiles measurement. Most remarkable is the comparison of the real part signal measured between aluminium (nonmagnetic material) and chrome steel (ferromagnetic material). These results could be used to differentiate between the types of object detected or the material from which the object is made from.

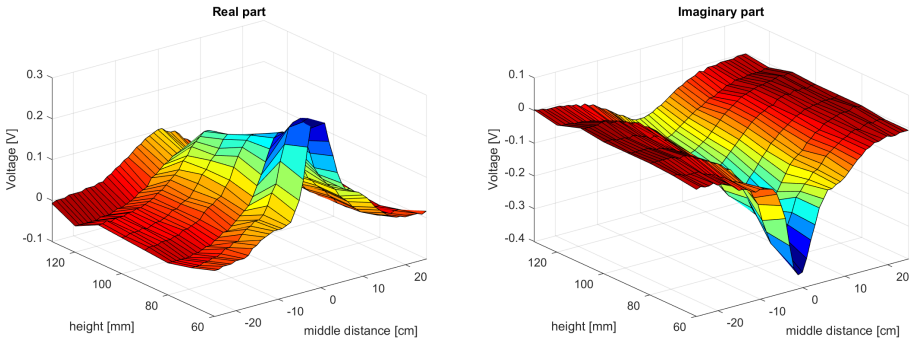

Figure 5.3: The signal height dependency of the metal detector for the bronze sphere (diameter $10mm$).

The second part of the paper describes the position dependence of the ATMID signal output during pinpoint movements above the detected object. This dependence is used in further work and will be discussed later. During the measurements, INOX AISIS 420 metal balls with diameters of 9.4 and $15mm$ were used as the objects detected. The testing system developed is able to monitor the metal detector position independently by camera. This system can be used for the calibration of the developed 3-D imager and provides a valuable tool for the training the operators. Operator training is time consuming and an expensive part of the demining mission. Basic training takes two weeks and requires experienced instructors. For field training, one instructor is required for each trained person. This part can be partly replaced by assisting the tracking system, which helps to teach the operator to perform correct scanning with constant ground distance and constant speed of motion even in complex terrain.

Journal of ELECTRICAL ENGINEERING, VOL 61. NO 7/s, 2010, 141-143

MINE DETECTOR WITH DISCRIMINATION ABILITY

Petr Nováček* — Pavel Ripka*— Ondrej Pribula* — Jan Fischer*

Metal detectors are widely used to detect Explosive Remnants of War such as landmines and Unexploded Ordnance. Almost all professional detectors are based on the eddy current principle. Currently count of false alarms rises up to 99.9% of total alarms count. Discrimination ability added to professional mine detector is therefore highly required by demining community. We show two complementary methods: using vertical signal profile and horizontal spatial maps. This is achieved by adding vertical distance sensor and inertial positioning unit to the search head. Image processing methods can be used to differentiate between metal ballast and dangerous objects. In this paper we show first steps in the development of the fully autonomous 3-D positioning unit for eddy current imaging.

Keywords: metal detection, mine detector, discrimination, signal height profile, eddy-current

1 INTRODUCTION

Detection and clearance of Explosive Remnants of War (ERW) such as landmines and Unexploded Ordnance from former military areas and after war conflicts is still made by human operators using eddy current metal detectors. All methods of remote sensing turned to be unpractical and the only real alternatives are two: 1. using trained animals such as dogs of rats to sniff explosives 2. hand-held ground penetrating radar (GPR). GPR is able to detect plastic mines, but fails in wet soil. Currently it is becoming very hard to differentiate between the ERW with low metal content and ordinary scrap metal such as cans or metal foils.

Increasing the sensitivity of metal detectors to detect low metal content mines also increases false alarms count [1]. Therefore the main objective of this paper is to introduce method to differentiate ordinary ballast and expected objects during demining procedures by adding discrimination ability to professional mine detector.

Several methods how to discriminate mine types were recently described in [2]. However the ultrasound tracking system used in that paper requires a minimum of three ultrasound receivers with precisely known locations being installed in the close vicinity. This is a configuration which can be used in the laboratory conditions but which is unsuitable for the field work such as routine demining of large areas.

Kellermann proposed method which registers the detector signal for several heights of the sensing head [3]. This technique helps to distinguish between shallow and deeply buried objects of different size. Measured signal intensity for small objects ideally decreases with $1/d^3$, where d is the distance.

In this paper we describe an effort to combine Kellerman's approach with x-y mapping. The proposed method of discrimination uses signal from the metal detector together with information of height above the ground and relative x-y position. Based on this information height profiles of metal detector signal can be constructed and estimation of detected object can be made by comparison with known signal profiles for different objects.

The signal profile depends on the size, shape, material and depth of the measured object, making the inverse problem very complex. A priori information about the possible buried objects should therefore be used. While the complete mine catalogue is very extensive, for practical applications the number of types of landmines in a given area is limited. Even an ability to discriminate between the deeply buried anti-tank mine and shallow anti-personnel mine can save lives of deminers.

2 EXPERIMENTAL EQUIPMENT

All Terrain Mine Detector (ATMID) [4,5] manufactured by Schiebel Austria was used in this study. This metal detector is based on eddy current principle and works with continuous wave. The ATMID was equipped with optical triangulation distance sensor [6] which enables measurement of the height above the ground and relative angle between the ground and the search head. The used setup is shown in Fig. 1. The distance sensor is installed above the search head to minimize the influence of its metal parts and also to avoid threshold limit for short distances.

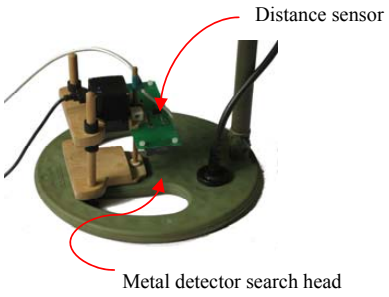

Fig. 1. Mine detector with optical ground distance sensor.

* Department of Measurement, Czech Technical University in Prague, Faculty of Electrical Engineering, Technicka 2, 166 27 Prague 6, Czech Republic; petr.novacek@fel.cvut.cz

ISSN 1335-3632

The non-metallic height adjustment stand, shown in Fig. 2, was developed for the testing. The stand allows fast change of the testing distance while keeping the search head parallel to the testing plane.

We have made experiments with the processing of the audio output of the metal detector. This is the only available standard output of professional metal detectors [6]. Unfortunately the signal processing used to generate the audible output limits the detector signal and thus highly reduces its information content. This effect is shown in Fig. 3.

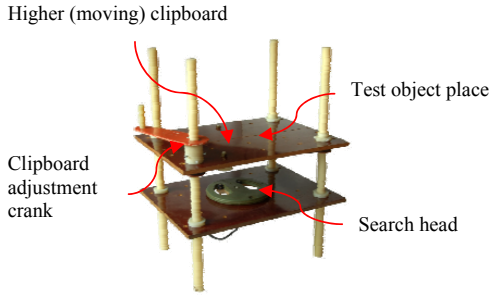

Fig. 2. Non-metallic height adjustment stand.

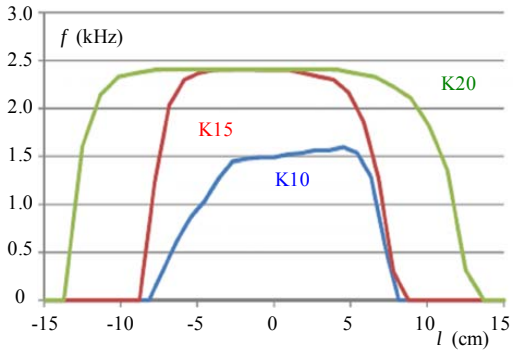

Fig. 3. Dependence of the acoustic signal frequency on horizontal position of the search head, for 3 sizes of metal balls [6,7].

We therefore decided to use the internal signal of the detector, namely the output of the logarithmic amplifier after the phase-sensitive detector.

For the field measurement of the relative position of the search head in the x-y plane we currently develop the aided inertial navigation system with 1 cm position accuracy. Large drifts of the used accelerometers and angular rate sensors are corrected by periodical nulling of the speed (using optical flow video sensor mounted on the detector head) and position (using magnetic, reflective optical or conductive markers). First steps in this effort have been reported in [7]. Here we report of using metal markers on both sides of the scanned area. This is in conformity with the commonly adopted procedures for the mine clearance: during the fast scan the location of the suspicious object is marked by two flags in a 1 distance with the "hot spot" between them. If the poles of the flags are made of the conductive material, the position of the detection head above these markers is sensed by the metal detector itself. The simplest situation is for the pendulum-like line pinpointing. In this case the marker position is reached every one or two seconds, which allows very frequent nulling of the navigation drift. Area scanning (typically in 1x1 m square) brings more demanding situation – the marker is reached only every 10 to 30 s. The integrated drift in position caused by the offset of inertial grade accelerometers is only in the order of 1 mm for the first second. Ideally the well-trained operator should keep the detector head always in the horizontal position. However in the real field scanning the tilt of the detector head is slightly changing. This changes the projection of g into the sensing axes of the accelerometers and brings much larger error. Our present effort is to use angular rate sensors to compensate for this effect. Standard adaptive filters used for inertial navigation should be modified to accommodate specific repetitive pattern of this motion.

For the calibration and testing purposes we use a digital laboratory USB camera with complementary metal oxide semiconductor (CMOS) image sensor of resolution 752 x 480 pixel and pixel size of 6μm. Camera was mounted 3 m above the testing area. The search head was equipped with an active marker (Light Emitting Diode) and center of image gravity algorithm [8] was used for marker position detection. Position of the search head was measured with resolution of 0.5 cm.

It should be noted that the described camera tracking system is not intended for the field work – in the final stage it will only be used for the calibration and testing of the portable inertial navigation system and for training of the operators.

3 RESULTS

Signal intensities were measured in the laboratory conditions in heights range from *50* to *300* mm for the simple testing objects of various size made of different metals. One example of the results is vertical signal intensity profile for the INOX AISI 420 steel balls shown in Fig. 4. The measurement was made using metal balls with diameters of 9.4 mm and 15 mm, shown in Fig. 5

Measured intensity function shows clear dependency on the object size. However the information content of such profile is not rich enough for practical applications.

In the following section we demonstrate the stability of the present laboratory tracking system: the detector head was marked by LED diode and its *x-y* position was tracked by video camera. Figure 6 shows time evolution of the repetitive pendulum-like scan over the clean area equipped with two large metallic markers. Figure 7 shows the signal of a metal ball positioned between the same markers.

The signal variations caused by interference can be averaged off the periodic signal record.

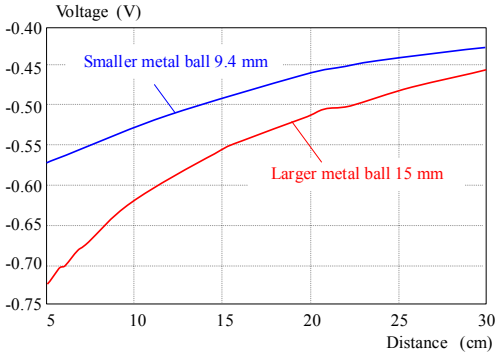

Fig. 4. Measured signal intensity as a function of the object distance.

Fig. 5. Tested metal balls, INOX AISI 420.

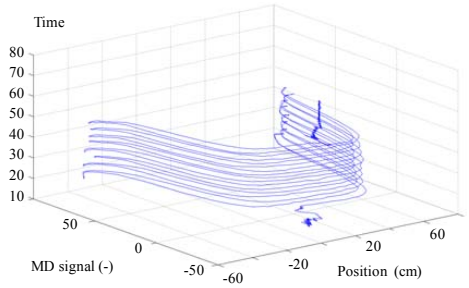

Fig. 6. Time evolution of the repetitive line scan. No detected object, only signal of two metal markers is visible

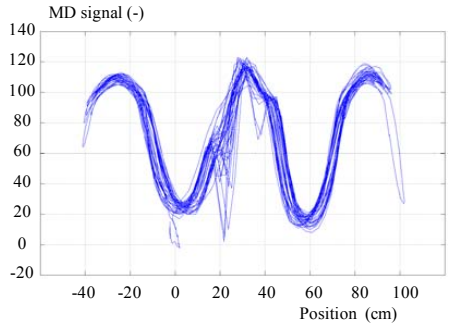

Fig. 7. Repetitive line-scan of metal ball (with two markers still present). Rough signal before averaging shows interference. object, only signal of two metal markers is visible

4 CONCLUSION

The described results present gradual achievements towards the fully portable 3-D imager for eddy-current metal detector. Metal detector with position tracker allows constructing eddy-current signal map, which is characteristic for specific objects. Mine signatures can be automatically recognized from these maps. Position sensing also allows detecting very weak signals buried in the environmental noise by repetitive scanning of the suspicious area. The developed system is also useful for the training of deminers.

Independent approach for increasing of the discrimination ability of metal detectors is using multiple excitation frequencies and processing both amplitude and phase information. This path is fully compatible with the path described in this paper.

Acknowledgement

This research was supported by the grant No 102-09-H082 from the Czech Science Foundation.

REFERENCES

[1] GUELLE, D *et al.*; Metal detector handbook for humanitarian demining, Luxembourg; Norwich: Office for Official Publications of the European Communities; Stationery Office distributor, 2003.
[2] KRUGER, H. – EWALD, H.: Handheld metal detector with online visualisation and classification for the humanitarian mine clearance, Sensors, 2008 IEEE, 2008, 415-418.
[3] KELLERMANN, G. :Metal detector, in particular mine detector US Patent US Patent 7265551, 9, 2007.
[4] SIEGENFELD, A.: ATMID – Technologie und Schaltungsbeschreibung, 2003.
[5] SCHIEBEL, Maintenance Manual MT5001/16/010E.
[6] VYHNÁNEK, J.: Distance sensor for mine detector, Bachelor thesis, CTU in Prague, 2009.
[7] RIPKA, P. – NOVÁČEK, P. – REINŠTEIN, M – ROHÁČ, J.: Position sensing system for eddy-current mine imager, Procedia Engineering, vol. 5, 2010, 276-279.
[8] R. SHORTIS, R. – CLARKE, T.A. T.A. T.A. SHORT, T.: A comparison of some techniques for the subpixel location of discrete target images, Videometrics III, SPIE Vol. 2350.,Boston 1994, 239-250

Received 30 September 2010

5.1.2 sin(x)/x Signal Utilization in Metal Detection and Discrimination

This second paper (Svatos, Novacek & Vedral 2012) presents the use of a multi-tone sinusoidal signal during the detection of metal objects. An unconventional signal, $sin(x)/x$ so-called *sinc* signal, was used for the testing. The use of a non-traditional signal increases the possibilities for the discrimination of the detected object and differentiation from conductive scrap. Furthermore, multi-tone usage would decrease the count of false alarms and would help with area clearance speed. For testing, the search head of an ATMID metal detector was used and a programmable waveform generator AFG 3102 was the source of the excitation signal. For the measurement, the 14-bit mode of the MSO 4034 oscilloscope was chosen. In this case, my role in the team was to generate an excitation sinc signal using the MATrix LABoratory (MATLAB) software tool together with spectral analyses during the gathering of results. As with testing object metal spheres, various diameters and materials were used. Results presented in the paper show the potential to increase the possibilities of distinguishing between UXO and conductive garbage by additional information from the phase spectra to ordinarily used amplitude spectra.

Journal of ELECTRICAL ENGINEERING, VOL 63. NO 7s, 2012, 110-113

sin(*x*)/*x* SIGNAL UTILIZATION IN METAL DETECTION AND DISCRIMINATION

Jakub Svatoš* — Petr Nováček — Josef Vedral*****

This paper presents usage of an unusual signal (sinc signal) for metal detection and discrimination. Even in present days, differentiate between Anti-Personnel (AP) mine or unexploded ordnance (UXO) and metal garbage is a matter of high interest for scientists. In some areas, especially with contaminated or magnetic soil, 999 form 1000 alarms are false. Decrease of these false alarms is enticing and necessary in humanitarian demining. For the experiment Schiebel All-Terrain Mine Detector with testing spheres from different materials and different sizes were used. Signal from the detector was processed in frequency domain, especially phase spectra are shown and compared.

Keywords: metal detection, metal discrimination, de-mining, polyharmonic signals, signal processing

1 INTRODUCTION

From the beginning of 20th century scientists make an effort to devise a device which can pinpoint metal. In these days metal detectors are still used in many sectors. Detectors help amateur treasure hunters or archaeologists to detect artefacts and coins. At the airports or in the important buildings walk-through security metal detectors serve to improve security. Metal detectors are also used in the military, pharmacy, food and chemical industries. The last but not least is the humanitarian demining [1], where the detectors play key role during land clearance from Explosives Remnants of Wars (ERW).

There are many methods how to detect mine but eddy current metal detectors are still popular detectors in humanitarian demining. The major problem of eddy current detectors is number of their false alarms. False alarms account 999 from 1000 total alarms [2]. The decrease of these false alarms is therefore desirable.

There are two ways how to minimalize false alarms. Leave the idea of eddy current metal detectors or improve detectors by way of improved excitation signals of the detector and more sophisticated signal processing. For this the polyharmonic signals can be applied, which is not common approach for metal detection. In this paper signal - sin(x)/x, so called sinc signal [3], is presented. Thanks to multi-harmonic composition sinc signal seems to be perspective for better detection and discrimination i.e. reduction of false alarms.

This signal gives complex information about detected objects. Two others experiments with multi-harmonic signals are presented in [4], where linear frequency sweep sine signal and [5] step sweep sine signal were used and results were presented by polar graphs.

This paper complement presented results in [6] with new results. In [6] amplitude spectra are presented and this paper presents phase spectra dependency on detected object. Results were obtained on the same non–magnetic platform using excitation sinc signal with the frequencies range from 0.5 kHz to 10 kHz.

2 THEORY

Eddy current metal detectors are the most used detectors in humanitarian mine detection [7]. There are two main groups of eddy current metal detectors. Pulse Induction detectors which monitor a time delay of a pulse to indicate a presence of the mine. Second are very low frequencies detectors which operate with single or multi tone signals and use changes of the phase and the amplitude to detect and distinguish object. Briefly, these detectors have usually separated transmitting and receiving coil in one of many configurations [5]. The majority of metal have “double D" configuration. Transmitting coil transmit excitation signal and voltage sensing in receiving coil is inducted according to the Faraday Laws. For more details about these metal detectors please see [8].

Different excitation signal together with advance signal processing of the detector and output signal processing is a way how to improve detection and discrimination ability of the very low frequencies detector. One possible signal is sine cardinal or commonly referred sinc function shown in Fig. 1. Thanks to its multi-harmonic composition and spectrum sinc signal cover defined frequency range (which can be easily adjusted) i.e. frequency characteristic of the detected object. Combination of amplitude and phase spectra could lead to decreasing of false alarms.

3 EXPERIMENT

For the experiment the metal detector ATMID was used, same detector as in [6]. The ATMID detector search head had “double D” configuration and receiving coil have diameter of 267 mm. For more details about the detector see [9] and [10].

* Department of Measurement, Faculty of Electrical Engineering of the Czech Technical University in Prague, Technická 2, 133 27, Prague 6, Czech Republic, svatoja1@fel.cvut.cz, ** Department of Measurement, Faculty of Electrical Engineering of the Czech Technical University in Prague, Technická 2, 133 27, Prague 6, Czech Republic, petr.novacek@fel.cvut.cz@fel.cvut.cz, *** Department of Measurement, Faculty of Electrical Engineering of the Czech Technical University in Prague, Technická 2, 133 27, Prague 6,Czech Republic, vedral@fel.cvut.cz

ISSN 1335-3632

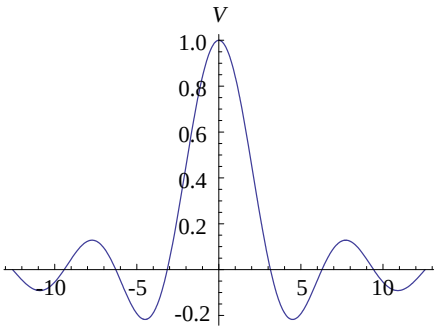

Fig. 1. Time plot of sinc signal.

Coil was excited by signal composed of two same sinc signals but half period inverted as shown in Fig. 2. One period of the signal is described by (1).

$$u(t) = H\left(t + \frac{T_1}{2}\right)\left(\frac{\sin\left(\frac{\omega t}{T_2}\right)}{\frac{\omega t}{T_2}}\right) - H\left(t - \frac{T_1}{2}\right)\left(\frac{\sin\left(\frac{\omega t}{T_2}\right)}{\frac{\omega t}{T_2}}\right) \quad (1)$$

where H is Heaviside function, which inverts the sinc function in time range $\langle -T_1/2, T_1/2)$ [11]. The anti-symmetric signal covers full scale of digitizer.

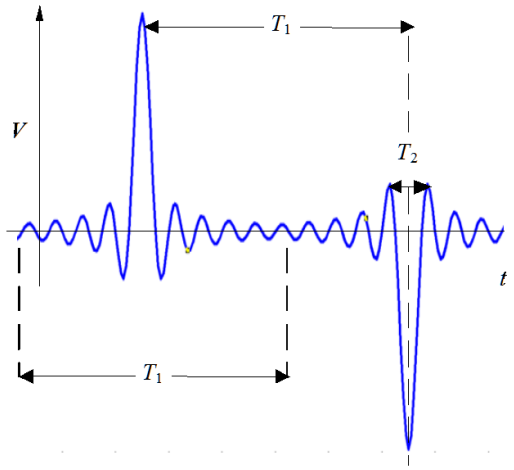

Fig. 2. Time plot of excitation sinc signal [6].

Sinc signal is driven through the coil and is derivate. First derivative of sinc signal, as shown in Fig. 3, is transmitted by primary coil and received by secondary coil. Received signal carries information about detected object.

As targets homogenous spheres of different materials and various sizes were used. Spheres were placed in open air to avoid ground effect [12] in a distance of 100 mm from the searching head on the axis of the greatest sensitivity.

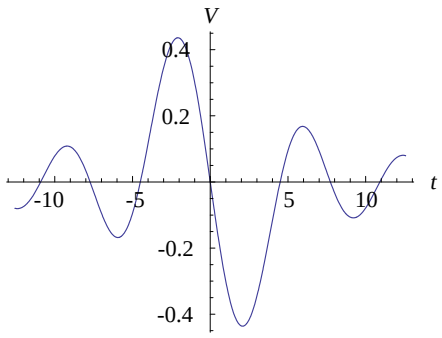

Fig. 3. Time plot of differentiate sinc signal [6].

The excitation signal was driven through the transmitting coil of ATMID metal detector. Following parameters describes the used signal: frequency $f_1 = 1/T_1 = 0.5$ kHz and $f_2 = 1/T_2 = 10$ kHz; 10 significant carrier frequencies; and amplitude of 10 V. Signal was generated by an AFG 3102 generator. The signals from the receiving and transmitting coils were measured by oscilloscope MSO 4034 in hi-res mode (14 bit) with sampling frequency 1 MHz.

In the future measuring instruments (generator oscilloscope and PC) will be replaced by intelligent modular system. The modular system will be based on three parts. Generator module for excitation signal based on Direct Digital Synthesizer (DDS), Amplifying module and Analog-to-Digital Converter (ADC). All this modules will be controlled by microprocessor with DSP unit (Fig 4).

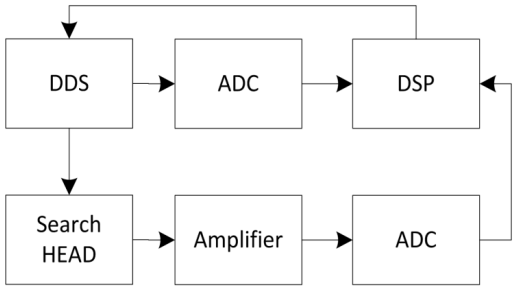

Fig. 4. Modular system concept block diagram.

4 DISCUSSION

Experimental measurements were done for four different materials and all measured data were processed in MATLAB. As testing materials were used bronze, stainless steel (INOX ANSI 320), brass, and chrome steel (UNI100Cr6) represented by spheres with diameter of 10, 20 and 25 mm. Phase spectra were calculated from complex variable definition. Obtained results are presented in Fig. 5 to 8.

Fig. 5 presents phase spectrum of spheres from different materials with diameter of 10 mm, 20 mm respectively in Fig. 6. In Fig. 7 influence of sphere diameter is shown for chrome steel Spheres diameters were 10, 20 and 25 mm in this case. And finally Fig. 8 shows same influence for brass (diameters 10 mm and 20 mm).

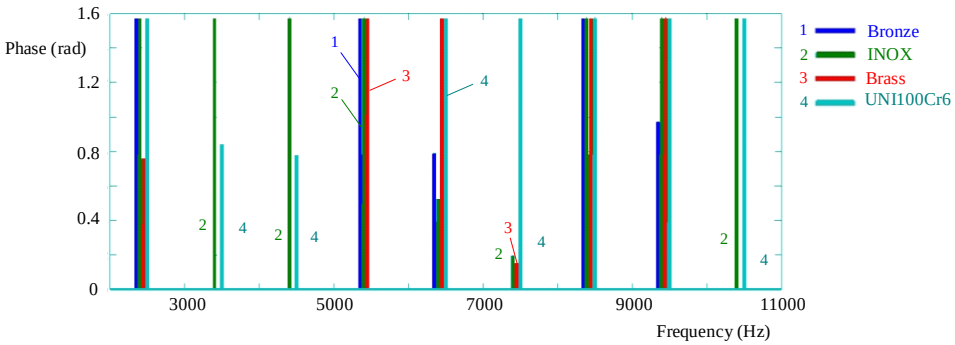

Fig. 5. Phase spectrum of signal from different spheres with diameter of 10 mm

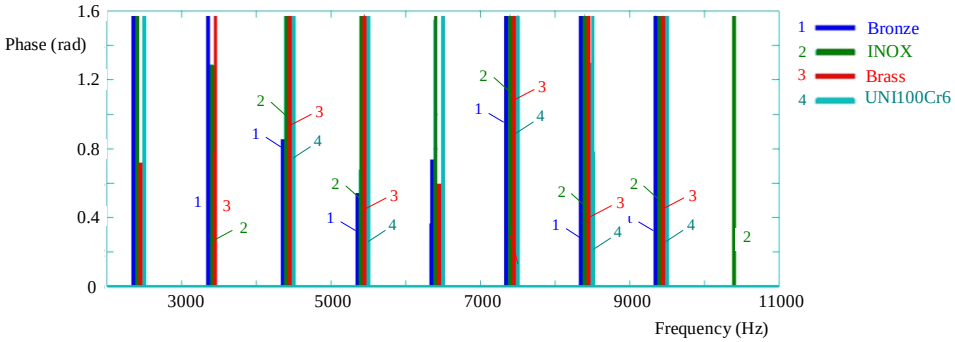

Fig. 6. Phase spectrum of signal from different spheres with diameter of 20 mm

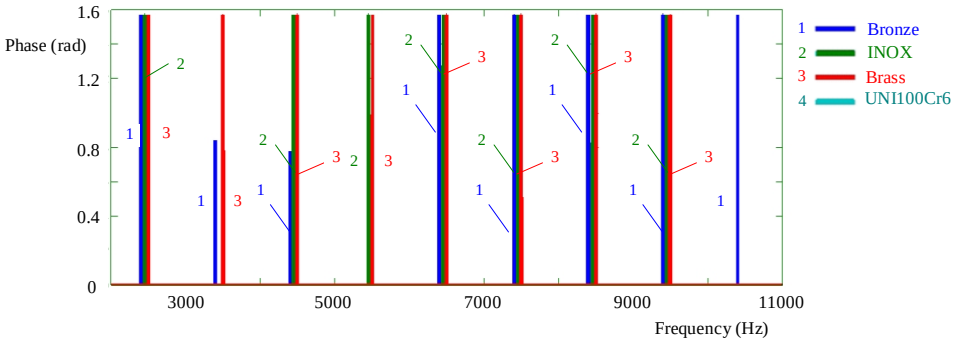

Fig. 7. Phase spectrum of signal UNI100Cr6 with different diameters

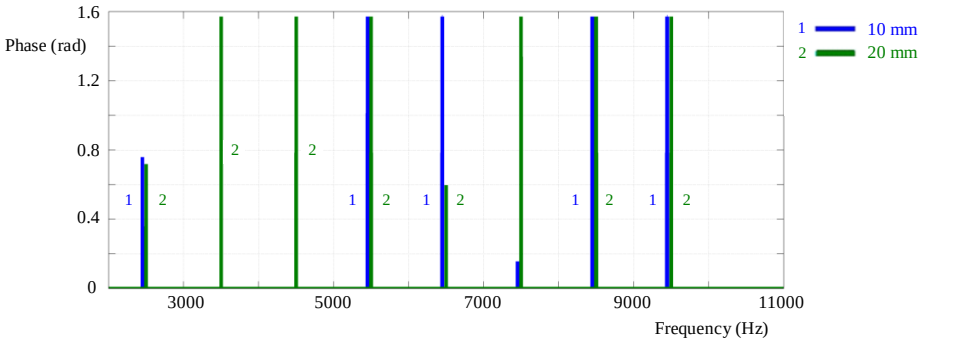

Fig. 8. Phase spectrum of signal brass with different diameters

Four different materials are presented in Figs. 5 and 6. There are differences in phase shift of the frequency characteristic. Thanks to multiple carriers we have possibilities to monitor differences in more frequencies. On Fig. 7 phase of the signal from UNI100Cr6 with diameter 20 mm and 25 mm are almost the same except second carrier frequency.

5 CONCLUSIONS

The non-traditional excitation signal, sinc signal, for metal detector was presented in this paper. Main goal was to decrease false alarms in humanitarian demining. Results presented in [6] together with this paper brings unite view into unusual metal detection and discrimination. Phase spectra supplement amplitude spectra with additional information about detected objects. Furthermore this additional information increases the chance of discrimination between unexploded ordnance and conductive garbage. Based on this experiments it is chance for better differentiation of the object in terms of geometric and electromagnetic properties.

Further work brings up the possible implementation on modern metal detector whose capabilities can be described by standards [13]. Modular subsystem will be part of the intelligent detector with the possibility of connection of navigation system. Thanks to navigation system position estimation of the objects can be done [14].

REFERENCES

[1] BROOKS, J.W.: The Detection of Buried Non-Metallic Anti-Personnel Land Mines, The University of Alabama in Huntsville, Huntsville, Alabama, 2000

[2] GUELLE, D.: Metal detector handbook for humanitarian demining, Luxembourg, Norwich: Office for Official Publications of the European Communities, Stationery Office distributor, 2003

[3] STENGER, F.: Handbook of Sinc Numerical Methods, CRC Press, 2010.

[4] SVATOS, J. — VEDRAL, J.: The Usage of Frequency Swept Signals for Metal Detection. IEEE Transactions on Magnetics, Volume: 48, Issue: 4, pp.1501-1504, 2012

[5] SVATOS, J. — VEDRAL, J. — FEXA, P.: Metal Detector Excited by Frequency Swept Signals, Metrology and Measurement Systems, vol. XVIII, no. 1, pp. 57-68, 2011

[6] SVATOS, J. — VEDRAL, J.: Metal Object Detection and Discrimination Using Sinc Signal. BEC2012, will be published in 2012

[7] International Test and Evaluation Program for Humanitarian Demining, Soil Electromagnetic Characteristics and Metal Detector Performance, European Commission Joint Research Centre Via E. Fermi, Ispra, 2002

[8] BRUSCHINI, C.: A Multidisciplinary Analysis of Frequency Domain Metal Detectors for Humanitarian Deminig, Vrije Universiteit Brussel, Brussel, 2002

[9] SIEGENFELD, A.: ATMID – Technologie und Schaltungsbeschreibung. 2003

[10] SCHIEBEL, Maintenance Manual. MT5001/16/010E

[11] VEDRAL, J. — FEXA, P.: DAC testing using impulse signals. Metrology and Measurement Systems, vol. XIX, No. 1, pp. 105-114. ISBN 0860-8229, 2012

[12] BRUSCHINI, C.: On the Low Frequency EMI Response of Coincident Loops Over a Conductive and Permeable Soil and Corresponding Background Reduction Schemes, IEEE Trans. Geosci. Remote Sens., vol. 42, no. 8, pp. 1706–1719, Aug. 2004

[13] PACES, P. — REINSTEIN, M. — DRAXLER, K..: "Fusion of smart sensor standards and sensors with self-validating abilities," *Digital Avionics Systems Conference, 2008, DASC 2008. IEEE/AIAA 27th*, vol., no., pp.4.B.5-1-4.B.5-13, 26-30 Oct. 2008, doi: 10.1109/DASC.2008.4702828

[14] NOVACEK, P. — RIPKA, P. — PRIBULA, O. — FISCHER, J.: Mine detector with discrimination ability, JEE 61(7), (2010), pp. 141-143, 2010,

Received 8 September 2012

Jakub Svatoš (Ing), was born in 1981 in Prague, Czech Republic received an Ing. degree (MSc equivalent) in February 2008 in specialization of Measurement and Distributed Systemsat at Dept. of Measurement, Faculty of Electrical Engineering (FEE) Czech Technical University in Prague (CTU), Czech Republic. Currently he is a PhD student under Assoc. Prof. Josef Vedral at the FEE, CTU. His research interests include metal detection and ADC testing using non-traditional excitation signals and digital signal processing.

Josef Vedral (Doc, CSc), was born in 1947 in Tachov, Czech Republic received an Ing. degree (MSc equivalent) in 1971 in specialization of Measurement Systems at Department of Measurement, Faculty of Electrical Engineering (FEE) Czech Technical University in Prague (CTU), Czech Republic. Currently he is an associate professor at the FEE, CTU. His research interests include analog signal processing and digitalization and ADC testing using polyharmonic signals.

Petr Nováček (Ing), was born in 1983 in Prague, Czech Republic. He received an Ing. degree (M.Sc. equivalent) with a specialization in aeronautical instrumentation systems from the Department of Measurement, Faculty of Electrical Engineering (FEE) Czech Technical University (CTU), Prague, in January 2010. He is currently pursuing the Ph.D. degree under prof. P. Ripka at the FEE, CTU. His research interests include sensors (magnetometers and accelerometers), electronics of sensors, digital signal processing, and microcontroller design for low-cost precise navigation systems.

5.1.3 Complex Markers for a Mine Detector

The publication (Novacek, Rohac & Ripka 2012) further involves the earlier paper (Novacek et al. 2010) by testing position marks based on a result obtained during metal detector movement above different materials. The position marks consist of metal nails from different materials (steel and aluminium) and by a different arrangement of nails together with a different metal combination - unique detected patterns were measured. Therefore, position marks can be used as reference position pointers during the estimation of the position of the metal detector search head. Together with Complex Magnetic Markers (CMMs), a local minimum or maximum algorithm was implemented to detect the exact centre position of the position mark.

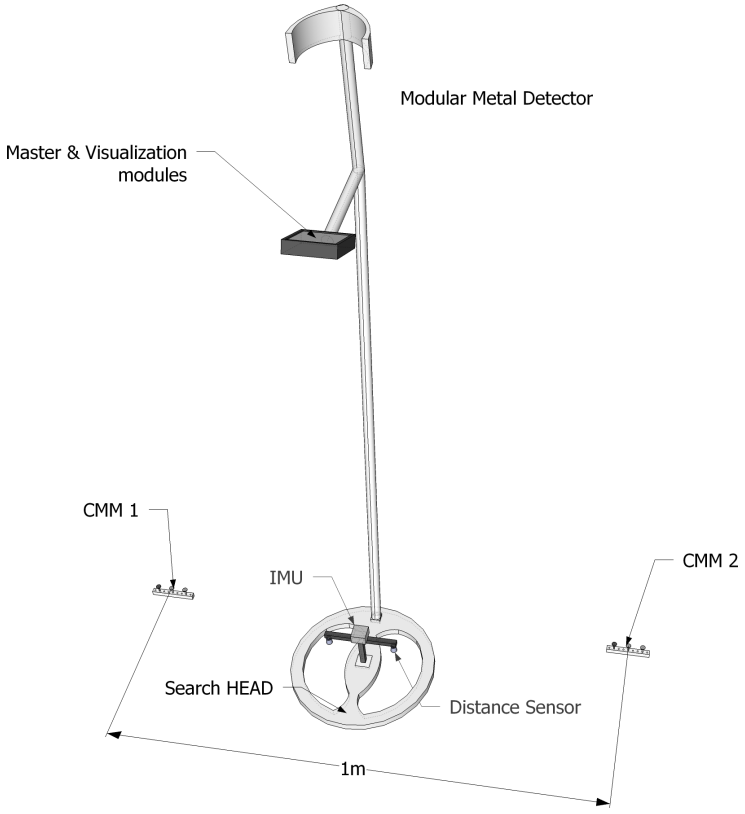

Figure 5.4: Modular metal detector modules setup, using Complex Magnetic Marks.

The real application setup of CMMs is shown in figure 5.4. The Metal detector is equipped with IMU and distance sensors installed on the search head. The distance between position marks is variable and depends on the exact application.

IEEE TRANSACTIONS ON MAGNETICS, VOL. 48, NO. 4, APRIL 2012

Complex Markers for a Mine Detector

Petr Nováček, Jan Roháč, and Pavel Ripka

Czech Technical University in Prague, Faculty of Electrical Engineering, 166 27 Prague, Czech Republic

This paper describes a novel type of metal markers for eddy current metal detection systems using precise positioning information. The new design for metal markers which are compounded by an ordered array of metal plates with different magnetic parameters has three fundamental advantages: 1. the markers are sensed directly by the metal detector, and no additional hardware is required; 2. the signatures are sharp; 3. not only the position but also the speed of the detector head can be evaluated. In the case of a stand-alone inertial navigation system for evaluating the position of the detector, the precision would be low due to the sensor noise and its integration. However, knowledge of the relative positions and potentially of the detector head speed over the markers can be used as auxiliary information, and so the eddy-current mapping system will be capable of determining the size of the magnetic imprint of a detected metal object and its position relative to the markers. This increases the reliability of the object discrimination during humanitarian demining, and decreases the numbers of false alarms, which nowadays constitute 99.9% of all alarms emitted by an ordinary mine detector.

***Index Terms*—Eddy currents, inertial navigation, magnetic field measurement, signal processing.**

I. Introduction

HUMANITARIAN demining is a very important activity, in which efforts are directed at clearing land contaminated with unexploded ordnance (UXO) after military conflicts all round the world. It is nowadays becoming more and more difficult to differentiate between UXO and clutter during demining procedures. Moreover, the detection ability of metal detectors is further decreased when searching in magnetic soils [1]. The numbers of false alarms can rise to 99.9% [2]. This high percentage of garbage that is detected instead of UXO enormously increases the cost of demining.

In recent years, several research groups have been developing innovative intelligent metal detectors with a high impact on decreasing the risk of injuries. Remotely controlled vehicles have been developed for demining, e.g. hovering detectors [3], unmanned vehicles [4], and robots [5], [6]. The improved ability of standard metal detectors to discriminate is mostly due to advanced signal processing [7], [8]. The magnetic signature of the suspected conducting object, in the form of a 2-D intensity map, is often compared with known patterns created by mines, and with ammunition used in the relevant region. In order to create this kind of map, it is necessary to scan the area using a metal detector and to have precise information about the position of the detector search head available.

The use of specialized vehicles or robots is mostly limited to flat terrain. Hand-held metal detectors, such as the All Terrain Mine Detector (ATMID) [9], equipped with additional systems, will offer a possible solution in areas that are difficult to access (forests, sloping terrain, etc.)

A precise positioning system for a hand-held metal detector is a challenging task, as the required resolution is 1 cm, and the required precision is 2 cm. We believe that only a simple, lightweight and inexpensive fully autonomous system has a chance of being adopted by the demining community. We therefore use an inertial positioning system based on acceleration and angular rates sensed by accelerometers and rate gyros. Metal detectors are generally equipped with low-cost Micro-Electro-Mechanical System (MEMS) sensors, which have significant drift and noise. Considering the integration from speed to position (and double integration from acceleration) these sensor errors very quickly lead to gross errors in evaluated position. In this paper, we use knowledge about metal marker relative positions to aid the positioning system. On the other hand, optical flow sensors provide information only about velocity, which alone is also not sufficient. The complex markers that we propose here provide information on both position and velocity, and this potentially allows all offsets in the system to be periodically nullified. The markers are sensed by the eddy-current detector itself. Unlike in the case of optical aiding methods, this requires no additional hardware.

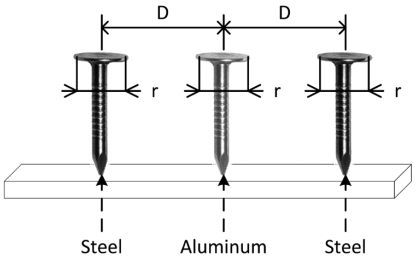

Fig. 1. Possible complex magnetic marker structure.

The novel contribution of this work is the utilization of complex markers as an auxiliary source of information for a precise positioning and navigation algorithm.

II. Methodology

Complex magnetic markers (CMMs) consist of a specially ordered array of tiny metal plates with known magnetic characteristics, see Fig. 1, where D represents plate distances and r is the diameter.

The proposed CMMs are designed to have precise center localization characteristics and to affect as small area as possible by their presence. The second characteristic enables the user to detect a UXO in a major part of the space between CMMs, which are commonly located in about 1 m distance, and does not decrease the sensitivity of the detector. The whole system is able to detect a UXO up to tens of centimeters in depth, depending on the environment, and to localize it due to the positioning capabilities of the detector head.

Manuscript received August 15, 2011; revised October 07, 2011; accepted October 11, 2011. Date of current version March 23, 2012. Corresponding author: P. Nováček (e-mail: petr.novacek@fel.cvut.cz).

Digital Object Identifier 10.1109/TMAG.2011.2172933

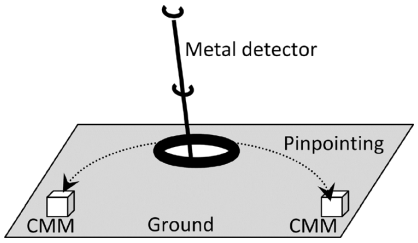

Fig. 2. "Pinpointing" character of the demining procedure (CMM—Complex Magnetic Marker).

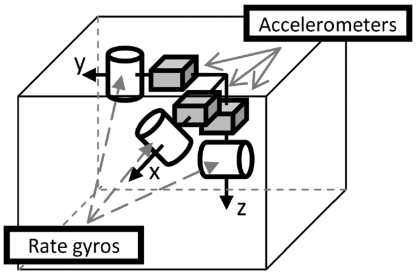

Fig. 3. Inertial measurement unit configuration.

We show that complex magnetic markers can be used not only to indicate the presence of the detector head above the markers, but also to measure the head velocity. In the case of complex markers with a known signal profile, the output voltage is highly dependent on the detector head velocity during the passage of the markers.

The standard demining process consists of two phases. In the first phase, the operator scans the strip of land using the conventional method. Once he detects a metal object, he stops moving forward and starts to pinpoint the exact location of the object. He signals the most probable location by two markers located on both sides of the object at a distance of 50 cm. The signal from the metal detector is collected during a pinpointing between these markers, see Fig. 2.

It must always be ensured that the detector head goes over the magnetic markers to identify the end of area being searched. This feature can be used to aid the positioning system, which continuously evaluates the position on the basis of the sensed acceleration and angular rates. This measurement is performed by the Inertial Measurement Unit (IMU), which generally consists of accelerometers and rate gyros, sometimes supplemented by magnetometers. According to the measured data, the position and attitude of the detector head can be estimated and then used to map the magnetic imprint of the detected object. This forms a system capable of observing the imprint more closely and determining its size and position. When low-cost sensors are used, it is necessary to have an auxiliary system to provide position corrections to reduce the effect of noise integration within the navigation data algorithm.

A. Inertial Sensors

Inertial sensors, i.e. a tri-axial accelerometer and a tri-axial rate gyro, form the Inertial Measurement Unit (IMU), see Fig. 3.

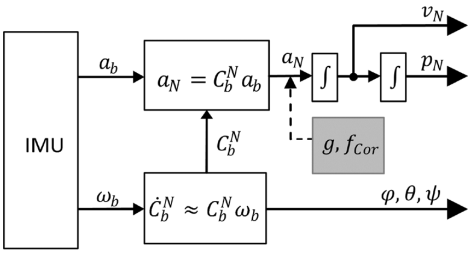

Fig. 4. Principle block scheme of the navigation algorithm.

Accelerometers measure the transitional acceleration, and rate gyros measure the angular rate. This data is used consecutively to evaluate the attitude (roll, pitch, and heading angle), based on which the sensed acceleration is transformed into the local navigation frame and then integrated to obtain the velocity and the position. A block scheme of this procedure is shown in Fig. 4, where ω_b, a_b denote the sensed angular rates and accelerations, $\mathrm{C}_\mathrm{b}^\mathrm{N}$ represents the transformation matrix from the body to the local navigation frame, v_N, p_N correspond to the velocity and the position in the local frame, and φ, θ, ψ are Euler angles related to the attitude.

The navigation algorithm further includes corrections for gravitational force and Coriolis force, denoted in Fig. 4 as g and f_{Cor}.

As mentioned above, both accelerometers and rate gyros suffer from noise which, after integration, causes unbounded error in the system output. This factor has to be minimized by an auxiliary system which is formed, in our case, by knowledge of the precise positions of the metal reference markers. In each sweeping cycle, the position estimated via the inertial sensors and the navigation algorithm is corrected, and this approach reduces the system error. In our experiments, we used IMU ADIS 16405, with a sampling frequency of 25 Hz. The usage, design and performance of the Kalman filter are not described in detail here, because they are beyond the scope of this paper.

B. Position Reference Markers

As presented by Bruschini [10], the signal phase measured by an eddy current metal detector depends on the material parameters, with the dependency defined as

$$\varphi = arctg\left(\frac{\mathrm{Im}(f)}{\mathrm{Re}(f)}\right), \tag{1}$$

where f represents the output signal of the metal detector, $\mathrm{Im}(f)$ and $\mathrm{Re}(f)$ denote the imaginary and real part of the output signal f, and φ is the evaluated signal phase.

In this paper, we propose a new design for metal markers which are compounded by a specially ordered array of metal plates with different magnetic parameters (permeability and conductivity). The array forms a magnetic marker with a defined impact on the detector output. This performance can be used to indicate the precise position of the detector head when the head is right above the marker.

The array of plates can be composed of different conductivity materials with a known relative permeability μ_r and conductivity σ. In our case, the marker consists of Aluminum (Al: $\mu_{r\,Al} = 1$, $\sigma_{Al} = 3.6\ 10^7$ S/m) and Chrome Steel (St: $\mu_{r\,St} = 150$, $\sigma_{St} = 0.46\ 10^7$ S/m) circular plates with the same diameter $r = 9.4$ mm.

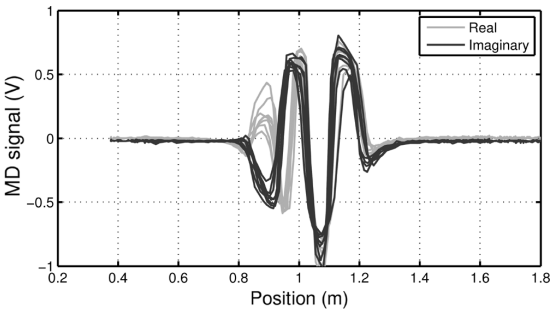

Fig. 5. Imprint of CMM consisting of two plates—Steel and Aluminum; distance between the plates: 50 mm.

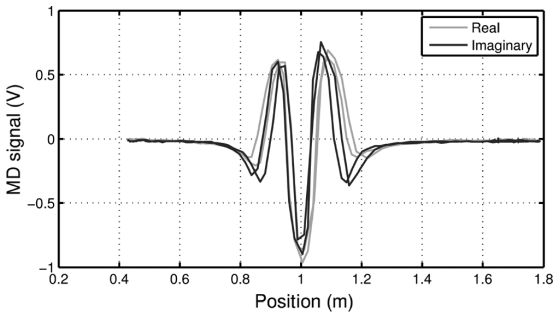

Fig. 6. Imprint of CMM consisting of two plates—Steel and Aluminum; distance between the plates: 40 mm; the signal phase shift is unobservable.

The possibility to differentiate CMMs just by choosing different plate array structures (the sequence of steel and aluminum plates) is another advantage of the proposed CMM. The use of a multiple CMM system with different structures (codes) enables more complex navigation tasks to be defined with absolute position accuracy, which is in contrast with the technology currently available on market.

III. Measurement Setup

The measurement setup included a modified ATMID metal detector equipped with a subsystem capable of measuring the real and imaginary part of the detector output signal and of communicating with a PC. Moreover, the IMU ADIS16405 was mounted on the detector head. An optical measurement system utilizing an industrial camera [11] was used as a position reference. All experiments were performed under laboratory conditions. The measured data was synchronized with a sampling frequency of 25 Hz.

IV. Experimental Results

The aim of this paper is to prove the suitability of CMM characteristics for providing adequate position determination accuracy. Precise navigation algorithms are beyond the scope this paper, and only CMM characteristics are therefore further analyzed and discussed here.

First of all, we analyzed the influence of the distance between the St and Al plates on the performance of the detector. Fig. 5 shows one imprint of a real and imaginary part of the detector output voltage. In this case, the distance between the plates was 5 cm. This was evaluated as the smallest distance in which the real and imaginary part was still distinguishable. When the distance was smaller, the difference decreased, as shown in Fig. 6, and the difference was hardly detectable. In contrast, when the distance was increased, no improvement was observed, and the CMM extended the size of its imprint, which was undesirable.

Knowledge of the precise position within the range of the imprint is defined by the local maximum or minimum (depending on the number of plates and on the structure). The sharper the local minimum or maximum is, the better the CMM localization accuracy will be. Therefore, due to the different design of CMM with more than two plates, a sharper local minimum or maximum can be achieved. A complex CMM imprint with four plates (Fe-Al-Fe-Al) is shown in Fig. 7. In this case, the local maximum is 2 times sharper than the local minimum in Fig. 5.

The imprints shown in Figs. 5–7 were evaluated from experiments in which the CMM was moved under the detector head.

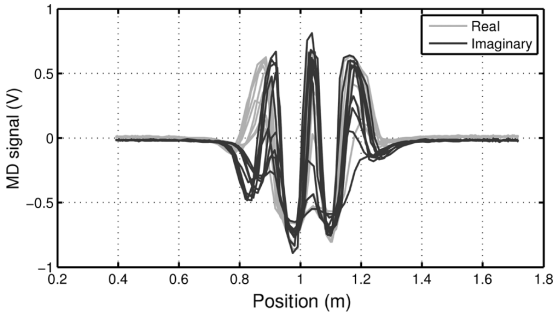

Fig. 7. Imprint of CMM consisting of four plates—Steel, Aluminum, Steel and Aluminum; distance between plates is 50 mm.

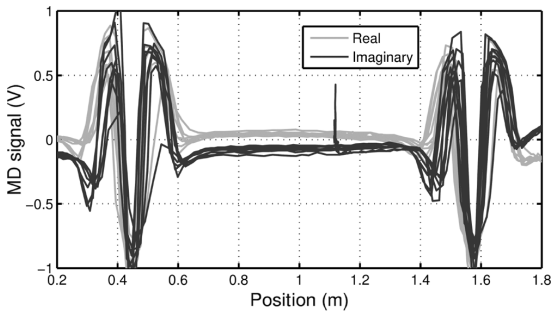

Fig. 8. CMM signal stamp for left and right CMM influenced by noise.

This ensured steady environmental conditions from the conductivity point of view. When the situation was opposite, i.e. when the detector head moved and the two CMMs were steady with a known relative position, the influence of the unsteady conductive conditions affected the mean values of the real and imaginary part, as shown in Fig. 8. The phase shift is small; however, it disables the use of CMM with a smaller distance than 5 cm the between plates. This situation corresponds to real demining conditions, and small phase shifts therefore have to be considered as undesirable.

We implemented an algorithm using a convolution function to localize the local minimum or maximum within the range of the imprint. This also took into account the differences between the minima and maxima in order to restrict false localization. In addition, the algorithm can compare the evaluated imprint

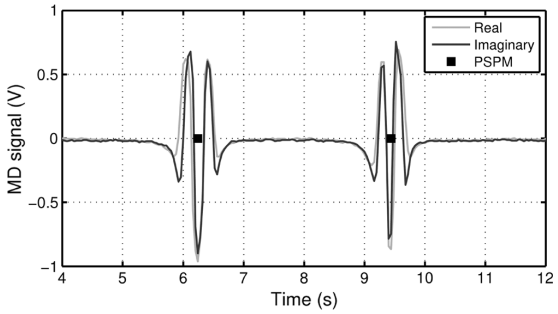

Fig. 9. CMM signal stamp for left and right CMM influenced by noise.

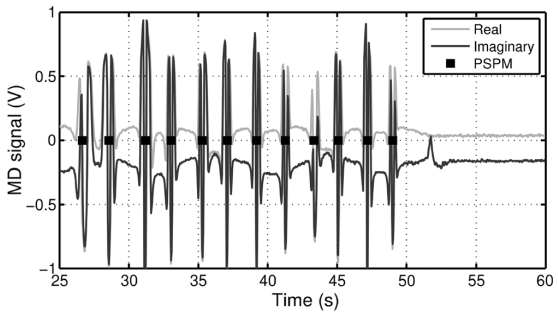

Fig. 10. Localization of imprint minima—unsteady conductive conditions.

with the imprint stored in the memory. This functionality further limits potential false imprint identification and localization. The algorithm is also able to estimate the metal detector search head transit time above the reference mark, and this enables it to be used in velocity estimation. The results of the algorithm are shown in Figs. 9 and 10. In the first case, the measurement was made under steady conductive conditions (CMM was moved under the detector head). By contrast, Fig. 10 depicts the measurement in which the detector head moved ("swept") between two CMMs, and thus the influence of an unsteady conductive environment can be seen in the imprint.

V. Conclusion

Continuous positioning of the metal detector is crucial in demining procedures. Since low-cost inertial sensors are used, additional (aiding) information about the position is needed. In this paper, we have proposed a new design for magnetic markers (CMM) composed of a specially ordered array of metal plates with different magnetic parameters. In the case of a complex marker (see Fig. 7), this design provides precise positioning capability due to the sharp identification of minima or maxima. The accuracy is better than 45 mm under all conditions. This accuracy makes the knowledge of proposed CMM relative positions, which are precise due to CMM parameters, suitable to aid an inertial sensor based position estimation process.

In addition, the character of CMM and its imprint minimize false localization of the marker. This is one of the main advantages of the design.

During preliminary experiments, we used markers in the form of nails made from two metal materials, non-magnetic aluminum and chrome steel, which are available in developing countries, where most demining operations are carried out. Some preliminary experiments have been performed under laboratory conditions; however, other tests are now planned under real conditions in the Joint Research Centre (ISPRA, Italy) testing area, where the whole metal detector system with magnetic markers will be tested.

Acknowledgment

This work was supported by the Grant Agency of the Czech Technical University in Prague under Project SGS10/288/OHK3/3T/13, by the Czech Science Foundation under Project 102/09/H082, and by Research Program MSM6840770015 Research on Methods and Systems for Measurement of Physical Quantities and Measured Data Processing of the CTU in Prague, sponsored by the Ministry of Education, Youth and Sport of the Czech Republic.

References

[1] P. Ripka, J. Vcelak, P. Kaspar, and A. M. Lewis, "Bomb detection in magnetic soils: AC versus DC methods," in *Proc. 5th IEEE Conf. Sens.*, 2006, pp. 1389–1391.

[2] D. Guelle, *Metal Detector Handbook for Humanitarian Demining*. Luxembourg, Norwich: Office for Official Publications of the European Communities; Stationery Office distributor, 2003.

[3] M. Hussain, "RF controlled GPS based hovering mine detector," in *Proc. 9th Int. IEEE INMIC*, 2005, pp. 1–4.

[4] M. Yagimli and H. Varol, "Mine detecting GPS-based unmanned ground vehicle," in *Proc. 4th Int. Conf. RAST*, 2009, pp. 303–306.

[5] E. Heußlein, B. W. Patullo, and D. L. Macmillan, "Robot navigation: Implications from search strategies in exploring crayfish," *Robotica*, vol. 28, no. 3, p. 465, May 2009.

[6] J. Estremera, J. A. Cobano, and P. Gonzalez de Santos, "Continuous free-crab gaits for hexapod robots on a natural terrain with forbidden zones: An application to humanitarian demining," *Robot. Autonomous Sys.*, vol. 58, no. 5, pp. 700–711, May 2010.

[7] P. Ripka, M. Janosek, and P. Novacek, "Depth estimation of metal objects," *Procedia Eng.*, vol. 5, pp. 280–283, 2010.

[8] J. Svatos, J. Vedral, and P. Fexa, "Metal detector excited by frequency-swept signal," *Metrology Meas. Syst.*, pp. 57–68, 2011.

[9] Schiebel, Maintenance Manual MT5001/16/010E 2003.

[10] C. Bruschini, "A Multidisciplinary Analysis of Frequency Domain Metal Detectors for Humanitarian Demining," PhD thesis, Vrije Universiteit Brussel, , Brussels, 2002.

[11] P. Novacek, P. Ripka, O. Pribula, and J. Fischer, "Mine detector with discrimination ability," *J. Electr. Eng.*, vol. 61, no. 7, pp. 141–143, 2010.

5.1.4 Metal Detector Signal Imprints of Detected Objects

This last publication (Novacek, Rohac, Simanek & Ripka 2013) addressing ATMID detectors, presents further work on CMMs (Novacek et al. 2012) and introduces position marks signal imprint. Furthermore, the signal intensity map of the INOX metal sphere detected is discussed.

As the journal publication had limited length, it was not possible to include all data measured, namely the comparison of signal intensity maps obtained for a different testing object. Here, the comparison of chrome steel and INOX sphere is presented.

Figure 5.5 illustrates the detection of the chrome steel sphere, again with a diameter of $10mm$.

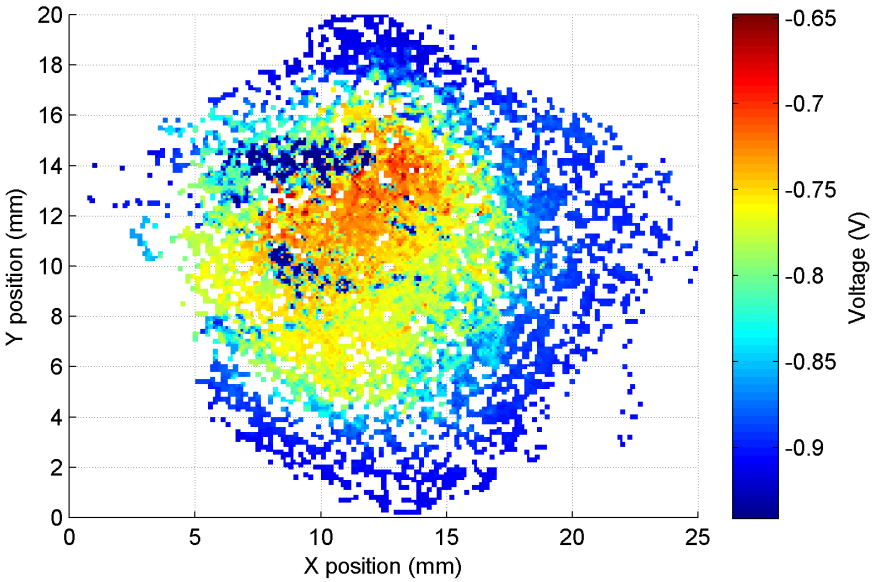

Figure 5.5: Chrome steel sphere ($10mm$) signal intensity map.

Figure 5.6 shows the measurement of the INOX AISI 420 sphere as the ferromagnetic material.

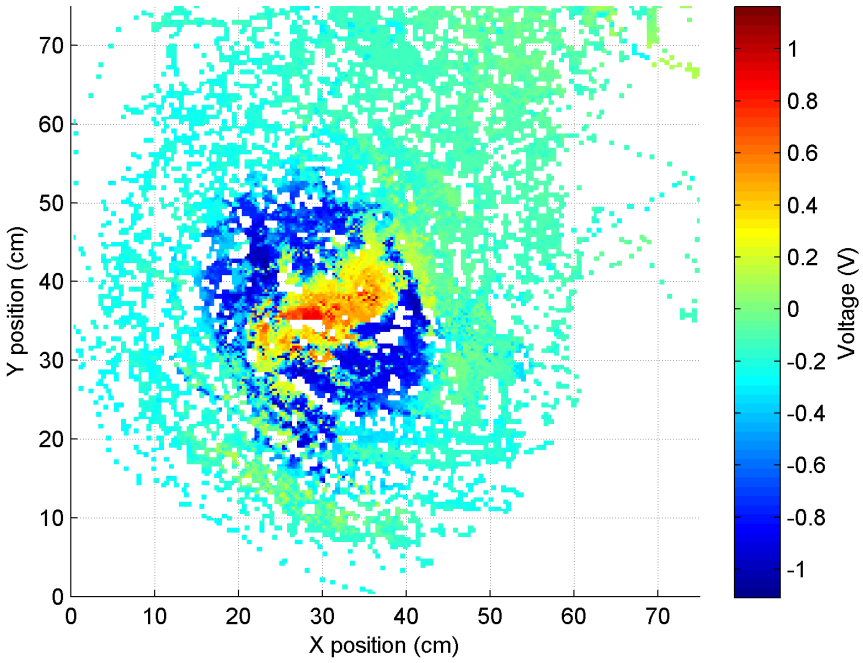

Figure 5.6: INOX AISI 420 sphere ($10mm$) signal intensity map.

The signal intensity map was constructed in post processing by the pinpoint movement of the ATMID and the use of a position reference system installed in the laboratory. The metal detector was moved by hand and missing points of signal intensity were approximated as the weighted average of surrounding known points. The figure seems to be non-symmetrical – which is caused by changing the sensing height by an unexperienced operator.

IEEE TRANSACTIONS ON MAGNETICS, VOL. 49, NO. 1, JANUARY 2013

Metal Detector Signal Imprints of Detected Objects

Petr Nováček, Jan Roháč, Jakub Šimánek, and Pavel Ripka

Department of Measurement, Faculty of Electrical Engineering, Czech Technical University in Prague, Prague 166 27, Czech Republic

Humanitarian demining missions are activities in which an operator safety and time consumption are key issues. To increase a discrimination ability of ATMID metal detector, which we have been using, we extended the capability of the detector with mounting inertial measurement unit (IMU) supplemented by two optical distance sensors on the detector head. That enabled us to perform dead reckoning based on accelerations and angular rates measured by IMU in all three axes. Optical distance sensors have been used for compensation purposes and an initial distance measurement. Our main aim was to interconnect magnetic imprint sensed by the detector with precise localization of its head, which led to imprint size estimation as well as its position. Due to low-cost micro-electro-mechanical system (MEMS) based IMU implementation we have had to deal with unstable dead reckoning outcomes. For this reason we used our designed complex magnetic markers (CMMs) which demarked a searched area plus provided us with precise positioning at its both edges. The main contribution of this paper is in the study and identification of CMM magnetic imprints characteristics and their differences related to various aspects of CMM usage during demining procedure and its conditions. The characteristics of CMMs have been studied and analyzed according to several laboratory experiments and results are presented.

***Index Terms*—Eddy currents, inertial navigation, magnetic field measurement, signal processing.**

I. Introduction

THIS paper deals with local navigation of a metal detector for detecting and discriminating mines. Precise localization and attitude estimation of the detector in space enables the user to create signal maps, which can be used to increase the discrimination ability of the metal detector [1]. The motivation is to reduce risks for detector operators during humanitarian demining missions [2]. Traditional systems of this type use multisensor arrays and feature extraction image processing methods [3].

Humanitarian demining is still actual problem. Especially in areas of recent military conflict, there is a need to return contaminated land to civilians. This land is needed for agricultural purposes and for other civilian activities, so it must be absolutely free of unexploded ordnance. Absolute land clearance sets high requirements on demining procedures. The problems are greater in areas that are difficult to access. In these areas, handheld mine and metal detectors are the only equipment that can be used [4]. As demining progresses, contaminated areas that are easy to access and demined are the first to be cleared. Other areas that need to be cleared are often handicapped by the presence of buried conductive or metal objects or by characteristics of the soils themselves [5]. Metal contamination and magnetic soils reduce the sensitivity of metal detectors; soil contamination also increases the numbers of false alarms which, in some areas, account for as much as 99.9% of all alarms [6]. False alarms additionally lower the operator's concentration, and the danger of injuries and casualties arises in combination with reduced detector sensitivity and the operator attention.

A simple system for increasing the discrimination ability of metal detectors needs to be developed in order to reduce humanitarian demining risks. Instead of multisensor arrays such a system should be based on a single metal detector which is manually scanning a small area while its position is monitored with cm precision. The first attempt towards such a system was reported in [7]. The position of a metal detector was evaluated from inertial navigation system. The integrated errors accumulated over time were unacceptable: up to 1 m after 90 s of operation. This was improved by aiding of zero-velocity sensor, but only for motion constrained to a plane. In this paper we suggested to use magnetic markers for position aiding. The advantage of the magnetic markers is that they are sensed directly by the metal detector itself unlike the optical markers which require additional camera [8]. A discrimination ability of metal detectors mainly depends on the level of output signal amplitude and its phase shift which are affected by the conductivity and permeability of a detected object. Thus, these parameters are considered as crucial factors. Furthermore, a lateral and vertical profiles also have to be taken into account [9].

The main contribution of our approach to increase discrimination ability of a metal detector relies on the development of complex magnetic markers (CMMs), for more details see [10]. When they are placed at both edges of searched area and are passed by a detector searching head they provide precise positioning capability as well as their identification, all provided by unique magnetic imprints with a known intensity map. In the case when a database of these intensity maps is built it provides a powerful tool increasing the precision of position evaluation during the demining procedure no matter the conditions. Therefore, we made several CMMs with a different structure and evaluated related reference intensity maps when the searching head was moved with a constant speed and distance above the CMMs. One example of CMM structure is shown in Fig. 1.

The CMMs were formed by the array of plates made from different conductivity materials with a known relative permeability μ_r and conductivity σ. In our case, the CMM consisted of the combination of aluminum $(\mathrm{Al}: \mu_{rAl} = 1, \sigma_{Al} = 3.6\ 10^7\ \mathrm{S/m})$ and chrome steel $(\mathrm{St}: \mu_{rSt} = 150, \sigma_{St} = 0.46\ 10^7\ \mathrm{S/m})$ circular headed nails with the same diameter $r = 9.4\ \mathrm{mm}$.

The bottom part under the nails was wooden with the possibility to change nails' structure and distance among them. The

Manuscript received July 11, 2012; revised September 05, 2012; accepted September 20, 2012. Date of current version December 19, 2012. Corresponding author: P. Nováček (e-mail: petr.novacek@fel.cvut.cz).

Digital Object Identifier 10.1109/TMAG.2012.2220959

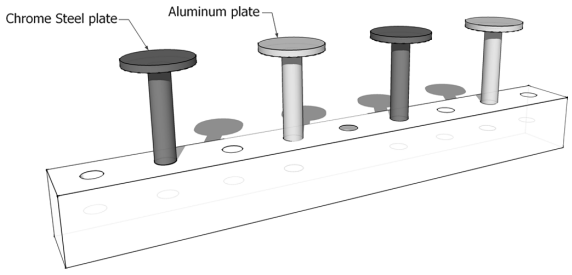

Fig. 1. Sample of the CMM structure with four nails (steel, aluminum, steel, and aluminum) with gaps of 2 cm.

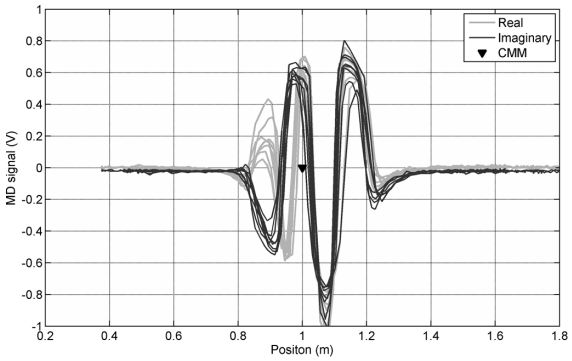

Fig. 2. Imprint of CMM consisting of two nails—steel and aluminum; distance between the nails: 50 mm. [10].

CMM imprints have different character than unexploded ordnance so the CMM and objects being searched can be clearly distinguished. The impact of different materials used in CMMs on the detector output voltage consisted of a real and imaginary part is shown in Fig. 2. When reference imprints are known it is possible to compare them with measured ones, which are influenced by the lateral and vertical distances between the CMM and the searching head and, of course, by the speed, and attitude of the head. All these aspects have been studied and characterized by performed experiments and results are presented.

II. Measurement Setup

All data and results presented were obtained under laboratory conditions. Our experiment setup consisted of ATMID [11] metal detector supplemented by additional information sources such as inertial measurement unit (IMU) for accelerations and angular rates sensing, plus two infrared distance sensors, and complex magnetic markers (CMMs). Usage of ground distance sensors is a second major improvement of the system described in [8].

For data validation purposes we placed a camera below the laboratory ceiling which provided us with the position and velocity reference to relate dead-reckoning outcomes to. The reference position estimation has had a sub pixel resolution and approximately 1 mm standard deviation, which guaranteed required precision for the CMM characteristics study.

All data measured by the detector itself, IMU, and distance sensors were synchronized by an acquisition unit and sent to a PC via communication interface. The sampling frequency of these data was 50 Hz. A principal schema is shown in Fig. 3.

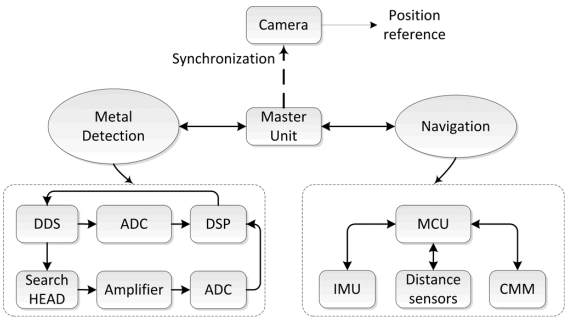

Fig. 3. Principle scheme of the measurement setup. A/D converter (ADC), digital signal processor (DSP), direct digital synthesizer (DDS), inertial measurement unit (IMU), micro-controller unit (MCU), complex magnetic marker (CMM).

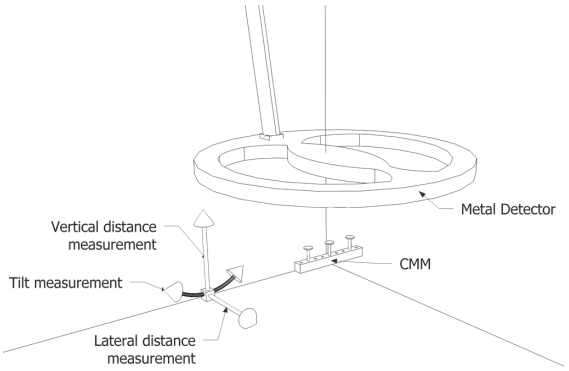

Fig. 4. Measurement setup and procedure.

For the CMM characteristics study the experiments observed only the detector output signals representing CMM imprints and the detector position obtained from the reference position camera system [12]. The reference position system was not synchronized with the other data; it is future possibility for the system capability extension; however, its update rate corresponded also to 50 frames per second.

III. Experimental Results

The experiments studying different aspects of CMM magnetic imprints characteristics were performed with more compositions of CMMs. The first one was formed by only aluminum nails and the other one consisted of a combination of aluminum and chrome steel nails. Nevertheless, results presented in this paper were related just to CMM formed by three aluminum plates (as shown in Fig. 4), because the dependencies were very similar.

A. Observation of the Detector Sensitivity

Evaluation of a metal detector output signal, when a small sphere with 10 mm diameter was observed, led to intensity map shown in Fig. 5. The intensity map was constructed by digitizing real and imaginary parts of detector output signal and then

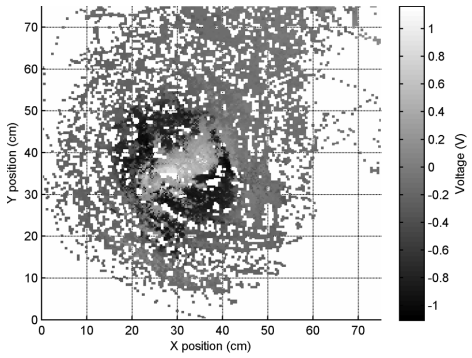

Fig. 5. Imprint intensity map measured by ATMID metal detector with INOX AISI 420 sphere of diameter 10 mm as the detected target.

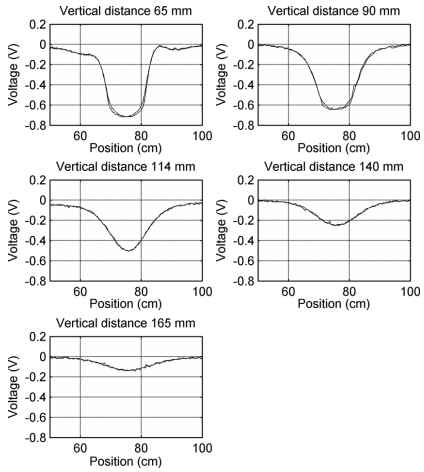

Fig. 6. Imprint dependency on a vertical distance between CMM and the detector head.

converted into voltage magnitude and corresponding phase. In Fig. 5 there is shown the evaluated magnitude with respect to the position and distance of the sphere from the detector head. A color representation corresponds to the value of the magnitude.

B. CMM Imprint Dependency on Lateral and Vertical Profile

Due to the fact that a detector operator does not need to pass the CMM precisely and the application still requires precise CMM identification we performed several experiments to study the imprint intensity map dependency on CMM vertical distance from the detector head as well as its dependency on CMM lateral distance from a detector main axis of sensitivity. Imprint parameters dependency on a vertical distance between CMM and the detector head is shown in Fig. 6. The detector head was moved above the CMM with different vertical distances (65, 90, 114, 140, and 165 mm). The values were chosen with respect to the ATMID detector sensitivity.

A similar character of the imprint parameters was also observed in the case of a lateral distance dependency. This distance was measured between the detector main axis and the axis of the CMM. The character is shown in Fig. 7. The detector head was moved above the CMM at the vertical distance 90 mm and lateral distances varied (-100, -50, 0, 50, and 100 mm). The distances were chosen with respect to the detector head diameter and its middle axis, which was kept constant, and the CMM position varied. The diameter of the ATMID detector head is 280 mm.

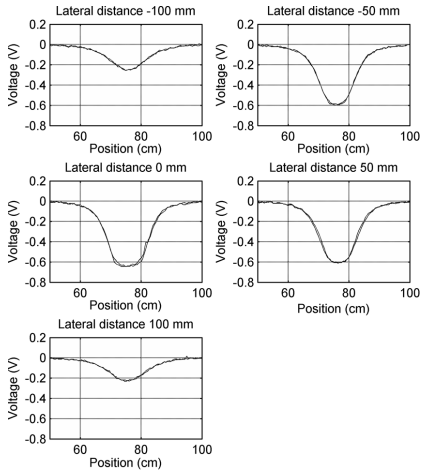

Fig. 7. Imprint dependency on a lateral distance between CMM axis and the detector main axis.

TABLE I
IMPRINTS AMPLITUDE DEPENDENCIES

Vertical Distance	Amplitude	Lateral Distance	Amplitude
65 mm	0.72 V	-100 mm	0.25 V
90 mm	0.65 V	-50 mm	0.60 V
114 mm	0.51 V	0 mm	0.65 V
140 mm	0.25 V	50 mm	0.61 V
165 mm	0.13 V	100 mm	0.23 V

Comparison of signal amplitudes related to specific vertical and lateral distances of CMM axis from the detector head main axis.

The results from experiments studying the imprint parameters dependency on CMM vertical and lateral distances from the detector head are summarized in Table I, in which maximal amplitudes of the detector output signal are provided.

C. CMM Imprint Dependency on the Detector Head Attitude

Because there is not possible generally to ensure null attitude of the detector head with respect to CMM origins, we also analyzed the impact of different attitude on the CMM imprint characteristics. We observed the amplitude of the imprint and the behavior did not show significant changes in the attitude range of $\pm 20°$. The resulting imprints for different attitude are shown in Fig. 8.

IV. CONCLUSION

This paper deals with CMMs and their magnetic imprints. The main contribution of this paper is in analyzing imprint char-

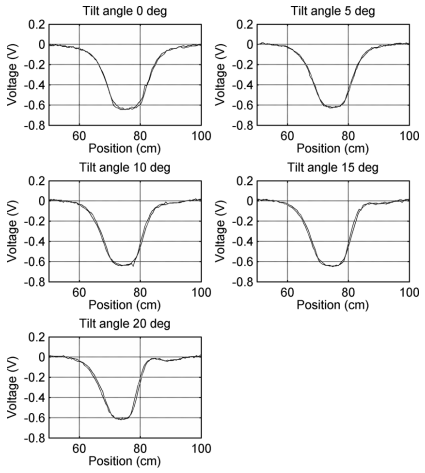

Fig. 8. CMM imprint dependency on a detector head attitude—tilt angle set in the range from 0° up to $+20^\circ$ with the step of 5°.

acteristics dependency on various conditions of a metal detector handling. Precise knowledge of CMMs position plays a crucial role in dead reckoning process in which the actual position of the detector head is estimated. CMMs position is used to compensate position errors mainly caused by uncompensated biased data measured by MEMS accelerometers and angular rate sensors. To localize CMMs it is required to identify CMMs correctly. The identification relies on correct matching of the measured CMM imprint with the reference one saved in the system memory. For the matching it is needed to know how the imprint can be affected by an operator handling the detector. During a demining procedure vertical and lateral distances between CMM and the detector head, and the detector head attitude can vary when CMM is passed by the detector head. Therefore, in this paper we analyzed all these aspects on two different CMMs. Even if all experiments were performed under laboratory conditions, we can clearly specify changes of CMM imprints according to mentioned handling conditions. Experiments proved the imprint amplitude was changing with lateral and vertical distances defined between CMM and the detector head. In ranges calculation we considered the environmental impact on the imprint on which it caused maximal amplitude perturbation of 0.1 V. Thus, to ensure correct identification we increased the minimal amplitude level for the CMM identification to be 0.2 V. In this case the correct identification as well as position determination can be done in ranges up to 105 mm in vertical distance and up to 90 mm in lateral distance. Both values were calculated based on Table I and progress approximations. Based on other experiments analyzing attitude changes impact on CMM identification it was proved that this aspect had no significant importance for its observation, because according to two different CMMs application we did not recognize any influence of different attitude in range of ± 20 deg on their magnetic imprints.

When CMM imprints are identified and their position precisely evaluated dead reckoning process can be strongly improved in the position estimation in the whole range of the metal detector application. It further increases discrimination ability of metal detectors during humanitarian demining missions as well as it decreases injury risks of detector operators because of better ability in differentiation among metal scraps and dangerous objects such as explosive remnants of wars.

Acknowledgment

This work was supported in part by the research program GD102/09/H082, “Sensors and Intelligent Sensor Systems,” at CTU, Prague, sponsored by the Czech Science Foundation; and by the Grant Agency of the Czech Technical University, Prague, under Grant SGS10/288/OHK3/3T/13, “Modular system for attitude and position estimation.”

References

[1] A. Brancaccio and G. Leone, “Localization of buried objects,” in *Proc. 13th Int. Conf. Ground Penetrating Radar (GPR)*, 2010, pp. 1–4.
[2] H. Kruger and H. Ewald, “Handheld metal detector with online visualisation and classification for the humanitarian mine clearance,” *IEEE Sens.*, 2008.
[3] M. D. Tran, C. Abeynayake, and L. C. Jain, “A target discrimination methodology utilizing wavelet-based and morphological feature extraction with metal detector array data,” *IEEE Trans. Geosci. Remote Sens.*, vol. 50, no. 1, pp. 119–129, Jan. 2012.
[4] G. Kellermann, “Metal detector, in particular mine detector,” US Patent 726555, 2007.
[5] P. Ripka, A. M. Lewis, and J. Kubik, “Mine detection in magnetic soils,” *Sens. Lett.*, vol. 5, no. 1, pp. 15–18, 2007.
[6] A. Lewis, T. Bloodworth, D. Guelle, and A. Smith, *Metal-Detector Handbook for Humanitarian Demining* 2003 [Online]. Available: http://publications.jrc.ec.europa.eu/repository/handle/111111111/13314
[7] B. Barrow and N. Khadr, “A combined EMI sensor and inertial motion system for localized UXO interrogation,” presented at the UXO COUNTERMINE RANGE Forum, Las Vegas, NV, 2006.
[8] X. Feng, M. Sato, and C. Liu, “Subsurface imaging using a handheld GPR MD system,” *IEEE Geosci. Remote Sens. Lett.*, vol. 9, no. 4, pp. 659–662, 2012.
[9] C. Bruschini, “A multidisciplinary analysis of frequency domain metal detectors for humanitarian demining,” Ph.D. dissertation, Faculty Appl. Sci., Vrije Univ., Brussels, Belgium, 2002.
[10] P. Novacek, J. Rohac, and P. Ripka, “Complex markers for a mine detector,” *IEEE Trans. Magn.*, vol. 48, no. 4, pp. 1489–1492, Apr. 2012.
[11] *“ATMID all Terrain Mine Detector Maintenance Manual MT5001/16/010E,”* Schiebel, Vienna, Austria, 2003, pp. 7–13.
[12] P. Novacek, P. Ripka, O. Pribula, and J. Fischer, “Mine detector with discrimination ability,” *JEE*, vol. 61, no. 7, pp. 141–143, 2010.

5.2 Inertial sensors analyses and calibration

The second part of the publications describes the enhancement of low cost inertial sensors utilizable for a wider range of navigation purposes. In these publications, I was only the co-author and my contribution consists mainly of the setup of the testing platform, data measurement and post processing preparation. However, the results achieved were fundamental to my work, as they allowed the realization of a practical autonomous tracking system that I could use in my main experiments.

5.2.1 Analyses of Triaxial Accelerometer Calibration Algorithms

This publication (Sipos, Paces, Rohac & Novacek 2011) addresses parameter improvements of a low-cost IMU. The paper describes three different calibration algorithms. Three different IMUs are used as a tested system. The results show the possibility of using only low cost equipment for the precise calibration of sensors using Levenberg–Marquardt and Thin-Shell calibration algorithms. The comparison of the two algorithms previously mentioned with MATLAB function *fminunc* is also presented. Conclusions of the publication show a significant improvement in attitude angles in addition to in-position determination.

IEEE SENSORS JOURNAL, VOL. 12, NO. 5, MAY 2012

Analyses of Triaxial Accelerometer Calibration Algorithms

Martin Šipoš, Pavel Pačes, *Member, IEEE*, Jan Roháč, and Petr Nováček

***Abstract*—This paper proposes a calibration procedure in order to minimize the process time and cost. It relies on the suggestion of optimal positions, in which the calibration procedure takes place, and on position number optimization. Furthermore, this paper describes and compares three useful calibration algorithms applicable on triaxial accelerometer to determine its mathematical error model without a need to use an expensive and precise calibration means, which is commonly required. The sensor error model (SEM) of triaxial accelerometer consists of three scale-factor errors, three nonorthogonality angles, and three offsets. For purposes of calibration, two algorithms were tested—the Levenberg–Marquardt and the Thin-Shell algorithm. Both were then related to algorithm based on Matlab *fminunc* function to analyze their efficiency and results. The proposed calibration procedure and applied algorithms were experimentally verified on accelerometers available on market. We performed various analyses of proposed procedure and proved its capability to estimate the parameters of SEM without a need of precise calibration means, with minimum number of iteration, both saving time, workload, and costs.**

***Index Terms*—Accelerometers, calibration, error analysis, inertial navigation.**

I. Introduction

OVER the last decades technological progress in the precision and reliability of Micro-Electro-Mechanical-Systems (MEMS) has enabled the usage of inertial sensors based on MEMS in a wide range of military and commercial applications, e.g., in Unmanned Aircraft Systems (UASs), indoor and personal navigation, human motion tracking, and attitude-control systems [1]–[5].

The Inertial Measurement Unit (IMU), which forms a basic part of Inertial Navigation System (INS), primarily contains only inertial sensors-accelerometers and angular rate sensors or gyroscopes to provide inertial data, and additionally magnetometers. The major errors of electronically-gimbaled navigation systems with accelerometers and magnetometers are caused by sensor triplet deviations (mutual misalignment) [6], and therefore, a calibration has to take a place for their proper function. The calibration is necessary to be performed to estimate sensor errors like nonorthogonalities (misalignment) and scale factor errors for their compensation. Factory based sensor calibration is an expensive and time-consuming process, which is typically done for specific high-grade IMUs. For low-cost inertial sensors, such as MEMS based ones, manufacturers perform only basic calibration [7] which is very often insufficient, because even small uncompensated imperfections can cause position deviation growth and also inaccuracy in tilt angle evaluation [8], [9].

There are already known different sensor error models (SEMs) [10] and calibration methods based on different principles, but they have limitations such as the necessity of precise position system or a platform providing precise alignment. This requirement increases manufacturing costs, and therefore, there is a need for investigating alternatives.

One example of a commonly used calibration procedure described by Titterton and Weston in ([11] p. 238) and by Won in [8] uses six static positions, in which the sensors' axes are consecutively aligned up and down along the vertical axis of the local level frame. The calibration is capable to determine only offsets and scale factor errors, not nonorthogonalities. The calibration accuracy strongly depends on the alignment precision [7]. To increase the precision of alignment an accurate reference system is usually used, as presented in [10], [11]. In the first case a 3-D optical tracking system and nonlinear least squares algorithm were applied, the other case used an *fminunc* Matlab function as a minimizing algorithm and a robotic arm. In both cases the calibration is capable to estimate sensor' axes misalignments, offsets, and electrical gains/scale factors, which define nine-parameter-error model. The same model for a triaxial accelerometer can be estimated by an iterative calibration procedure described by Petrucha *et al.* in [12] using an automated nonmagnetic system, or the one described by Syed *et al.* in [7], in which offset and scale factor initial values are required for a modified multiposition method. Other method for an accelerometer calibration, presented by Skog and Händel in [13], is based on the cost function formulation and its minimization with respect to unknown model parameters using Newton's method. The cost function can reach several local optima, and therefore, the initial starting values have to be determined. Automatic adaptive method of a 3-D field sensor based on a linearized version of an ellipsoid fitting problem has been published in [14]. It relies on a procedure that fits an ellipsoid to data using linear regression. Based on estimated ellipsoid parameters the unknown model parameters can be evaluated. An alternative to this method using modified ellipsoidal-fitting procedure has

Manuscript received May 13, 2011; revised August 01, 2011; accepted August 24, 2011. Date of publication September 08, 2011; date of current version April 11, 2012. This work was supported in part by the Czech Science Foundation project 102/09/H082; in part by the Research Program No. MSM6840770015 "Research of Methods and Systems for Measurement of Physical Quantities and Measured Data Processing" of the CTU in Prague sponsored by the Ministry of Education, Youth, and Sports of the Czech Republic; and in part by the Grant Agency of the Czech Technical University in Prague under Grant SGS10/288/OHK3/3T/13. The associate editor coordinating the review of this paper and approving it for publication was Prof. Boris Stoeber.

The authors are with the Department of Measurement, Faculty of Electrical Engineering, Czech Technical University in Prague, Technicka 2, 166 27 Prague, Czech Republic (e-mail: siposmar@fel.cvut.cz; pacesp@fel.cvut.cz; xrohac@fel.cvut.cz; petr.novacek@fel.cvut.cz).

Digital Object Identifier 10.1109/JSEN.2011.2167319

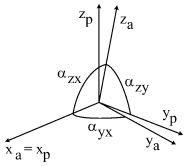

Fig. 1. Orthogonalization of sensor frame; a—nonorthogonal sensor frame; p—orthogonal sensor frame.

been described by Bonnet *et al.* in [15]. He proved that an ellipsoid fitting using either linear optimization (Merayo's algorithm) or nonlinear optimization (Quasi-Newton factorization algorithm) is robust with data sets from static positions obtained within free rotations along a vertical axis in case of accelerometers and free rotations along East-West axis in case of magnetometers.

In Section II, the SEM of triaxial accelerometer is described. We present three algorithms for its calibration in Section III; the Levenberg–Marquardt algorithm, the Thin-Shell algorithm, and an algorithm based on Matlab *fminunc* function. First two algorithms were related to third one, which was used as a reference, in order to have a means for the comparison of algorithms efficiency. In Section IV, we shortly present the most important parameters of calibrated sensors and used measurement setup. To compare a calibration effect on measured and evaluated data based on applied algorithms and SEMs we used a Rotational-Tilt Platform with precise positioning capability to provide precise tilt angles. The experiments, analyses, and result accuracy are provided in Section V.

II. Sensor Error Model

For triaxial accelerometer calibration we considered the sensor error model (SEM), which consisted of nine unknown parameters—three scale factor corrections, three angles of nonorthogonality, and three offsets. The SEM can be defined as (1). Offset forms a stochastic part of biases and can be modeled as a random constant. The time variant part of the bias is drift, which changes based on environmental and other sensor conditions. The calibration process is supposed to be performed during short-time period; therefore, drift can be considered as zero

$$\begin{aligned} a_p &= T_a^p \mathrm{SF}_a (a_m - b_a) \\ &= \begin{pmatrix} 1 & 0 & 0 \\ \alpha_{yx} & 1 & 0 \\ \alpha_{zx} & \alpha_{zy} & 1 \end{pmatrix} \begin{pmatrix} \mathrm{SF}_{ax} & 0 & 0 \\ 0 & \mathrm{SF}_{ay} & 0 \\ 0 & 0 & \mathrm{SF}_{az} \end{pmatrix} \\ &\quad \times \left(\begin{pmatrix} a_{mx} \\ a_{my} \\ a_{mz} \end{pmatrix} - \begin{pmatrix} b_{ax} \\ b_{ay} \\ b_{az} \end{pmatrix} \right) \end{aligned} \tag{1}$$

where $a_p = [a_{px}, a_{py}, a_{pz}]^T$ is the compensated vector of a measured acceleration defined in the orthogonal system (platform frame); T_a^p denotes matrix providing transformation from nonorthogonal frame to orthogonal one with nondiagonal terms $\alpha_{yx}, \alpha_{zx}, \alpha_{zy}$ that correspond to the axes misalignment (nonorthogonality angles) (Fig. 1); SF_a represents a scale factor matrix; $b_a = [b_{ax}, b_{ay}, b_{az}]^T$ is the vector of sensor offsets; $a_m = [a_{mx}, a_{my}, a_{mz}]^T$ denotes the vector of measured accelerations. The SEM and its derivation are described in more detail in [13] and [16].

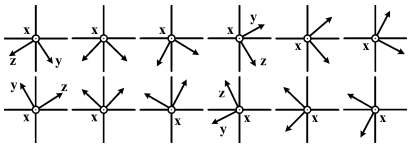

Fig. 2. Positions for calibration; rotation around x axis.

III. Calibration Algorithms

This section briefly describes the algorithms for triaxial accelerometer calibration—Levenberg–Marquardt (LM) algorithm, Thin-Shell (TS) algorithm, and algorithm based on Matlab *fminunc* function. The fundamental principle of the proposed calibration procedure is based on the fact that the magnitude of measured acceleration should be equal to the gravity magnitude, which is ensured by static conditions (2). It corresponds to "scalar field calibration" used in [17]. The proposed procedure uses only general knowledge about the applied quantity, which is in contrast to the case when precise positioning system is available, and thus, the knowledge about precise tilt angle is also provided in all steps of iteration

$$g_x^2 + g_y^2 + g_z^2 = |g|^2 \tag{2}$$

where g_i denotes sensed acceleration in direction of i axis and $|g|$ is the magnitude of gravity vector, ideally equal to $1g$.

To obtain the most accurate estimation without the need of having a precise positioning system, the sensor should be consecutively placed to positions in manner to cover the whole globe surface and the sensor should be influenced only by gravity. In practice, it is not possible to do so, because the number of measurements would be infinite. Therefore, in the proposed procedure, the number of positions is optimized and suggested their orientation, in which a high influence of all errors is expected. Only 36 positions are used, 3 times 12 positions along x, y, z axis. The positions along x axis are shown in Fig. 2. Precise knowledge of their orientations is not required, only 3 positions per quadrant are recommended.

A. Principle of Levenberg–Marquardt Algorithm

The Levenberg–Marquardt (LM) algorithm is one of the most efficient and popular algorithms. It has better convergence than the other ones for nonlinear minimization. The LM algorithm is widely utilized in software applications, neural networks, and curve-fitting problems [18]–[21]. The LM algorithm combines two algorithms: the Gradient Descent (GD) and the Gauss–Newton (GN) algorithm [22]. The LM algorithm can be described by (3)

$$S(\beta) = \sum_{i=1}^{m} [y_i - f(x_i, \beta)]^2 = \sum_{i=1}^{m} q_i(\beta)^2 \tag{3}$$

where $S(\beta)$ denotes the sum of residuals $q_i(\beta)^2$; m is the number of measurements; x_i are measured data; y_i are the reference values, and β is a vector of parameters being estimated

and forming the SEM defined in (1). The LM algorithm is iterative algorithm reducing $S(\beta)$ with respect to the parameters in vector β.

1) Gradient Descent Algorithm: The Gradient Descent (GD) algorithm is a minimization algorithm updating the estimated parameters in the direction opposite to the gradient of the cost function. The GD algorithm is highly convergent and can be used for problems with thousands of parameters forming the cost function. The h_{GD} modifies the GD algorithm step to reduce $S(\beta)$ in the direction of steepest descent and is defined by (4) [22]

$$h_{\mathrm{GD}} = \alpha J^T W(y_i - f(x_i, \beta)) \tag{4}$$

where α is a parameter corresponding to the length of step in the steepest descent direction; J is the Jacobian related to the vector β; W is the weighting diagonal matrix [22].

2) Gauss–Newton Algorithm: A main advantage of Gauss–Newton (GN) algorithm is its rapid convergence; however, it depends on the initial conditions. The GN algorithm does not require the calculation of second-order derivatives [21]. The equation for GN algorithm reducing $S(\beta)$ is given by (5)

$$\lfloor J^T W J \rfloor h_{\mathrm{GN}} = J^T W(y_i - f(x_i, \beta)) \tag{5}$$

where h_{GN} denotes the GN algorithm update of estimated parameter leading to a minimization of $S(\beta)$.

3) Levenberg–Marquardt Algorithm: As was mentioned, the Levenberg–Marquardt (LM) algorithm combines both the GD and GN algorithm. In the LM algorithm, the parameter h_{LM} is adaptively weighted with respect to h_{GD} and h_{GN} to reach optimal progress in $S(\beta)$ minimization, and thus, the LM algorithm equation is given by (6)

$$\lfloor J^T W J + \lambda \operatorname{diag}(J^T W J) \rfloor h_{\mathrm{LM}} = J^T W(y_i - f(x_i, \beta)) \tag{6}$$

where λ is a damping parameter and h_{LM} is the LM algorithm update. The parameter λ has several characteristics [23]:

- for all $\lambda > 0$, the coefficient matrix $(J^T W J + \lambda \operatorname{diag}(J^T W J))$ is positive definite, and this fact ensures that h_{LM} is descent directional;
- for large values of λ the iteration step (parameter modification) is in the steepest descent direction, which is good when the current stage is far from required solution;
- for small values of λ, the $h_{\mathrm{LM}} \cong h_{\mathrm{GN}}$ and it is good for final phases of iteration, when estimated parameters are close to required solution.

In other words, if the iteration step decreases the error, it implies that quadratic assumption $f(x_i)$ is working and λ can be reduced (usually by a factor of 10) to decrease the influence of GD. On the other hand, if $S(\beta)$ increases, λ is increased by the same factor increasing GD influence and the iteration step is repeated.

B. Thin-Shell Algorithm

The Thin-Shell (TS) algorithm is based on an estimation of Linear Minimum Mean Square Error, which is applied on SEM (1) of calibrated sensor. According to (1) nine parameters have to be estimated. The iteration is based on successive halving of intervals, in which the estimated parameter is searched for. The intervals are halved based on a standard deviation defined by (7) and if-conditions related to Fig. 3

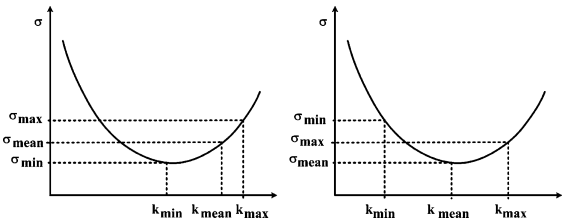

Fig. 3. Criterions for halving the interval, for which the estimated parameters are searched.

$$\sigma = \sqrt{\frac{\sum_{i=1}^{m} \left(\widehat{a}_{xi}^2 + \widehat{a}_{yi}^2 + \widehat{a}_{zi}^2 - |g|^2 \right)^2}{m-1}} \tag{7}$$

where σ is the standard deviation; m is the number of positions; $\widehat{a}_{xi}$, $\widehat{a}_{yi}$, $\widehat{a}_{zi}$ are estimations of compensated measured gravity vector components and $|g|$ is the magnitude of gravity vector corresponding to the reference value.

At the beginning of the algorithm, the minimal and maximal values of each parameter must be set (it defines the interval, in which the unknown parameter is searched for); the mean value is computed as an average of them. Each iteration cycle can be divided into three steps:

1) Min, max, and mean values of the parameter being searched for ($\mathrm{k_{min}}, \mathrm{k_{mean}}$, and $\mathrm{k_{max}}$) are used for the estimation of compensated accelerations in all positions.
2) Three corresponding standard deviations ($\sigma_{\mathrm{min}}, \sigma_{\mathrm{mean}}$, and σ_{max}) are then obtained based on (7). Other parameters are set to their mean values.
3) Based on $\sigma_{\mathrm{min}}, \sigma_{\mathrm{mean}}$, and σ_{max} the interval, in which estimated parameter should be, is halved according to Fig. 3 and following conditions:
   - if $(\sigma_{\mathrm{min}} > \sigma_{\mathrm{mean}})$ and $(\sigma_{\mathrm{max}} > \sigma_{\mathrm{mean}})$, the interval is reduced to a half around the mean value k_{mean}.
   - if $(\sigma_{\mathrm{min}} < \sigma_{\mathrm{mean}})$ and $(\sigma_{\mathrm{mean}} < \sigma_{\mathrm{max}})$ the true value of the parameter should be in the interval $(k_{\mathrm{min}}, k_{\mathrm{mean}})$; for the following iteration cycle $k_{\mathrm{max}} = k_{\mathrm{mean}}$ and k_{mean} is computed as a mean value of k_{min} and new k_{max}.
   - if $(\sigma_{\mathrm{max}} < \sigma_{\mathrm{mean}})$ and $(\sigma_{\mathrm{mean}} < \sigma_{\mathrm{min}})$ the true value of the parameter should be in the interval $(k_{\mathrm{mean}}, k_{\mathrm{max}})$; for the following iteration cycle $k_{\mathrm{min}} = k_{\mathrm{mean}}$ and k_{mean} is computed as a mean value of new k_{min} and k_{max}.

The steps described above are repeated until the computed standard deviation is less than the required value or required number of iteration cycles is reached. Consequently the rest of the parameters are estimated in the same manner. The final value of standard deviation defines the calibration algorithm accuracy. This algorithm is described in more detail in [24].

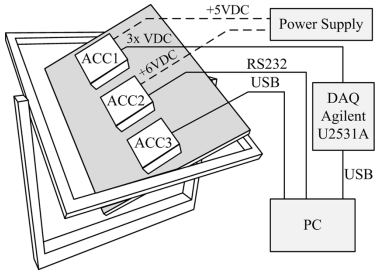

Fig. 4. Measurement setup for triaxial accelerometer calibration; ACC1—CXL02LF3; ACC2—AHRS M3; ACC3—ADIS16405.

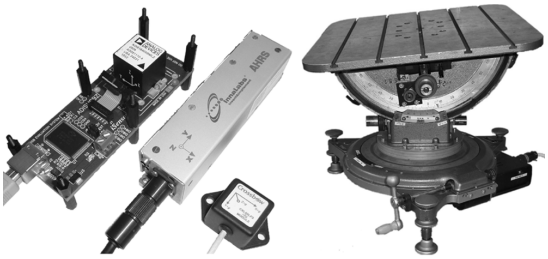

(a) (b)

Fig. 5. (a) Calibrated systems (from left): ADIS16405; AHRS M3; CXL02LF3; (b) Rotational-tilt platform.

C. Algorithm Based on Fminunc Matlab Function

To evaluate the efficiency of Levenberg–Marquardt (LM) and Thin-Shell (TS) algorithms with respect to minimum required number of iterations and reached accuracy Matlab functions *fminunc, lsqnonlin*, and *fminsearch* were tested. Based on their performances the function *fminunc* was chosen as a reference and a means for LM and TS algorithm evaluation. Function *fminunc* is based on quasi-Newton minimization with numerical gradients [25]. Its description is not the subject of this paper and can be found [26].

IV. Calibrated Sensors and Measurement Setup

In this section, we briefly present the systems used for the calibration and measurement setup (Fig. 4) which uses a simple platform enabling to measure accelerometer data in the static positions defined approximately as shown in Fig. 2. Furthermore, we used a Rotational-Tilt Platform (RoTiP), see Fig. 5(b), as a reference for analyses needed to verify the results of the proposed calibration procedure according to applied algorithms. The RoTiP parameters are shown in Table I. Although we evaluated five sensors in sum, such as AHRS M3's accelerometer (Innalabs [27]), ADIS16405's accelerometer (Analog Devices [28]), CXL02LF3 accelerometer (Crossbow [29]), 3DM-GX2's accelerometer (MicroStrain [30]), and STEVAL-MKI062V2's accelerometer (STMicroelectronics [31]), we present the results of analyses only from first three accelerometers of calibrated systems [see Fig. 5(a)]. The analyses of last two sensors were very similar.

TABLE I
Parameters of Rotational-Tilt Platform

Parameter	Range	Speed of Motion	Resolution
Pitch	±45 deg	±42 deg/s	0.00033 deg
Roll	±25 deg	±60 deg/s	0.00065 deg
Heading	0 to 360 deg	±310 deg/s	0.00074 deg

V. Calibration Analyses

Three aforementioned algorithms were used to estimate SEMs of three triaxial accelerometers described in Section IV according to measured data in suggested positions. It helped to decrease the influence of manufacturing imperfection on the sensor precision. As said in [32] other problematic errors can show up with incorrect determination of sensor error parameters; therefore, for results, a comparison Root Mean Square Error (RMSE) defined by (8) was used

$$\mathrm{RMSE}(p,g) = \sqrt{\frac{\sum_{i=1}^{n}(x_i - g)^2}{n}} \qquad x_i = \sqrt{g_{xi}^2 + g_{yi}^2 + g_{zi}^2} \tag{8}$$

where $p = (x_1, \ldots, x_n)^T$ is n-dimensional vector; n—number of evaluated positions; g is an ideal magnitude of the gravity vector equal to $1g$; g_{xi}, g_{yi}, g_{zi} are components of the estimated gravity vector.

For the calibration purposes and consecutive analyses we measured the raw data from sensors and evaluated data in 364 positions. The number was chosen with respect to the number of suggested positions in Section III multiplied by 10 and modified to have uniformly spaced data along all axes. The analyses included the observation of estimated parameters of SEM with respect to algorithms applied, the RMSE dependence on the number of taken positions and the number of iterations, and the observation of a long-period permutation of estimated SEMs. Furthermore, the calibration effect on the precision of evaluated tilt angles and the calibration effect from the sensors' drift point of view were performed.

A. Sensor Error Models

We estimated Sensor Errors Models (SEMs) of three accelerometers. Results are listed for LM and TS algorithms in Table II. Although we estimated the SEMs using three algorithms, only LM and TS algorithms' results are listed due to the fact that the results estimated by LM algorithm were identical to the ones from algorithm based on *fminunc* function. From Table II, it can be seen that SEMs estimated by LM and TS algorithms are comparable for all tested units, which also proves the values of RMSE. The effect of SEM applying on measured data is shown in Fig. 6, where magnitude of compensated acceleration vector has approximately 100 times smaller deviation from $1g$ than the one before calibration.

B. Dependence of RMSE on Evaluated Data Positions

To prove that only 36 static positions are sufficient for the calibration purposes, we measured 364 positions uniformly spaced, and analyzed the variation of RMSE for the different number of

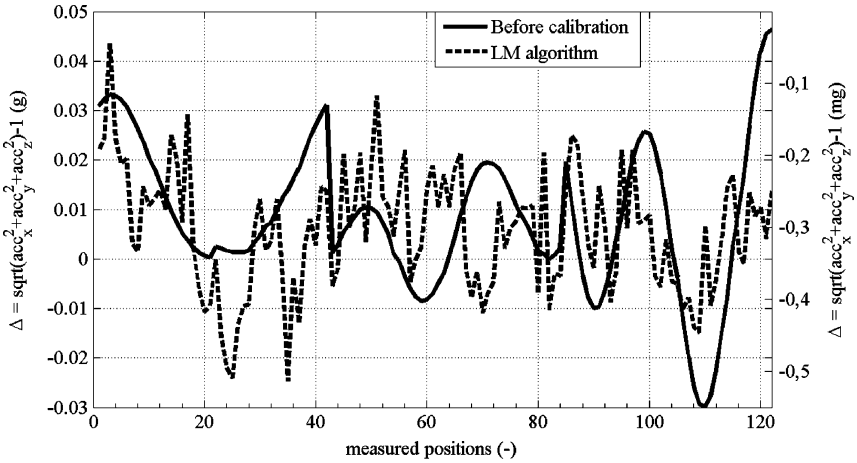

Fig. 6. Dependence of deviations of measured accelerations before (left vertical axis) and after (right vertical axis) calibration using LM algorithm applied on AHRS M3's accelerometer data in evaluated different positions.

TABLE II
SENSOR ERROR MODELS OBTAINED USING LEVENBERG–MARQUARDT (LM) AND THIN-SHELL (TS) ALGORITHM FOR ACCELEROMETERS OF AHRS M3'S (AHRS) AND ADIS16405'S (ADIS) AND CXL02LF3 (CXL) ACCELEROMETER

Par	LM AHRS	LM ADIS	LM CXL	TS AHRS	TS ADIS	TS CXL
α_{yx} (deg)	-0.8758	-0.0230	1.0237	-0.8760	-0.0227	1.0235
α_{zx} (deg)	3.0286	0.0351	-0.5217	3.0229	0.0350	-0.4476
α_{zy} (deg)	0.1765	-0.1639	-1.4939	0.1784	-0.1639	-1.4829
SF_{ax} (-)	0.99865	0.99956	1.05591	0.99866	0.99957	1.05664
SF_{ay} (-)	0.98946	1.00194	1.06517	0.98946	1.00194	1.06508
SF_{az} (-)	0.98611	0.99828	1.06144	0.98608	0.99828	1.06128
b_{ax} (g)	0.00173	-0.01354	-0.00255	0.00172	-0.01353	-0.00272
b_{ay} (g)	-0.00602	-0.00671	-0.03445	-0.00598	-0.00678	-0.03675
b_{az} (g)	0.01440	-0.00402	0.03690	0.01427	-0.00400	0.04003
RMSE [1]	0.01810	0.00948	0.06628	0.01810	0.00948	0.06628
RMSE [2]	0.00015	0.00252	0.01527	0.00017	0.00252	0.01545

Superscript 1 denotes RMSE before calibration and 2 after calibration.

positions (NoP) in intervals from 12 to 364. NoP can be seen in Table III, where N represents the relationship between Figs. 7–9 horizontal axes and the NoP used for calculation. In each static position, an average of 100 measured data samples was calculated to reduce noise. The dependence between RMSE defined in (8) and NoP is shown in Fig. 7 for AHRS M3, in Fig. 8 for ADIS16405, and in Fig. 9 for CXL02LF3. The RMSE was evaluated between an ideal magnitude of gravity vector and the magnitude of compensated measured gravity. The compensated measured gravity obtained from the measured data multiplication with SEM is further notified as a compensated result. The left vertical axes of Figs. 7–9 correspond to RMSE before calibration and right vertical axes correspond to RMSE after calibration. As a criterion for the evaluation of RMSE dependence on the number of evaluated positions we considered a maximum deviation of RMSE from RMSE in $\mathrm{N} = 1$ position to be equal or less than 1 mg, which corresponds to sensor resolutions. From Figs. 7–9 it can be seen, that 21 positions and more satisfy desired limitation no matter which algorithm was used. This means that the variation of the compensated results in the case of usage

TABLE III
RELATIONSHIP BETWEEN THE NUMBER OF EVALUATED POSITIONS (NOP) AND NOTATION OF FIGS. 7–9 HORIZONTAL AXES (N)

N	NoP	N	NoP	N	NoP	N	NoP	N	NoP
1	364	7	52	13	28	19	20	25	14
2	182	8	46	14	26	20	19	26	13
3	122	9	41	15	25	21	18	27	12
4	91	10	36	16	23	22	17		
5	73	11	34	17	22	23	16		
6	61	12	31	18	21	24	15		

21 positions or more (up to 364) differs under the required value; therefore, further differences are considered as negligible. Because having 7 positions in 360 deg and also in 4 quadrants does not have a uniform distribution with a constant number of positions per quadrant, it is suitable to increase the number to 12. This leads to having 36 positions covering all axes, which was the number we used in Section III-A. The result optimizes the number of positions needed for the calibration with respect to a workload and precision.

C. Dependence of RMSE on Number of Iterations

Based on the data measured in 36 positions as described in Section III and proven in Section V-B, we analyzed the dependency of RMSE calculated between compensated results and an ideal gravity vector on the number of iterations for LM and TS algorithms. The iteration denotes a calibration cycle, in which all measured data (in our case in 36 positions) are used for an unknown SEM parameter estimation. This analysis relied on the progress of RMSE with respect to the number of iteration. When the deviation from the steady-state value was less than 1 mg we considered the accuracy of calibration to be sufficient. Fig. 10 shows the RMSE dependency on number of iterations for TS algorithm applied on AHRS M3 accelerometer. The comparison between LM and TS algorithms from the number of iterations point of view is presented in Table IV.

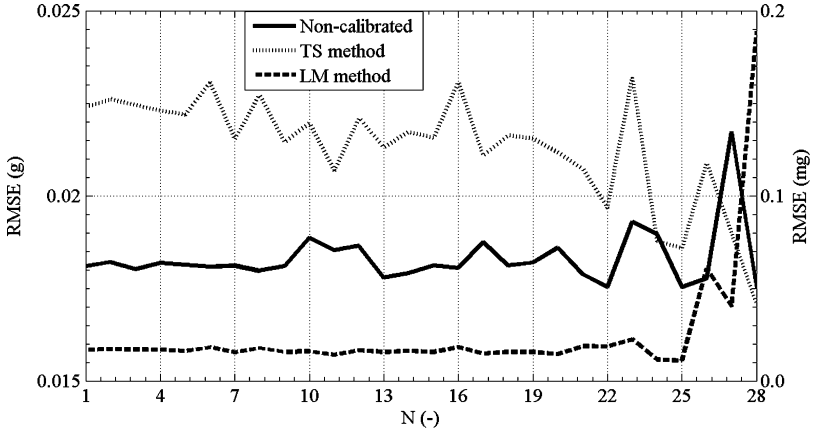

Fig. 7. Dependence of RMSE before (left axis) and after (right axis) calibration on the number of positions using AHRS M3's accelerometer.

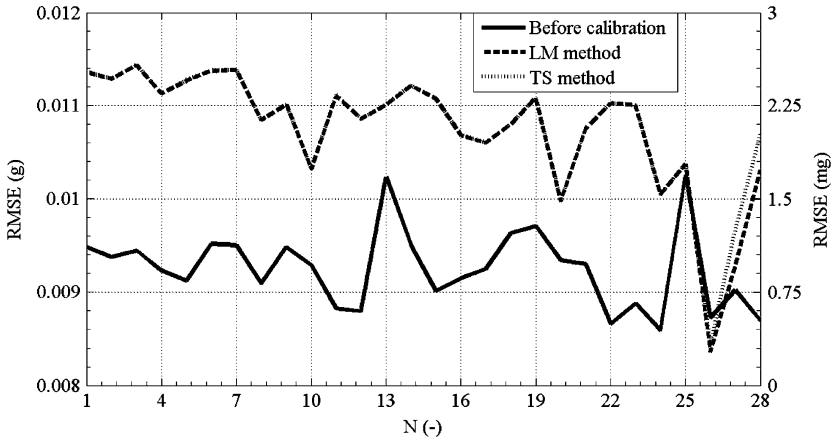

Fig. 8. Dependence of RMSE before (left axis) and after (right axis) calibration on the number of positions using ADIS16405's accelerometer.

D. Comparison of SEM During Time Period

We analyzed the variation of SEMs obtained by LM and TS algorithms during a longer time period corresponding to one and half years (the first measurement was taken in April 2009 and the second one was taken in November 2010). We measured 122 positions in both cases with different distributions as shown in Fig. 11. We analyzed the SEMs permutation and their accuracy. The SEMs evaluated based on two data sets using LM and TS calibration algorithms are presented in Table V. In each position the average of 100 data samples was used as in previous analyses.

From Table V it can be seen that parameters are slightly different, which we think was caused by reaching the resolution of the method applied. The influence of different distribution of evaluated positions shown in Fig. 11 is considered as negligible, because the number of evaluated positions was always higher than 21.

E. Comparison of Tilt Angles Before and After Calibration

To see the effect of calibration, we performed another analysis in which the tilt angles estimated based on calibration results were compared to the reference ones measured by Rotational-Tilt Platform (RoTiP).

We mounted the accelerometers on RoTiP and tilted them along two axes. A tilt corresponded to pitch (θ) and roll (ϕ) angles. Specification of RoTiP is listed in Section IV. The pitch angle calculation is defined as (9) and roll angle calculation as (10)

$$\theta = \operatorname{arctg}\left(-f_{by} \Big/ \sqrt{f_{bx}^2 + f_{bz}^2}\right) \tag{9}$$

$$\phi = \operatorname{arctg}(f_{bx}/-f_{bz}) \tag{10}$$

where θ is the pitch angle; ϕ is the roll angle; f_{bx}, f_{by}, f_{bz} are measured accelerations. For computation of *arctg* function, the Matlab function *atan2*, which returns the four-quadrant invert tangent (arctangent) of real parts x and y. [2], was used.

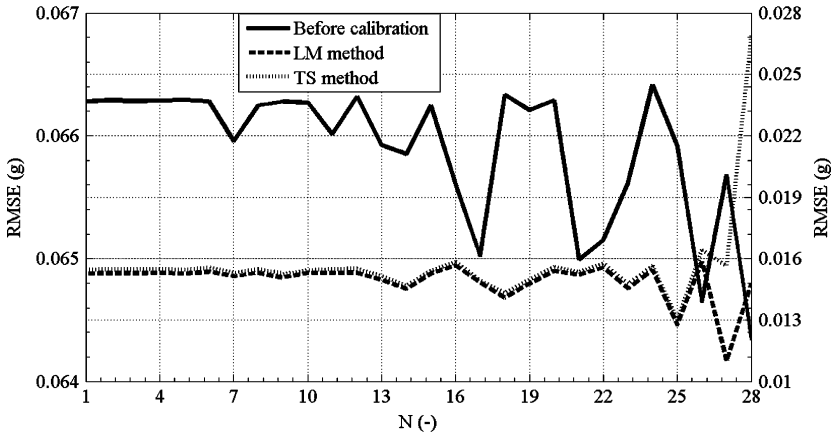

Fig. 9. Dependence of RMSE before (left axis) and after (right axis) calibration on the number of positions using CXL02LF3 accelerometer.

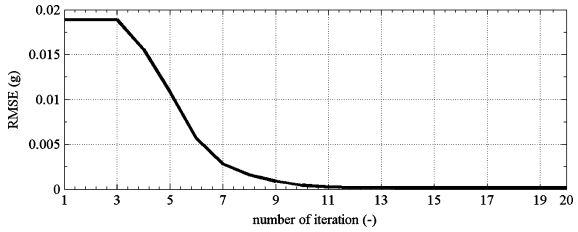

Fig. 10. Dependence of RMSE on the number of iterations for AHRS M3's accelerometer using TS calibration algorithm.

TABLE IV
NUMBER OF ITERATIONS FOR LM AND TS CALIBRATION ALGORITHMS

	AHRS M3	ADIS16405	CXL02LF3
LM Algorithm	2	1	1
TS Algorithm	9	7	6

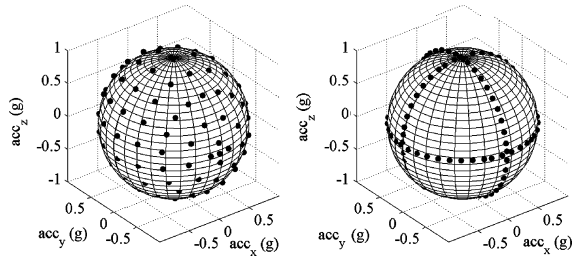

Fig. 11. Evaluated positions in April 2009 (left) and in November 2010 (right).

We analyzed the variation of results when LM and TS algorithms had been applied. The last column of Tables VI–VIII (AHRS M3, ADIS16405, CXL02LF3) describes an Error Percentage Improvement (EPI) which corresponds to the difference between particular deviations (relative errors) related to the maximum angle, i.e., 20 deg. From these tables it can be seen that due to the calibration the tilt angles are more accurate than

TABLE V
SENSOR ERROR MODELS OBTAINED USING LM ALGORITHM (LM) AND TS ALGORITHM (TS) DURING TIME INTERVAL OF ONE AND HALF YEARS FOR ACCELEROMETER CONTAINED IN AHRS M3

Parameter	LM Apr 2009	LM Nov 2010	TS Apr 2009	TS Nov 2010
α_{yx} (deg)	-0.8769	-0.8758	-0.8830	-0.8760
α_{zx} (deg)	3.0261	3.0286	3.0253	3.0229
α_{zy} (deg)	0.1794	0.1765	0.1818	0.1784
SF_{ax} (-)	0.99868	0.99865	0.99902	0.99866
SF_{ay} (-)	0.98951	0.98946	0.98828	0.98946
SF_{az} (-)	0.98609	0.98611	0.98640	0.98608
b_{ax} (g)	0.00153	0.00173	0.00156	0.00172
b_{ay} (g)	-0.00541	-0.00602	-0.00527	-0.00598
b_{az} (g)	0.01461	0.01440	0.01448	0.01427
RMSE [1]	0.01957	0.01810	0.01957	0.01810
RMSE [2]	0.00014	0.00015	0.00055	0.00017

Superscript 1 denotes RMSE before calibration and 2 after calibration.

TABLE VI
COMPARISON OF TILT ANGLES BEFORE AND AFTER CALIBRATION USING LM AND TS ALGORITHMS FOR AHRS M3; θ—PITCH, ϕ—ROLL

Reference Angle θ; ϕ (deg)	Without Calibration θ; ϕ (deg)	LM Algorithm θ; ϕ (deg)	TS Algorithm θ; ϕ (deg)	LM EPI θ; ϕ (%)
0; 0	-0.77; -0.59	-0.70; -0.30	-0.68; -0.26	0.4; 1.5
10; 0	9.18; -0.62	9.61; -0.16	9.62; -0.12	2.2; 2.3
20; 0	19.18; -0.63	20.13; 0.01	20.14; 0.05	3.4; 3.1
0; -10	-0.96; -10.83	-0.90; -10.72	-0.89; -10.69	0.3; 0.6
0; -20	-0.83; -21.10	-0.76; -21.00	-0.75; -21.06	0.4; 0.5
10; -10	9.31; -10.98	9.76; -10.82	9.77; -10.79	2.3; 0.8
20; -20	19.00; -19.62	19.98; -19.76	19.99; -19.72	4.9; 0.7

in case without calibration for all tested sensors and tilt angles.

F. Position Determination With and Without Calibration

Furthermore, we analyzed the drift influence on the accuracy of position determination when a compensated model was used. The accelerations were measured for 200 s in a static position with different tilt angles and then two times integrated to get the position. The effect of compensation applied on an

TABLE VII
COMPARISON OF TILT ANGLES BEFORE AND AFTER CALIBRATION USING LM AND TS ALGORITHMS FOR ADIS16405; θ—PITCH, ϕ—ROLL

Reference Angle θ; ϕ (deg)	Without Calibration θ; ϕ (deg)	LM Algorithm θ; ϕ (deg)	TS Algorithm θ; ϕ (deg)	LM EPI θ; ϕ (%)
0; 0	0.85; -0.29	0.07; 0.10	0.07; 0.10	3.9; 1.0
10; 0	10.80; -0.46	10.09; -0.07	10.09; -0.07	3.6; 2
20; 0	20.66; -0.36	20.04; 0.05	20.04; 0.05	3.1; 1.6
0; -10	1.11; -10.51	0.34; -10.22	0.34; -10.22	3.9; 1.5
0; -20	1.07; -20.35	0.31; -20.15	0.31; -20.15	3.8; 1.5
10; -10	10.92; -10.51	10.23; -10.20	10.23; -10.20	3.5; 1.0
20; -20	20.73; -20.21	20.16; -19.99	20.16; -19.97	2.9; 1.0

TABLE VIII
COMPARISON OF TILT ANGLES BEFORE AND AFTER CALIBRATION USING LM AND TS ALGORITHMS FOR CXL02LF3; θ—PITCH, ϕ—ROLL

Reference Angle θ; ϕ (deg)	Without Calibration θ; ϕ (deg)	LM Algorithm θ; ϕ (deg)	TS Algorithm θ; ϕ (deg)	LM EPI θ; ϕ (%)
0; 0	4.69; -3.84	-0.43; -0.92	-0.37; -0.75	21.3; 14.6
10; 0	13.48; -3.76	10.71; 0.29	10.54; 0.24	13.9; 17.4
20; 0	21.37; -3.78	20.47; 0.15	20.47; 0.09	4.6; 18.2
0; -10	4.56; -13.25	0.90; 10.37	0.71; -10.31	18.3; 9.4
0; -20	4.63; -22.52	0.94; -20.30	0.74; -20.24	18.5; 11.1
10; -10	13.67; -13.30	10.25; -10.92	10.19; -10.73	17.1; 11.9
20; -20	22.12; -22.37	18.82; -20.75	18.76; -20.54	4.9; 8.2

TABLE IX
POSITION DETERMINATION IN PLATFORM FRAME BEFORE AND AFTER CALIBRATION USING SEMS GOT FROM LM AND TS ALGORITHMS FOR AHRS M3'S ACCELEROMETER; δ_X, δ_Y, δ_Z—DEVIATIONS IN X, Y, Z AXES

Reference Angle θ; ϕ (deg)	Without Calibration δ_X; δ_Y; δ_Z (m)	LM Algorithm δ_X, δ_Y, δ_Z (m)	TS Algorithm δ_X, δ_Y, δ_Z (m)
0; 0	-239; -56; 5867	7; 2; -160	5; 9; -160
10; 0	-1516; -36; 7224	27; 1; -116	22; 9; -117
20; 0	-3105; 51; 7987	20; -30; -50	10; -22;- 54
0; -10	-350; -1078; 6061	-121; 40; -88	-123; 44; -87
0; -20	-721; -2116; 5921	-508; 85; -67	-507; 84; -67
10; -10	-2299; -635; 7555	-674; 828; -30	-680; 832; -31
20; -20	-7555; 1618; 7981	-4553; 5026; 64	-4561; 5025; 22

TABLE X
POSITION DETERMINATION IN PLATFORM FRAME BEFORE AND AFTER CALIBRATION USING SEMS GOT FROM LM AND TS ALGORITHMS FOR ADIS16405'S ACCELEROMETER; δ_X, δ_Y, δ_Z—DEVIATIONS IN X, Y, Z AXES

Reference Angle θ; ϕ (deg)	Without Calibration δ_X; δ_Y; δ_Z (m)	LM Algorithm δ_X, δ_Y, δ_Z (m)	TS Algorithm δ_X, δ_Y, δ_Z (m)
0; 0	-679; -107; -1825	-30; -1; 136	-27; -4; 135
10; 0	-420; 66; -2403	93; 62; 222	95; 60; 222
20; 0	-2366; 93; -6110	-1157; -70; -3050	-1156; -72; 3051
0; -10	-171; 296; 1618	-44; 156; 821	-42; 153; 821
0; -20	-693; -1492; -4065	-328; -497; -1447	-327; -501; -1423
10; -10	-1629; -548; -2659	-933; 1005; 193	-931; 1002; 194
20; -20	-8276; -1733; -2077	-7422; 6714; -1015	-7120; 6710; -1015

AHRS M3's accelerometer, ADIS16405's accelerometer, and CXL02LF3 can be seen in Tables IX–XI.

Results from Tables IX–XI show that, in most cases, the deviations in position decreased due to the calibration. The deviations in position can be partially caused by imprecise alignment of the compensated sensor frame with respect to the platform frame which lies along main axes of the moving object. Due to imprecise sensor-platform, the alignment measured acceleration deviates from the true one and causes a deviation in position as well. This can be reduced by a successive alignment procedure which was not the subject of this analysis.

TABLE XI
POSITION DETERMINATION IN PLATFORM FRAME BEFORE AND AFTER CALIBRATION USING SEMS GOT FROM LM AND TS ALGORITHMS FOR CXL02LF3 ACCELEROMETER; δ_X, δ_Y, δ_Z—DEVIATIONS IN X, Y, Z AXES

Reference Angle θ; ϕ (deg)	Without Calibration δ_X; δ_Y; δ_Z (m)	LM Algorithm δ_X, δ_Y, δ_Z (m)	TS Algorithm δ_X, δ_Y, δ_Z (m)
0; 0	-2951; -339; -586	1668; -169; 15	1683; -190; 40
10; 0	-5867; -3609; -804	-3487; -3541; 32	-3628; -3561; 44
20; 0	-8388; -6863; -794	-6479; -6863; 162	-6534; -6824; 179
0; -10	-6187; 2908; -796	-3224; 3226; 103	-3773; 3198; 164
0; -20	-9345; 5971; 942	-6485; 5481; 210	-7059; -6455; 153
10; -10	-9140; -393; -1022	-1585; -158; 136	-1265; -184; 305
20; -20	-14242; -547; -1202	-1314; -182; 336	-1273; -205; 610

VI. CONCLUSION

The main aim of this paper was to prove the effectiveness of the calibration approach, which does not need to use precise positioning devices and thus is not expensive and time-consuming. These characteristics are the main benefits of the proposed approach. Based on Levenberg–Marquardt (LM) and Thin-Shell (TS) algorithms we evaluated sensor error models (SEMs) for accelerometers of AHRS M3, ADIS16405, CXL02LF3 units and compared them with ones obtained from a Matlab *fminunc* function, which was used as a reference. We provided various analyses to show different aspects of the calibration such as reached values of SEM when LM or TS algorithm was applied, how many taken positions had to be used and how many iterations had to be performed to reach the required precision, or how greatly SEMs changed when they were compared with long-period perspectives. In all cases, the calibration had significant effect on results, e.g., according to Fig. 6 they were approx. 100 times improved. All results proved the suitability of the proposed calibration approach.

REFERENCES

[1] D. Jurman, M. Jankovec, R. Kamnik, and M. Topic, "Calibration and data fusion solution for the miniature attitude and heading reference system," *Sens. Actuators A, Phys.*, vol. 138, no. 2, pp. 411–420, Aug. 2007.

[2] M. Soták, "Coarse alignment algorithm for ADIS16405," *Przegląd elektrotechniczny*, vol. 86, no. 9, pp. 247–251, 2010.

[3] M. Sipos, P. Paces, M. Reinstein, and J. Rohac, "Flight attitude track reconstruction using two AHRS units under laboratory conditions," in *Proc. IEEE Sensors*, Nov. 2009, vol. 1–3, pp. 630–633.

[4] M. Reinstein, J. Rohac, and M. Sipos, "Algorithms for heading determination using inertial sensors," *Przeglad Elektrotechniczny*, vol. 86, no. 9, pp. 243–246, 2010.

[5] N. Barbour and G. Schmidt, "Inertial sensor technology trends," *IEEE Sensors J.*, vol. 1, no. 4, pp. 332–339, Dec. 2001.

[6] J. Včelák, P. Ripka, J. Kubik, A. Platil, and P. Kašpar:, "AMR navigation systems and methods of their calibration," *Sens. Actuators A, Phys.*, vol. 123–124, pp. 122–128, 2005.

[7] Z. Syed, P. Aggarwal, C. Goodall, X. Niu, and N. El-Sheimy, "A new multi-position calibration method for MEMS inertial navigation systems," *Meas., Sci., Technol.*, vol. 18, no. 7, pp. 1897–1907, Jun. 2007.

[8] S. P. Won and F. Golnaraghi, "A triaxial accelerometer calibration method using a mathematical model," *IEEE Trans. Instrum. Meas.*, vol. 59, no. 8, pp. 2144–2153, Aug. 2010.
[9] S. Luczak, W. Oleksiuk, and M. Bodnicki, "Sensing tilt with MEMS accelerometers," *IEEE Sensors J.*, vol. 6, no. 6, pp. 1669–1675, Dec. 2006.
[10] A. Kim and M. F. Golnaraghi, "Initial calibration of an inertial measurement unit using optical position tracking system," in *Proc. PLANS 2004: Position Location and Navigation Symp.*, 2007, pp. 96–101.
[11] D. H. Titterton and J. L. Weston, *Strapdown Inertial Navigation Technology*. London, U.K.: Peter Peregrinis, 1997, p. 238.
[12] V. Petrucha, P. Kaspar, P. Ripka, and J. M. G. Merayo, "Automated system for the calibration of magnetometers," *J. Appl. Phys.*, vol. 105, no. 7, 2009.
[13] I. Skog and P. Händel, "Calibration of a MEMS inertial measurement unit," presented at the XVII IMEKO World Congr., Rio de Janeiro, Brazil, 2006.
[14] T. Pylvanainen, "Automatic and adaptive calibration of 3D field sensors," *Appl. Math. Model.*, vol. 32, no. 4, pp. 575–587, Apr. 2008.
[15] S. Bonnet, C. Bassompierre, C. Godin, S. Lesecq, and A. Barraud, "Calibration methods for inertial and magnetic sensors," *Sens. Actuators A, Phys.*, vol. 156, no. 2, pp. 302–311, Dec. 2009.
[16] M. Reinstein, M. Sipos, and J. Rohac, "Error analyses of attitude and heading reference systems," *Przeglad Elektrotechniczny*, vol. 85, no. 8, pp. 114–118, 2009.
[17] J. Včelák, V. Petrucha, and P. Kašpar, "Electronic compass with miniature fluxgate sensors," *Sensor Lett.*, vol. 5, no. 1, pp. 279–282, 2007.
[18] B. M. Wilamowski and H. Yu, "Improved computation for Levenberg & Marquardt training," *IEEE Trans. Neural Netw.*, vol. 21, no. 6, pp. 930–937, Jun., 2010.
[19] L. S. H. Ngia and J. Sjoberg, "Efficient training of neural nets for nonlinear adaptive filtering using a recursive Levenberg–Marquardt algorithm," *IEEE Trans. Signal Process.*, vol. 48, no. 7, pp. 1915–1927, Jul. 2000.
[20] A. Ranganathan, The Levenberg–Marquardt Algorithm. Atlanta, GA, College of Computing, Georgia Inst. Technol., 2004.
[21] L. M. Saini and M. K. Soni, "Artificial neural network based peak load forecasting using Levenberg–Marquardt and quasi-Newton methods," *Proc. IEEE Proc.*, vol. 149, no. 5, pp. 578–584, 2002, Generation, Transmission and Distribution.
[22] H. Gavin, "The Levenberg–Marquardt method for nonlinear least squares curve-fitting problems," Dept. Civil and Environmental Engineering, Duke Univ. Durham, NC, 2011.
[23] K. Madsen, H. B. Nielsen, and O. Tingleff, *Methods for Non-Linear Least Squares Problems*, 2nd ed. Lyngby, Denmark: Tech. Univ. Denmark, 2004, Informatics and Mathematical Modelling.
[24] M. Soták, M. Sopata, R. Bréda, J. Roháč, and L. Váci, Navigation System Integration, Košice: Robert Breda. Kosice, Slovak Republic, 2006.
[25] E. L. Renk, W. Collins, M. Rizzo, F. Lee, and D. S. Bernstein, "Calibrating a triaxial accelerometer-magnetometer—Using robotic actuation for sensor reorientation during data collection," *IEEE Control Syst. Mag.*, vol. 25, no. 6, pp. 86–95, Jun. 2005.
[26] Find Minimum of Unconstrained Multivariable Function—MATLAB [Online]. Available: http://www.mathworks.com/help/toolbox/optim/ug/fminunc.html [Accessed: 29-Apr-2011].
[27] Attitude and Heading Reference System, Innalabs AHRS M3, Datasheet [Online]. Available: http://www.galaxynav.com/AHRS_M3_datasheet_2008.10.08.pdf [Accessed: 29-Apr-2011].
[28] ADIS16405 | High Precision Tri-Axis Gyroscope, Accelerometer, Magnetometer | Inertial Sensors | Sensors | Analog Devices [Online]. Available: http://www.analog.com/en/sensors/inertial-sensors/adis16405/products/product.html [Accessed: 24-Apr-2011].
[29] Crossbow Accelerometers, High Sensitivity, LF Series [Online]. Available: http://www.datasheetarchive.com/cxl-datasheet.html [Accessed: 29-Apr-2011].
[30] MicroStrain: Inertial Systems—3DM-GX2® [Online]. Available: http://www.microstrain.com/3dm-gx2.aspx [Accessed: 29-Apr-2011].
[31] STEVAL-MKI062V2—STMicroelectronics [Online]. Available: http://www.st.com/internet/evalboard/product/250367.jsp [Accessed: 29-Apr-2011].
[32] J. Vcelak, P. Ripka, A. Platil, J. Kubik, and P. Kaspar, "Errors of AMR compass and methods of their compensation," *Sens. Actuators A, Phys.*, vol. 129, no. 1–2, pp. 53–57, 2006.

Martin Šipoš was born in Prague, Czech Republic, in 1983. He received the Engineering degree (M.Sc. equivalent) with a specialization in aeronautical instrumentation systems from the Department of Measurement, Faculty of Electrical Engineering, Czech Technical University, Prague, in 2008, where he is currently pursuing the Ph.D. degree in the Laboratory of Aeronautical Information Systems with a dissertation titled "Improvement of INS accuracy using alternative sensors."

His main research activity is INS, GPS, Earth's magnetic field navigation, and adaptive filtering.

Pavel Pačes (M'09) was born in Prague, Czech Republic, in 1978. He received the M.Sc. degree in aerospace engineering from the Faculty of Electrical Engineering, Czech Technical University, Prague, in 2005, and the Ph.D. degree from the air traffic control program with two patent applications in 2011.

He gained industrial experience as a programmer and tester of avionics instruments at DevCom, as an HW and SW developer for the Aircraft Research Institute of the Czech Republic, etc.

Dr. Pačes is member of the IEEE Aerospace and Electronic Systems Society and the American Institute of Aeronautics and Astronautics. Currently, he is a National Point of Contact for the Space Generation Advisory Council in support of the United Nations Program on Space Applications.

Jan Roháč received the Ing. degree (M.Sc. equivalent) and the Ph.D. degree from the Faculty of Electrical Engineering (FEE), Czech Technical University (CTU), Prague, Czech Republic, in 2000 and 2005, respectively.

He is an Assistant Professor and Researcher with the Department of Measurement, FEE, CTU. He teaches courses concerning aircraft and space systems. His main research interests are in avionics, space technologies, inertial navigation systems, GNSS, AOCS, sensors and their modeling, and data processing methods.

Dr. Roháč is a member of the Czech Aeronautical Society and one of the representatives of the CTU in the PEGASUS Network.

Petr Nováček was born in 1983 in Prague, Czech Republic. He received an Ing. degree (M.Sc. equivalent) with a specialization in aeronautical instrumentation systems from the Department of Measurement, Faculty of Electrical Engineering (FEE) Czech Technical University (CTU), Prague, in January 2010. He is currently pursuing the Ph.D. degree under Prof. P. Ripka at the FEE, CTU.

His research interests include sensors (magnetometers and accelerometers), electronics of sensors, digital signal processing, and microcontroller design for low-cost precise navigation systems.

5.2.2 Improvement of Electronic Compass Accuracy Based on Magnetometer and Accelerometer Calibration

An additional sensor, which can be used for search head navigation is a magnetometer. The published paper (Sipos, Rohac & Novacek 2012*a*) addresses sensor calibration and its use for low cost Electronic Compass output precision improvement. The calibration presented in the paper is also suitable for inexpensive IMU. Such an IMU is also used for the estimation of the search head position of the metal detector. Two parts of the work presented is generally usable: Sensor error model and calibration procedure. The error model is similarly based (Sipos et al. 2011) as a Thin-Shell calibration procedure; as the result of calibration, low cost sensors precision is improved fivefold.

Vol. **121** (2012) *ACTA PHYSICA POLONICA A* No. 4

Proceedings of the the Tenth Symposium of Magnetic Measurements, Warsaw, 17–19.10.2011

Improvement of Electronic Compass Accuracy Based on Magnetometer and Accelerometer Calibration

M. Šipoš*, J. Roháč, P. Nováček
Czech Technical University in Prague, Faculty of Electrical Engineering, Department of Measurement
Technická 2, 166 27, Prague, Czech Republic

This paper describes the process used for an electronic compass compensation according to accelerometer based tilt evaluation. Tilt angles have to be estimated first for sensed magnetic vector components to be aligned and horizontal components evaluated. Therefore the precision of accelerometer based tilt angles plays a key role in this whole process as well as the magnetometer characteristics. Hence accelerometers plus magnetometers have to be calibrated to improve the accuracy of a tilt and an azimuth angle evaluation. The calibration uses Thin-Shell method to determine sensor error models. Both the effect of calibration and precision of estimated error models have been observed and are presented. The electronic compass consisted of tri-axial magnetometer and tri-axial accelerometer contained in the Inertial Measurement Unit ADIS16405 from Analog Devices manufacturer.

PACS: 85.75.Ss, 91.10.–v, 06.20.fb, 91.25.–r, 07.07.Df

1. Introduction

Since 1500 years ago, the mechanical compasses have been used for an azimuth determination and a guidance using Earth magnetic field. Due to the technology development and improvement, current electronic compasses (ECs) have much better parameters which are, of course, influenced by sensor type applied. The most simple low accuracy compasses use Hall sensors. In contrast, more accurate ones use Anisotropic Magneto Resistors (AMR) and the most accurate compasses use the fluxgate sensors [1]. The final accuracy of EC depends not only on used magnetic sensors, but also on tilt sensors, which have to be utilized to mathematically align magnetic sensors (compasses with tilt compensation) into the local navigation frame. Characteristics of tilt sensors also affect the EC accuracy, and therefore they have to be calibrated, which eliminates the sensors imperfections [2]. For low-cost sensors like MEMS (Micro-Electro-Mechanical System) based ones, manufacturers mostly perform only basic calibration and the rest is left on customers. Thus, for better accuracy the system needs to be recalibrated [3]. There exists a wide range of calibration procedures and techniques, e.g. the calibration using redundant heading information computed from rate gyroscopes [4] or the calibration procedure based on ellipsoid fitting problem which does not need heading reference information obtained from redundant sensors [5].

Nowadays, the ECs have become useful in a wide range of consumer applications such as mobile phones, PDAs, robot navigation, human head and hands tracking, attitude determination of inertial navigation systems used in aerospace engineering, etc. [1, 2, 6–8].

In this paper, the EC system and the tilt compensation is briefly described in section 2, the sensor error model (SEM) is further discussed in chapter 3 and Thin-Shell calibration method is mentioned in section 4. A measurement setup and a measured unit are briefly introduced in section 5. The most important results are summarized in section 6.

* corresponding author; e-mail: siposmar@fel.cvut.cz

2. Electronic compass

The simplest electronic compass (EC) can be constructed using only a dual-axis magnetometer. This type of EC can measure accurate only azimuth (yaw angle) in horizontal plane. The resulting azimuth ψ can be computed using simple eq. (1):

$$\psi = \arctan\left(f_y/f_x\right) - D \tag{1}$$

where f_x, f_y are horizontal magnetic field components measured in sensor (body) frame, and D is a magnetic declination [2].

Although this type of compasses is very simple and easy to manufacture, a main disadvantage of this EC construction is in the obligation to place the sensor accurately into horizontal plane. If it cannot be ensured, the errors are not negligible as was proved by Vcelak in [2]. Generally, it is not possible to ensure this condition providing horizontal mounting of magnetic sensor, so the electronic compass has to be equipped with tilt compensation functionality. The compass with tilt compensation (Fig. 1) usually consists of tri-axial magnetometer and tilt sensor, which can be formed by tri-axial accelerometer [9] or an electronic inclinometer commonly used in Honeywell compasses.

The EC uses magnetometer platform mathematically aligned to the horizontal plane using pitch and roll angles defined by (2) and (3). The azimuth can be then computed using (4).

$$\theta = \arctan\left(-a^{by}\Big/\sqrt{\left(a^{bx}\right)^2 + \left(a^{bz}\right)^2}\right), \tag{2}$$

$$\varphi = \arctan\left(a^{bx}/\left(-a^{bz}\right)\right), \tag{3}$$

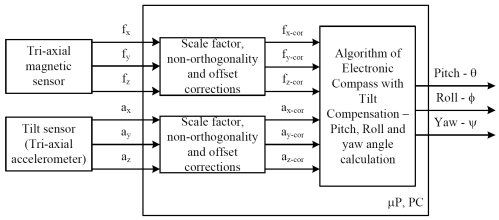

Fig. 1. The block scheme of an EC with a tilt compensation and the compensation of sensor imperfections formed in the sensor error model (5).

$$\psi = \arctan \frac{f_y \cos\varphi + f_z \sin\varphi}{f_x \cos\varphi + f_y \sin\varphi \sin\theta - f_z \cos\varphi \sin\theta} - D, \tag{4}$$

where: θ, φ denote the pitch and roll angle; a^{bx}, a^{by}, a^{bz} are measured accelerations in the sensor body frame; f_x, f_y, f_z represent magnetic field vector components measured in sensor frame [10].

3. Sensor error model

In the chapter 1 it was mentioned that the calibration is necessary to be performed for the elimination of the sensor imperfections. Generally, sensors have many error sources; nevertheless, our sensor error model (SEM) defined by (5) includes the main ones [11]. They correspond to scale factor deflections, axes misalignment described in our case by three non-orthogonality angles [11], and offsets for all three axes. The offset forms a stochastic time-invariant part of the bias; in contrast, a drift characterizes a time-variant part of the bias. Because the calibration process is commonly performed during short-time period, the drift can be considered as zero [11].

$$\boldsymbol{y_p} = \boldsymbol{T_a^p SF_a}(\boldsymbol{y_m} - \boldsymbol{b_a}) \begin{pmatrix} 1 & 0 & 0 \\ \alpha_{yx} & 1 & 0 \\ \alpha_{zx} & \alpha_{zy} & 1 \end{pmatrix} \times \begin{pmatrix} SF_{ax} & 0 & 0 \\ 0 & SF_{ay} & 0 \\ 0 & 0 & SF_{az} \end{pmatrix} \left[\begin{pmatrix} y_{mx} \\ y_{my} \\ y_{mz} \end{pmatrix} - \begin{pmatrix} b_{ax} \\ b_{ay} \\ b_{az} \end{pmatrix} \right], \tag{5}$$

where $\boldsymbol{y_p}$ represents the compensated vector of either measured acceleration in the case of accelerometers or magnetic field vector in case of magnetometers and is defined in the orthogonal platform frame; $\boldsymbol{T_a^p}$ denotes the matrix providing the transformation from the non-orthogonal frame to the orthogonal one with non-diagonal terms α_{yx}, α_{zx}, α_{zy} that correspond to the axes misalignment; SF_a represents a scale factor matrix; $\boldsymbol{b_a} = [b_{ax}, b_{ay}, b_{az}]^T$ is the vector of offsets; $\boldsymbol{y_m} = [y_{mx}, y_{my}, y_{mz}]^T$ denotes the vector of measured acceleration/magnetic field vector. The SEM and its derivation are described in more detail in [12].

4. Calibration procedure

There already exist several calibration procedures for tri-axial sensors using different principles, e.g. the method using an ellipsoidal-fitting procedure [5, 13], a calibration procedure which uses a robotic arm [14] or a procedure with the usage of 3D optical tracking system that measures the position coordinates of markers attached to a measurement unit [15].

In our case, we used the thin-shell (TS) calibration method. A fundamental principle of the proposed method is based on the fact that the magnitude of measured quantity $|y|$ (gravity acceleration, magnetic field vector) should be always equal to the constant value when static conditions are ensured and also equal to the square root of the sum of squared vector components (6):

$$y_x^2 + y_y^2 + y_z^2 = |y|^2, \tag{6}$$

where y_i denotes sensed quantity in direction of i axis and $|y|$ is the magnitude of measured quantity. In the case of the gravity vector, it is ideally equal to lg and in the case of the magnetic field vector $|F|$ it is equal to $0.48125G$ for the location (area) where the measurements were taken. The value of Earth magnetic field vector was calculated using International Geomagnetic Reference Field model (IGRF 11) which depends on the date of measurement, GPS position, and the altitude [16].

For the calibration purposes, according to [11], 36 positions are recommended to measure, 3 times 12 positions along x, y, z axis. The advantage of the method is that the precise knowledge of position orientations is not required. It is only recommended to provide at least 3 positions per each quadrant and each axis. After the measurements are taken, the Thin-Shell algorithm can be applied on the measured data. The TS algorithm is based on a lineaer minimum mean square error principle minimizing the standard deviation σ defined by (7), which is calculated from compensated vector component estimates and the known number of measurements.

$$\sigma = \sqrt{\frac{\sum_{i=1}^{m} \left(\widehat{y}_{xi}^2 + \widehat{y}_{yi}^2 + \widehat{y}_{zi}^2 - |y|^2 \right)^2}{m-1}}, \tag{7}$$

where $\widehat{y}_{xi}$, $\widehat{y}_{yi}$, $\widehat{y}_{zi}$ are estimations of compensated acceleration/magnetic field vector components and $|y|$ is the magnitude of the reference value corresponding to measured quantity. The more detailed description of this calibration method is presented in [11, 17].

In each iteration step the interval defines the minimum, maximum, and mean value of the parameter being searched for and these values are then used to update the SEM. Thus, 3 SEMs are obtained coresponding to min., max., and mean values of the given parameter. Based on the updated SEMs new estimates of compensated vector are determined for each position and used for σ calculations. With respect to obtained 3 values of σ the interval is halved to find the local minimum of a standard deviation according to Fig. 2. When σ_{mean} reaches the smallest value, the interval is halved around k_{mean}, where "k" rep-

resents the parameter being searched for. Unlikely, when other σ reaches the smallest value and σ_{mean} is the second, the new interval is defined between k, whose σ was the smallest and k_{mean}. For instance, when k_{min} has the smallest σ, the k_{mean} becomes k_{max} for another iteration step and the new k_{mean} is calculated as the average of the new k_{max} and previous k_{min}. The same principle can be applied for the other case [11].

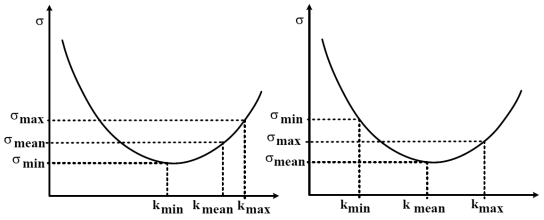

Fig. 2. Criterions for halving the interval, in which the estimated parameters are searched for [11].

5. Measurement setup

In our case the measurement setup was built up by the inertial measurement unit (IMU) ADIS16405 [18] (Analog Devices) and the non-magnetic theodolite T1c (Meopta Prague, Czech Republic). The IMU was used to evaluate the EC algorithm with tilt compensation and to prove the improvement of applied calibration procedure. The IMU (Fig. 3) contains the tri-axial magnetometer (MAG), tri-axial accelerometer (ACC), and tri-axial angular rate sensor (ARS). The measurements were performed in the area with minimal magnetic field disturbances in the local time from 18:00 to 19:00 CET when the variations of magnetic field are minimal. For the evaluation of EC accuracy, the IMU was mounted on the non-magnetic theodolite, see Fig. 3, which was used as a reference with an average error 4.17×10^{-3} deg.

In all performed experiments we used for calibration purposes and a final EC evaluation the average of 100 ACC and MAG samples taken in each position under static conditions as a value we consequently calculated with. A main reason for the usage of average values was the elimination of a noise influence.

6. Results

6.1. Calibration of Magnetometer and Accelerometer of IMU ADIS16405

From the output data provided by IMU ADIS16405 we used only information from the magnetometer (MAG) and the accelerometer (ACC). After the data had been preprocessed, the calibration was performed using the Thin-Shell algorithm to estimate three misalignment angles (non-orthogonality angles), three scale factor corrections, and three biases, all formed in SEM (5). The

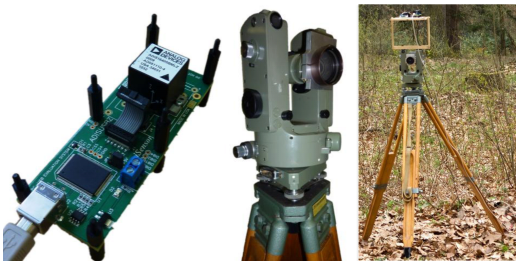

Fig. 3. The Inertial measurement unit ADIS16405 (on the left); theodolite T1c (in the middle); the whole measurement setup (on the right).

parameters of MAG and ACC SEMs are listed in Table I. The deviation between the measured and the ideal vector of applied quantity (corresponds to the magnetic field vector for MAG and to the gravity vector for ACC) is shown in Fig. 4 and Fig. 5. In contrast with the chapter 4, in which 36 positions are recommended for a correct calibration, we used only 21 positions in the case of MAG. The measurement took shorter time and thus we minimized the risk of potential magnetic field variations. In [11] it was proven that 21 positions is a sufficient number without a final accuracy decrease. For ACC calibration, the 36 positions were measured as was recommended.

TABLE I

Sensor error models obtained using Thin-Shell algorithm for magnetometer (MAG) and accelerometer (ACC) of IMU ADIS16405 (Superscript 1 denotes RMSE before calibration and 2 after calibration)

Parameter	MAG	ACC
α_{xy} [deg]	0.1355	–0.0230
α_{zx} [deg]	–0.6628	0.0351
α_{zy} [deg]	–0.0818	–0.1639
SF_x [–]	1.0049	0.9996
SF_y [–]	1.0050	1.0019
SF_z [–]	1.0004	0.9983
b_x	–0.71 mG	–13.54 mg
b_y	–0.83 mG	–6.71 mg
b_z	0.23 mG	–4.02 mg
RMSE^1	1.9 mG	9.5 mg
RMSE^2	0.4 mG	2.5 mg

6.2. Influence of MAG and ACC Calibration to Electronic Compass Accuracy

Finally, we analyzed in previous chapter performed calibration from the final accuracy of realized electronic compass (EC) point of view. We performed four measurements at all. In each measurement the EC was differently tilted in two directions to set values of 0 deg and 20 deg in various combinations. Then, the azimuth was

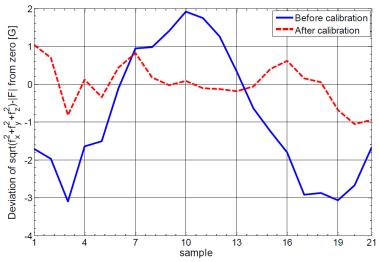

Fig. 4. The dependence of deviations of measured magnetic field vector before and after calibration — MAG of ADIS16405 — 21 evaluated positions.

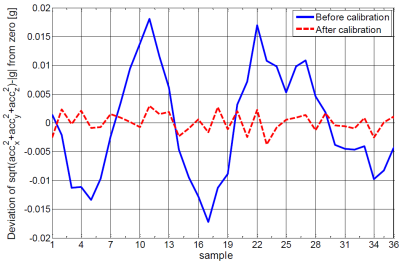

Fig. 5. The dependence of deviations of measured accelerations before and after calibration — ACC of ADIS16405 — 36 evaluated positions.

changing with the step of 22.5 deg and a tilt compensation observed as well as the effect of MAG and ACC calibration on the azimuth accuracy. As a criterion for the azimuth accuracy evaluation the RMSEs were computed and the final values with and without calibration (applied SEM) summarized, see Table II. The table provides the final RMSEs depending on set tilts in two direction (pitch and roll angles). In all four data sets, the application of evaluated SEMs led to the improvement of the final EC accuracy.

TABLE II
Final accuracy of yaw angle estimation with and without applied ACC and MAG SEM; θ - pitch, φ - roll, ψ - yaw

θ [deg]	φ [deg]	without calibration $\Delta\psi_{\mathrm{RMSE}}$ [deg]	with calibration $\Delta\psi_{\mathrm{RMSE}}$ [deg]
0	0	1.663	0.534
0	20	1.270	0.462
20	0	2.012	0.567
20	20	1.303	0.563

7. Conclusion

This paper deals with an electronic compass (EC) algorithm and procedures needed for its correct functionality. The EC performance generally depends on used tri-axial magnetometer (MAG) and its parameters as well as on parameters of an aligning system. In our case we used tri-axial accelerometer (ACC) for this purpose. To improve EC performance we applied a calibration procedure Thin-Shell to estimate sensor error models of MAG and ACC. The methods were shortly introduced; nevertheless, a main focus was pointed to present experimental results. We performed the calibration of MAG, which approximately five-times improved its accuracy and in the case of ACC the accuracy was four-times improved. Although the calibration procedure recommended 36 positions to use, we measured data only 21 in the case of MAG which was in accordance to [11]. In contrast, for the ACC calibration we kept 36 positions as was recommended. We analyzed the influence of MAG and ACC calibration on the final EC accuracy by analyzing the differences between the evaluated azimuth and the reference angle obtained from our reference system formed by theodolite T1c. The evaluated azimuth reflected estimated SEMs' parameters, which were: three scale-factors corrections, three non-orthogonality angles, and three offsets. In all tested experiments the application of MAG and ACC SEMs led to improvement of final EC accuracy as was presented.

Acknowledgement

This research has been partially supported by Czech Science Foundation project 102/09/H082, partially by the research program No. MSM6840770015 "Research of Methods and Systems for Measurement of Physical Quantities and Measured Data Processing" of the CTU in Prague sponsored by the Ministry of Education, Youth and Sports of the Czech Republic and partially by Grant Agency of the Czech Technical University in Prague grant No. SGS10/288/OHK3/3T/13.

References

[1] R. Racz, Ch. Schott, S. Huber, *Proceedings of the IEEE sensors 2004*, Vienna, Austria **1-3**, 1446, (2005).

[2] J. Vcelak, V. Petrucha, P. Kaspar, *Sensor Letters* **5**, 279, (2005).

[3] Z. Syed, P. Aggarwal, C. Goodall, X. Niu, N. El-Sheimy, *Measurement Science & Technology* **18**, 1897, (2007).

[4] B. Hoff, R. Azuma, *IEEE and ACM International Symposium on Augmented Reality*, Munich, Germany, 159, (2000).

[5] X. Hu, Y. Liu, Y. Wang, Y. Hu, D. Yan, *4th IEEE/ACM International Symposium on Mixed and Augmented Reality 2005*, Vienna, Austria, 182-183, (2005).

[6] V.Y. Skvortzov, HK. Lee, S.W. Bang, YB. Lee, *Proceedings of the 2007 IEEE International Conference on Robotics and Automation* **1-10**, 2963, (2007).

[7] M. Reinstein, *Przegląd Elektrotechniczny* **87**, 255, (2011).

[8] M. Reinstein, M. Sipos, J. Rohac, *Przegląd Elektrotechniczny* **85**, 114, (2009).

[9] J. Včelák, P. Ripka, J. Kubík, A. Platil, P. Kaňpar, *Sensors and Actuators A: Physical* **123-124,**, 122, (2005).

[10] M. Soták, *Przegląd Elektrotechniczny* **86**, 247, (2010).

[11] M. Sipos, P. Paces, J. Rohac, P. Novacek, *IEEE Sensors Journal*, (2011), accepted for publication.

[12] I. Skog, P. Händel, *XVII IMEKO World Congress*, Rio de Janeiro, (2006).

[13] S. Bonnet, C. Bassompierre, C. Godin, S. Lesecq, A. Barraud, *Sensors and Actuators A: Physical* **156**, 302, (2009).

[14] E.L. Renk, M. Rizzo, W. Collins, F. Lee, D.S. Bernstein, *IEEE Control Systems Magazine*, **25**, 86, (2005).

[15] A. Kim, MF. Golnaraghi, *Plans 2004: Position location and Navigation Symposium*, Monterey, CA, 26, (2004).

[16] *NOAA's Geophysical Data Center - Geomagnetic Online Calculator.* Available: http://www.ngdc.noaa.gov/ geomagmodels/ IGRFWMM.jsp [Accessed: 09-Sep-2011].

[17] M. Soták, M. Sopata, R. Bréda, J. Roháč, L. Váci, *Navigation System Integration*, Košice: Robert Breda, Kosice, the Slovak Republic (2006).

[18] *ADIS16405 High Precision Tri-Axis Gyroscope, Accelerometer, Magnetometer, Inertial Sensors, Sensors, Analog Devices.* Available: http://www.analog.com/en/sensors/inertial-sensors/adis16405/products/product.html [Accessed: 24-Apr-2011].

5.2.3 Analyses of Electronic Inclinometer Data for Tri-axial Accelerometer's Initial Alignment

The paper (Sipos, Rohac & Novacek 2012*b*) follows a previously published paper (Sipos et al. 2012*a*). The publication describes an analysis of an electronic inclinometer EZ-TILT-2000-008 and its usage for the IMU ADIS16405 accelerometers start-up setup. The IMU used is based on MEMS and it is necessary to setup its parameters correctly after each cold start. The electronic inclinometer is used to improve the initial orientation estimation of the IMU.

Martin ŠIPOŠ, Jan ROHÁČ, Petr NOVÁČEK

Czech Technical University in Prague (1)

Analyses of Electronic Inclinometer Data for Tri-axial Accelerometer's Initial Alignment

Abstract. *This paper deals with the usage of a dual-axis electronic inclinometer EZ-TILT-2000-008 to improve an initial alignment of a tri-axial accelerometer, which forms a part of the inertial measurement unit ADIS16405. There were performed several measurements under various initial conditions with the usage of a precise Rotational-Tilt Platform as a reference. Based on measured data the alignment procedure accuracy, null repeatability, stability of initial null angle, hysteresis, and cross-axis dependence were analyzed and the results of these analyses are presented.*

Streszczenie. *Zaprezentowano wykorzystanie dwuosiowego inklinometru EZ-TILT-2000-008 do poprawy ustawiania trzyosiowego przyśpieszeniomierza. Przeprowadzono badania dokładności, powtarzalności zera, histerezy i wpływu osi w opracowanym przyśpieszeniomierzu. (**Zastosowanie elektronicznego inklinometru do ustawiania trzyosiowego miernika przyśpieszeń**)*.

Keywords: electronic inclinometer, tri-axial accelerometer, initial alignment, cross-axis dependence.
Słowa kluczowe: inklinometr, przyśpieszeniomierz.

Introduction

Recently, a technological improvements in the precision and reliability of Micro-Electro-Mechanical-Systems (MEMS) have enabled the usage of low-cost MEMS inertial sensors in wide range of civil and military applications, such as a car navigation, personal navigation, indoor navigation, navigation of unmanned aerial vehicles, underwater navigation, human motion tracking, etc. [1, 2, 3, 4, 5, 6].

A basic part of common navigation systems, which is an Inertial Measurement Unit (IMU), primarily contains accelerometers (ACCs) and angular rate sensors (ARSs) for providing inertial data, and additionally magnetometers (MAGs). These sensors' data are used for various navigation computations such as attitude, velocity and position estimation, initial alignment, etc. In navigation systems, first of all, it is necessary to determine the initial attitude of the navigation system including the determination of initial Euler angles (the roll, pitch, and yaw). They describe the relationship between the sensor frame (SF) and the local navigation frame (LNF) in which the navigation is performed.

For IMUs with low-cost ARSs the initial attitude cannot be determined by a self-alignment procedure using only ARSs them-selves [7, 8], because aforementioned sensors are not able to sense the Earth rotation, which is usually below the noise level [9]. Therefore, the initial attitude has to be determined using the ACCs and MAGs. The procedure of initial attitude determination is called the coarse alignment and its accuracy depends on the level of imperfections of ACCs and MAGs (scale factor corrections, angles of non-orthogonality, biases, etc.). These can be partially compensated using a sensor error model [3, 10]. After the coarse alignment has been done, the Euler angles are initialized and regular Euler angles estimation process, for details see [11], can take place.

This paper extends the analyses presented in [1] and deals with the usage of an electronic inclinometer (EI) EZ-TILT-2000-008 (Advanced Orientation Systems Inc. [12]). The EI is used to improve the initial levelling done based on tri-axial accelerometer, in our case, contained in the IMU ADIS16405 (Analog Devices [13]). The levelling procedure forms the part of initial attitude determination, in which the pitch and roll angles are estimated. The accuracy of initial attitude determination depends on biases of ACCs which cause non-negligible errors in pitch and roll estimates and vary with each system turning-on. This mentioned imperfection of accelerometers was a motivation for using other system with a different principle of angles estimation. In our case, the EI was used, which enabled the estimation of accelerometer biases. There were performed several measurements under various initial conditions with the usage of the Rotational-Tilt Platform (RoTiP) as the reference. Based on the measured data the accuracy analyses were performed.

Initial Attitude Determination

The initial attitude determination is a procedure, in which Euler angles are estimated. There exist various algorithms for initial attitude determination, e.g. a coarse/fine alignment, static/in-motion alignment, analytic alignment and so on [9]. In this paper, the initial attitude is evaluated using the coarse alignment procedure only. This procedure can be divided into two steps. First one includes the levelling procedure to determine the pitch and roll angles. The following one is named a course alignment and determines the yaw angle [8]. For IMUs consisted of tri-axial MAG as well as ACC and ARS, the yaw angle can be determined easily. In the following part only the levelling procedure is described.

Levelling procedure

A main aim of the levelling is determine the pitch (1) and roll (2) angles according to the gravity vector measured by tri-axial ACC under static conditions [7, 8].

$$\theta = arctg\left(- f^{by} \Big/ \sqrt{\left(f^{bx}\right)^2 + \left(f^{bz}\right)^2} \right) \tag{1}$$

$$\phi = arctg\left(f^{bx} \Big/ - f^{bz}\right) \tag{2}$$

where: θ is the pitch angle, ϕ denotes the roll angle, f^{bx}, f^{by}, f^{bz} are measured accelerations in the sensor frame.

The procedures of the levelling and course alignment were described in detail by Soták in [7, 8]. Based on the real tests performed by Soták it can be seen that the estimated values of pitch and roll angles are not identical with the reference ones due to the influence of accelerometer biases. Based on the specifications of ADIS16405 the initial bias error is up to ±50 mg (for 1σ corresponding 68% probability) and thus can cause the error of ±2.9 degree in zero tilt. This error negatively influences the final accuracy of estimated initial attitude as well as the following position evaluation. This imperfection of the process was the motivation for a usage of a different system to measure and correct the pitch and roll angles determined from the accelerometer during the coarse alignment procedure [1].

Applied Systems and Measurement Setup

This section describes basic specifications of applied measurement systems. The performance of the ADIS16405's tri-axial ACC (Analog Devices [13]) is provided in Table 1. In the case of the electronic inclinometer (EI) EZ-TILT-2000-008 (Advanced Orientation Systems Inc. [12]) it is in Table 2.

Table 1. The parameters of the ADIS16405's accelerometer [13]

Accelerometer's parameter	Typical value
Dynamic range	±18 g
Initial sensitivity	3.33 mg/LSB
Initial bias error (± 1σ)	±50 mg
In-run bias error (± 1σ)	0.2 mg
Velocity random walk (± 1σ)	0.2 m/s/√hr
Output noise (no filtering, rms)	9 mg
Noise density (no filtering)	0.5 mg/√Hz

Table 2. The parameters of the EZ-TILT-2000-008 [12]

EI's parameter	Typical value
Range	±8 deg
Analog output	1 to 4 VDC
Power supply	6 to 12 VDC
Resolution of A/D convertor	12 bit
Response (10% - 90%)	40 ms
Repeatability	<0.02 deg
Temperature range	-40 to +60 degC

The EI (Fig. 1a) is an advanced programmable dual-axis linear analog/digital module with CMOS microprocessor which includes a dual-axis polymer based electrolytic tilt sensor (ETS) DX-008. The EI module provides analog, PWM, and RS-232 tilt information in two axes. Full description is specified in [12]. In our case, the viscosity of ETS was about 50% higher than viscosity of standard ETS.

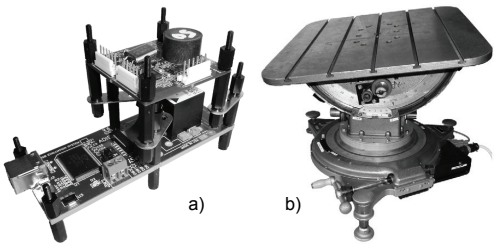

Fig.1. a) ADIS16405 board with EZ-TILT-2000-008 mounted on; b) Rotational-Tilt Platform

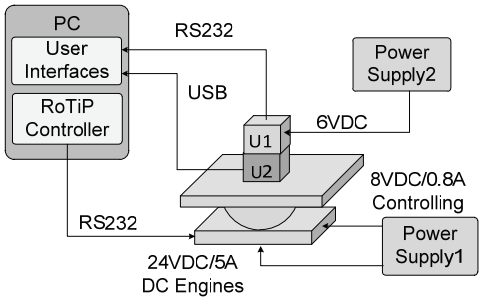

Fig.2. A block scheme of measurement setup; U1 – electronic inclinometer EZ-TILT-2000-008, U2 – IMU ADIS16405

As a reference system for the results comparison and analyses we used the Rotational-Tilt Platform (RoTiP), see Fig. 1b. The RoTiP is capable to set positions with required attitude and speed along three axes. The specification of RoTiP is provided in Table 3.

Table 3. The parameters of Rotational-Tilt Platform

Parameter	Range	Speed of motion	Resolution
Pitch	± 45 deg	± 42 deg/s	0.00033 deg
Roll	± 25 deg	± 60 deg/s	0.00065 deg
Heading	0 to 360 deg	± 310 deg/s	0.00074 deg

A block scheme of measurement setup is shown in Fig. 2. It includes the RoTiP with its power supply, two measurement systems (EI, IMU) powered by other DC power supply and USB, and a PC control station. The PC software controls the RoTiP position via RS232 bus and collects the data from the measurement systems.

Tests and Results

This chapter provides the results of EI and ACCs tests which helped to analyse the measurements system performances from their accuracy point of view. The tests covered the effect of EI correction on the final accuracy, the correction of ACC's transfer characteristics, a null repeatability, the stability of the initial null angle, the hysteresis, and cross-axis dependence.

During all experiments and analyses the data from ADIS16405 were sampled and recorded with the frequency 100 Hz and the data from EZ-TILT-2000-008 with 14 Hz. To eliminate the influence of a noise contained in the data we made a mean value of 100 samples for each channel and each position under steady-state conditions and a resultant averaged value was used as a representative for that particular position and channel.

For a result comparison Root Mean Square Error (RMSE) defined by (3) was used.

$$RMSE(x_1, x_2) = \sqrt{\frac{\sum_{i=1}^{n}(x_{1,i} - x_{2,i})^2}{n}} \tag{3}$$

where: $x_{1,i}$ is the vector of reference values, $x_{2,i}$ denotes the vector of measured/estimated values, and n represents the number of measurements.

Transfer Characteristics

The transfer characteristics of both measurement systems were measured using RoTiP platform in the range approximately ±8 deg with the step of 1 deg. The systems were consequently tilted among steady-state positions with angular velocity 2 deg/s. Measured transfer characteristics of EI related to the reference values were then approximated using 2nd order polynomials to get corrections for both pitch (4) and roll (5) angles.

$$\theta_{cor} = 0.001761 \cdot \theta_{nc}^2 + 1.031 \cdot \theta_{nc} + 0.6138 \tag{4}$$

$$\phi_{cor} = 0.001761 \cdot \phi_{nc}^2 + 1.033 \cdot \phi_{nc} + 0.2546 \tag{5}$$

where: θ is the pitch angle, ϕ denotes the roll angle, subscript cor represents the angles after the polynomial correction, subscript nc corresponds to the measured non-corrected angles.

The deviations of EI transfer characteristics from the reference values before and after the correction are shown in Fig. 3. The effect of EI transfer characteristics correction on the precision of ACC biases estimation and consecutive ACC based angles estimation can be seen in Fig. 4. The experiment in each position considered that based on corrected value of EI ACCs were newly initialized, which means that the biases of ACCs were newly estimated and corrected. The RMSE and variance values from Fig. 3 and Fig.4 are listed in Table 4.

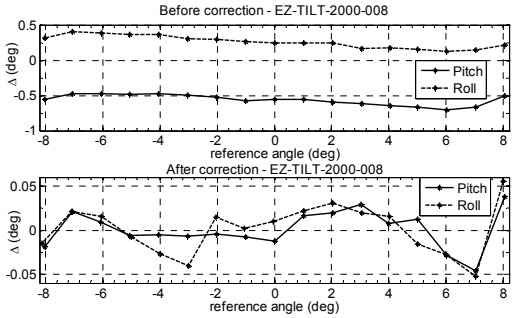

Fig.3. Deviations (Δ) of pitch and roll angles from the reference values before and after corrections using 2nd order polynomials – electronic inclinometer EZ-TILT-2000-008

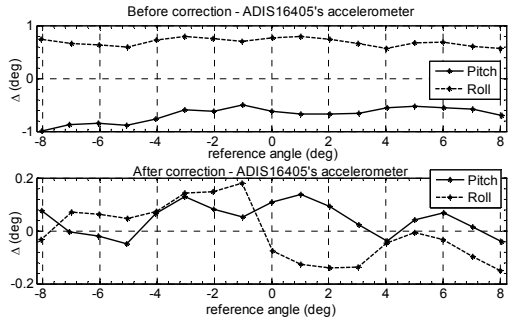

Fig.4. Deviations (Δ) of pitch and roll angles from the reference values before and after bias corrections using corrected data of electronic inclinometer – ACC of IMU ADIS16405

Table 4. The RMSE and variance values before and after correction for EI and ACC (according to Figs. 3-4)

	EI (deg)		ACC (deg)	
	Pitch	Roll	Pitch	Roll
RMSE before correction	0.57	0.27	0.69	0.70
RMSE after correction	0.04	0.05	0.07	0.10
Variance before corr.	0.0057	0.0077	0.0213	0.0053
Variance after corr.	0.0005	0.0005	0.0114	0.0034

Null Repeatability

The repeatability is defined as an angular error calculated from angle deviations when the measurement system is repeatedly placed in the same position and consequently replaced from it. A special angle of importance is the null angle, which is characterized by the null repeatability characteristics [14]. As in the previous case, the RoTiP was used to set the positions and to refer the angles. The ACC and EI were tilted within the range of ±8 deg along combined directions (positive pitch and negative roll and conversely). The angular rate between subsequent positions was kept at the value of 2 deg/s in all cases. For each channel of EI and ACC and steady-state conditions the average of 100 samples was calculated. Fifty times the null angle position was subsequently set up. The performances of EI and ACC are shown in Fig. 5.

Based on obtained data from the null repeatability experiment the RMSE of EI performance was 0.12 deg for the pitch and 0.09 deg for the roll angle. In the case of ACC the RMSE was higher in both cases, i.e. 0.81 deg for the pitch and 0.40 deg for the roll angle. From Fig. 5 it is clear that the null repeatability of ACC is influenced by the initial bias error, which can be compensated using the bias correction obtained from EI.

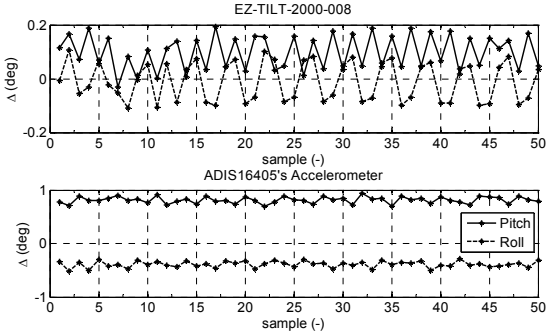

Fig.5. The Null repeatability of pitch and roll angles for the EI and the ACC, where "Δ" means a deviation between measured angle and the reference angle equal in this case to 0 deg

Stability of Initial Null Angle

The stability of an initial null angle, which corresponds to an initial bias error defined by Analog Devices [13], was also observed. For both systems there were performed 20 measurements during 4 days. Each measurement was performed after the power was 60 seconds switched-on to stabilize the system operating conditions. As well as in previous cases in each position and steady-state conditions 100 data samples were averaged to obtain the value we then worked with.

The RMSE for the pitch and roll angles of EI was 0.05 deg in both axes. The RMSE for the pitch and roll of ACC was 0.87 deg and 0.25 deg, respectively. The stability of initial null angle characteristics for both EI and ACC is shown in Fig. 6. From the ACC characteristics it can be seen that the pitch and roll angles were again influenced by an initial bias error, unlike the EI. According to Fig. 6, the initial bias error has smaller influence on EI than on ACC. It proves the EI to be suitable for initial ACC corrections from the null angle stability point of view.

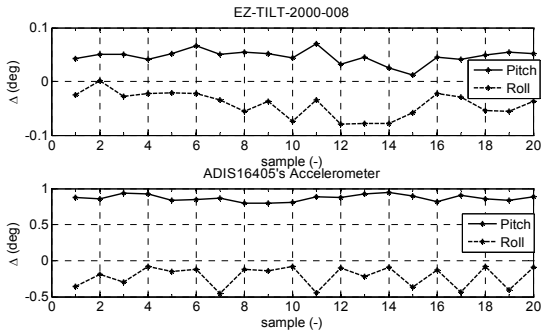

Fig.6. The Stability of an initial null angle for EI and ACC, where "Δ" represents a deviation between a measured angle and a reference angle equal to 0 deg

Hysteresis

The hysteresis characteristics were measured in the range of ±8 deg forward and backward for both angles of tilt. As in previous measurements, the average of 100 samples was taken as a representative value of particular steady-state position. The hysteresis was observed on the sensor data already compensated for the nonlinearity and initial offset. According to tilt angles evaluated based on measured data when the RoTiP was tilted from -8 deg up to +8 deg and back, we evaluated differences between obtained angles of both directions and a particular reference angle of RoTiP. The progresses of those

differences for both sensors are presented in Fig. 7. The hysteresis δ_H can be then calculated according to (6).

$$\delta_H = \left(\frac{y_{up} - y_{down}}{y_{max} - y_{min}} \right)_{max} .100(\%) \quad (6)$$

where $y_{up,}$ denotes an evaluated value from a forward measurement (tilt being increased), y_{down} corresponds to a backward measurement (tilt being decreased), and y_{min}, y_{max} are the minimal and maximal values of the measurement.

With respect to (6) and measured data the EI hysteresis was 0.51 % for the pitch and 0.43 % for the roll angle. The hysteresis for ACC was 0.71 % for the pitch and 1.19 % for the roll angle.

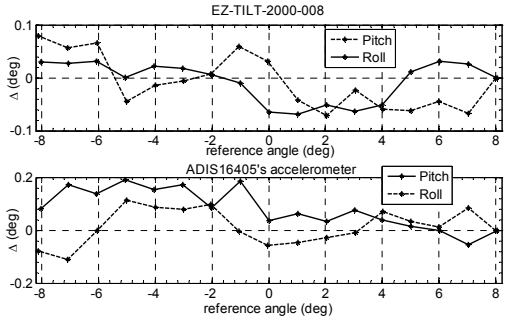

Fig.7. The progress of differences "Δ" defined between tilt angles evaluated from measurements in which the RoTiP was tilted from -8 deg up to +8 deg and in backward direction. The differences correspond to the same reference angle of RoTiP set within a forward and backward direction of the measurement

Cross-axis Dependence

The cross-axis dependence was measured for both systems using the same procedure and the same number of samples to be averaged for representing values as in previous cases. In the cases of the pitch angles being changed, the roll angle deviations were measured. In the other case, the roll angles were changed and pitch angle deviations were measured. The measured data for both systems were analysed. The cross-axis dependencies for ACC are shown in Fig. 8. The RMSE was 0.08 deg for the pitch and 0.06 deg for the roll angle.

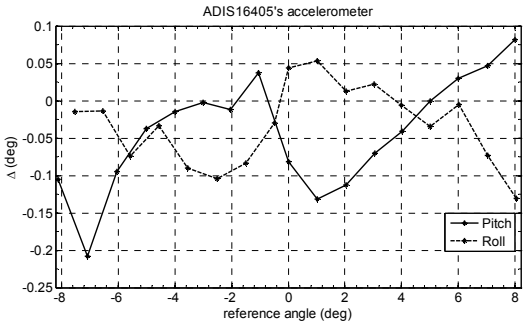

Fig.8. Cross-axis dependence of ACC where "Δ" represents cross-axis deviation

According to measured characteristics of ACC it can be seen that the cross-axis error is negligible with respect to other error sources. Unfortunately, performed analyses of EI showed the strong cross-axis dependence and the additional measurements had to be performed. The cross-axis dependencies for the pitch and roll angles of EI are shown in Fig. 9 and Fig. 10, respectively.

The measured characteristics were analysed and approximated by two-variable polynomials. We analysed different order of polynomials from the computational cost and the accuracy points of view. The RMSEs which were computed from deviations between measured and reference angles before and after cross-axis correction using different order polynomials are shown in Table 5.

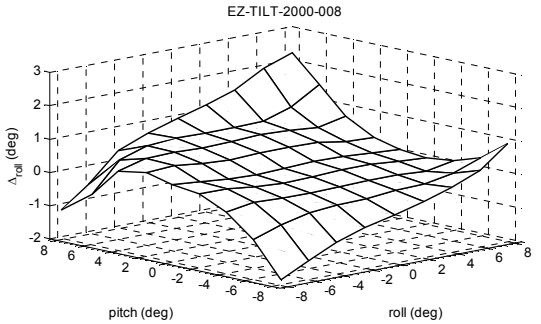

Fig.9. Cross-axis dependence of EI – pitch angle tilted, roll angle deviations observed

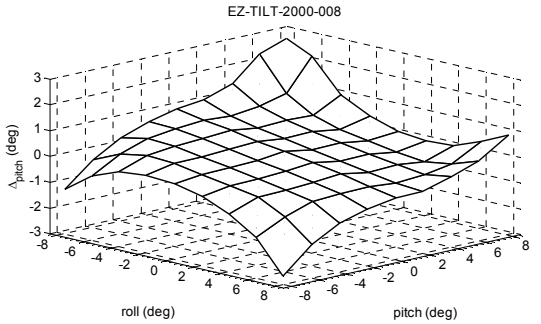

Fig.10. Cross-axis dependence of EI – roll angle tilted, pitch angle deviations observed

Furthermore, we performed the correction using other mathematical algorithm – LOcally WEighted Scatterplot Smoothing (LOWESS), but the application of this algorithm did not lead to well-marked improvement of the accuracy. Finally, we chose 3rd order polynomials described by (7) and (8) for pitch and roll correction, respectively.

$$\Delta\theta = 0.093 - 0.081\theta - 0.082\phi - 0.002\theta^2 - 0.003\theta\phi + 0.001\theta^3 + 0.003\theta\phi^2 - 0.0001\phi^3 \quad (7)$$

$$\Delta\phi = 0.273 + 0.077\theta - 0.050\phi - 0.001\theta^2 + 0.001\theta\phi - 0.001\phi^2 + 0.0003\theta^3 + 0.003\theta^2\phi + 0.0005\phi^3 \quad (8)$$

where: $\Delta\theta$, $\Delta\phi$ are the pitch and roll corrections, θ, ϕ are estimated pitch and roll angles.

Table 5. The RMSEs of applied polynomials for EI cross-axis correction

Applied polynomial	RMSE (deg)	
	Pitch	Roll
No correction	0.67	0.77
Correction using 1st order polynomial	0.44	0.39
Correction using 2nd order polynomial	0.43	0.38
Correction using 3rd order polynomial	0.13	0.14
Correction using 4th order polynomial	0.12	0.12
Correction using 5th order polynomial	0.09	0.10

Conclusion

This paper concerns a levelling procedure of navigation systems using tri-axial accelerometer (ACC) and electronic inclinometer (EI). The levelling forms the part of coarse alignment process which is needed to be performed within the initialization of inertial navigation systems. The levelling is generally done by ACCs; however, ACC biases negatively affect its precision. Due to this reason other system is required and thus we analysed how the precision can be improved by EI utilization and what weak points the system has.

In our case we used ACCs of IMU ADIS16405 and electrolytic tilt sensor of EZ-TILT-2000-008 EI system. Both systems belong to the low-cost category. The main aim was to analyse different effects of their characteristics on the levelling precision. For both systems we analysed the transfer characteristics, null repeatability, stability of initial null angle, hysteresis, and cross-axis dependence. All these characteristics were measured in the range of ±8 deg using a Rotational-Tilt Platform (RoTiP) which provided us with reference values of tilt. These values were related with ACC and EI data and used for analyses.

The RMSEs of performed analyses are summarized in Table 6. From this table, it can been seen that the main error affecting accuracy of the EI was caused by a cross-axis dependence with the RMSE equal to 0.13 deg for the pitch angle and 0.14 deg for the roll angle. These errors can be further reduced by using higher order polynomials or using other correction algorithms, such as aforementioned LOWESS. Nevertheless, with more and more complicated functions applied the computation cost will increase and the accuracy improvement will not change so much.

The measured characteristics of EI were slightly different from values specified by manufacturer. It was probably caused by using an electrolyte with higher viscosity than the one generally used in standard EI systems. However, according to measured data and performed analyses we proved that the corrections based on EI data led to the improvement of the levelling accuracy, which was our main purpose.

Table 6. The results of performed analyses for EI EZ-TILT-2000-008 and ACC ADIS16405's

Performed analyses	EI		ACC	
	Pitch	Roll	Pitch	Roll
No correction: RMSE (deg)	0.57	0.27	0.69	0.70
After correction: RMSE (deg)	0.04	0.05	0.07	0.10
Null repeatability: RMSE (deg)	0.12	0.09	0.81	0.40
Init. null angle stability: RMSE (deg)	0.05	0.05	0.87	0.25
Hysteresis (%)	0.51	0.43	0.71	1.19
Cross-axis dependence: RMSE (deg)	0.13	0.14	0.08	0.06

This research has been partially supported by Czech Science Foundation project 102/09/H082, partially by the research program No. MSM6840770015 "Research of Methods and Systems for Measurement of Physical Quantities and Measured Data Processing" of the CTU in Prague sponsored by the Ministry of Education, Youth and Sports of the Czech Republic and partially by Grant Agency of the Czech Technical University in Prague grant No. SGS10/288/OHK3/3T/13.

REFERENCES

[1] Šipoš M., Roháč J., Usage of Electrolytic Tilt Sensors for Initial Alignment of Tri-axial Accelerometer, *ICMT'11 International Conference on Miltary Technologies 2011*, 2011, Brno, Czech Republic, 685-691

[2] Šipoš M., Roháč J., Calibration of Tri-axial Angular Rate Sensors, *MDS2010 - Measurement, Diagnostics, Dependability of Aircraft Systems*, 2010, Brno, Czech Republic, 148-152

[3] Reinstein M., Šipoš M., Roháč J., Error Analyses of Attitude and Heading Reference Systems, *Przegląd Elektrotechniczny*, 85 (2009), nr 8, 114-118

[4] Sipos M., Paces P., Reinstein M., Roháč J., Flight Attitude Track Reconstruction Using Two AHRS Units under Laboratory Conditions, *IEEE Sensors 2009, Christchurch, New Zealand*, 2009, 675-678

[5] Jurman D., Jankovec M., Kamnik R., Topic M., Calibration and Data Fusion Solution for the Miniature Attitude and Heading Reference System, *Sensors and Actuators A-Physical*, 138 (2007), 411-420

[6] Reinstein M., Roháč J., Šipoš M., Algorithms for Heading Determination Using Inertial Sensors, *Przegląd Elektrotechniczny*, 86 (2010), nr 9, 243-246

[7] Soták M., Testing the coarse alignment algorithm using rotation platform, *Acta Polytechnica Hungarica,* ISSN 1785-8860, 7 (2010), nr 5, 87-107

[8] Soták M., Coarse alignment algorithm for ADIS16405, *Przegląd elektrotechniczny*, ISSN 0033-2097, 86 (2010), nr 9, 247-251

[9] Reinstein M., Evaluation of Fine Alignment Algorithm for Inertial Navigation, *Przegląd Elektrotechniczny*, 87 (2011), nr 7, 255-258

[10] Šipoš M., Pačes P., Roháč J., Nováček P., Analyses of Triaxial Accelerometer Calibration Algorithms, *IEEE Sensors Journal*, 2011, accepted for publication.

[11] Jalovecký R., Janů P., Computation Method Analysis of Turn Angle, *International Conference on Military Technologies 2010*, Bratislava, Slovak Republic, 2010.

[12] EZ-TILT-2000-008-rev2 Multi-Output Dual Axis High Res. Conversion Module w/RS232, *Advanced Orientation Systems*, Linden, USA, 2009, URL: <http://www.aositilt.com/Ez208.htm>, [cit. 2011-07-20]

[13] Triaxial Inertial Sensor with Magnetometer ADIS16400/ ADIS16405, *Analog Devices*, Nordwood, USA 2009, URL: : <http://www.analog.com/static/imported-files/data_sheets/ ADIS16400_16405.pdf>, [cit. 2011-07-20]

[14] General Application Notes, *Advanced Orientation Systems*, Linden, USA, 2009, URL: <http://www.aositilt.com/Ap0good.htm>, [cit. 2011-07-20]

***Authors**: Ing. Martin Šipoš*, E-mail: siposmar@fel.cvut.cz, Ing. Jan Roháč*, Ph.D., E-mail: xrohac@fel.cvut.cz, Ing. Petr Nováček*, E-mail: petr.novacek@fel.cvut.cz *Czech Technical University in Prague, Technická 2, Prague, Czech Republic.*

Chapter 6

Conclusions

This thesis shows modern approaches in metal detection, especially in the case of eddy-current metal detector usage. The main objective of the work was position estimation implementation on a standard metal detector. A collection of publications shows one possible solution that deals with low cost inertial sensor implementation on the detector sensing head. My original scientific contribution is the utilization of the Complex Magnetic Markers directly detected by the metal detector itself. The position markers can be utilized for the correction of the velocity and position information.

The usage of a multi-tone excitation signal was presented as the second part of the dissertation. The usage of such a signal shows the improvement of discrimination abilities for metal detection. This cooperative work, completed with Dr. Svatoš, promises perspective applicability. However, further development is needed.

Finally yet importantly, problematic sensor calibration was addressed. In practise, this analysis improves the accuracy of the low-cost inertial sensors used several times in a Microelectromechanical Systems. Therefore, this task is essential for the first part of this thesis and helps with position estimation precision.

Complex Magnetic Markers are partly evolved, but future development tasks are also awaited. In particular, additional differentiable types need to be found. Later on, the implementation of more than two markers in one measurement will be provided to improve the aiding of inertial sensors.

6.1 Future work

The work presented shows prospective results, but it will need future development. In particular, the final assembly of combined navigation and multi-tone excitation is needed. The concept of a modular metal detector has been

presented which combines Complex Magnetic Markers, and is expected to implement the use of a complex excitation signal.

The results presented regarding a *sinc* signal were obtained only in laboratory conditions with laboratory instruments; which is not suitable for field-testing. The development of an excitation and processing unit would therefore be one of the future evolution steps. It will be essential to obtain synchronous channels digitalization with high resolution and a sample rate. The future work also includes the adaption of image processing methods for magnetic images.

Appendix A

Bibliography

Aires, K. R. T., Santana, A. M. & Medeiros, A. A. D. (2008), OPTICAL FLOW USING COLOR INFORMATION: PRELIMINARY RESULTS, *in* 'APPLIED COMPUTING 2008, VOLS 1-3', ACM SIGAC; Univ Fortaleza; Federal Univ Ceara, pp. 1607–1611. 23rd Annual ACM Symposium on Applied Computing, Fortaleza, BRAZIL, MAR 16-20, 2008.

Ambrus, D., Vasic, D. & Bilas, V. (2016), 'Robust estimation of metal target shape using time-domain electromagnetic induction data', *IEEE Transactions on Instrumentation and Measurement* **65**(4), 795–807.

Beauchemin, S. S. & Barron, J. L. (1995), 'The computation of optical flow', *ACM Comput. Surv.* **27**(3), 433–466.
URL: *http://doi.acm.org/10.1145/212094.212141*

Bruschini, C., Marinella, A. & Sorpresa, M. (2002), A multidisciplinary analysis of frequency domain metal detectors for humanitarian demining, *in* 'Ph.D. thesis, Faculty of Applied Sciences, Vrije Universiteit'.

Butler, D. K. (2003), 'Implications of magnetic backgrounds for unexploded ordnance detection', *Journal of Applied Geophysics* **54**(1-2), 111–125.

Estremera, J., Cobano, J. A. & de Santos, P. G. (2010), 'Continuous free-crab gaits for hexapod robots on a natural terrain with forbidden zones: An application to humanitarian demining', *Robotics and Autonomous Systems* **58**(5), 700–711.
URL: *http://www.sciencedirect.com/science/article/pii/S0921889009002012*

Fracchia, M., Benson, M., Kennedy, C., Convery, J., Poultney, A., Anderson, J. W., Tan, A., Wright, J., Ermilio, J. & Clayton, G. M. (2015), Low-cost explosive ordnance disposal robot for deployment in southeast asia, *in* 'International Humanitarian Technology Conference (IHTC2015), 2015 IEEE Canada', pp. 1–4.

Habib, M. K. (2001), Mine detection and sensing technologies-new development potentials in the context of humanitarian demining, *in* 'IEEE Industrial Electronics Society (IECON '01), The 27th Annual Conference of the', Vol. 3, p. 1621 vol.3.

Habib, M. K. (2011), Humanitarian demining mine detection and sensors, *in* 'Industrial Electronics, IEEE International Symposium on', pp. 2237–2242.

Heußlein, E., Patullo, B. W. & Macmillan, D. L. (2009), 'Robot navigation: implications from search strategies in exploring crayfish', *Robotica* **28**(03), 465–465. ID: 31; M3: 10.1017/S0263574709005785.

Hussain, M. (2005), Rf controlled gps based hovering mine detector, *in* '2005 IEEE International Multitopic Conference', pp. 1–4.

Hussain, M. (2007), Wireless controlled laser tracking based hovering mine detector, *in* '2007 IEEE International Multitopic Conference', pp. 1–7.

Hyland, J. C. & Smith, C. M. (2009), Nonparametric spatial analysis for mine line detection, *in* 'OCEANS 2009, MTS/IEEE Biloxi - Marine Technology for Our Future: Global and Local Challenges', pp. 1–10. ID: 1.

Jin, Y., Ko, D., Seok, J., Lee, W. & Kang, S. (2013), 'Strategy and Development of Mine Detection Robot System'. 13th International Conference on Control, Automation and Systems (ICCAS), Gwangju, SOUTH KOREA, OCT 20-23, 2013.

King, T. L., Horine, F. M., Daly, K. C. & Smith, B. H. (2004), 'Explosives detection with hard-wired moths', *IEEE Transactions on Instrumentation and Measurement* **53**(4), 1113–1118.

Kong, X., Li, J., Yu, H. & Wu, W. (2014), Robust kalman filtering for attitude estimation using low-cost mems-based sensors, *in* 'Proceedings of 2014 IEEE Chinese Guidance, Navigation and Control Conference', pp. 2779–2783.

Krüger, H. (2010), Solutions for 3d position referencing for handheld metal detectors used in humanitarian demining, *in* 'IEEE Instrumentation Measurement Technology', pp. 447–451.

Kruger, H. & Ewald, H. (2008), Handheld metal detector with online visualisation and classification for the humanitarian mine clearance, *in* 'Sensors, 2008 IEEE', pp. 415–418. ID: 1.

Lewis, A., Bloodworth, T., Guelle, D. & Smith, A. (2003), 'Metal-detector handbook for humanitarian demining'. JRC Scientific and Technical Reports (EUR collection); JRC.G-Institute for the Protection and the Security of the Citizen (Ispra).
URL: *http://publications.jrc.ec.europa.eu/repository/handle/111111111/13314*

Miles, R. B., Dogariu, A. & Michael, J. B. (2012), 'Bringing BOMBS to Light', *IEEE SPECTRUM* **49**(2), 38–43.

Novacek, P., Ripka, P., Pribula, O. & Fischer, J. (2010), 'Mine detector with discrimination ability', *Journal of Electrical Engineering* **61**(7), 141–143. ID: 45.

Novacek, P., Rohac, J. & Ripka, P. (2012), 'Complex markers for a mine detector', *Magnetics, IEEE Transactions on* **48**(4), 1489–1492. ID: 1.

Novacek, P., Rohac, J., Simanek, J. & Ripka, P. (2013), 'Metal detector signal imprints of detected objects', *IEEE Transactions on Magnetics* **49**(1), 69–72.

Reinstein, M., Rohac, J. & Sipos, M. (2008), 'Improving performance of a low-cost ahrs', *Acta Avionica* **X**(16), 132–137.

Reinstein, M., Rohac, J. & Sipos, M. (2010), 'Algorithms for heading determination using inertial sensors rid g-7754-2011', *Przeglad Elektrotechniczny* **86**(9), 243–246. PT: J; NR: 22; TC: 3; J9: PRZ ELEKTROTECHNICZN; PG: 4; GA: 662OT; UT: WOS:000282820700057.

Ripka, P., Novacek, P., Reinstein, M. & Rohac, J. (2010), 'Position sensing system for eddy-current mine imager', *Procedia Engineering* **5**, 276–279. ID: 38; M3: 10.1016/j.proeng.2010.09.101.
URL: *http://www.sciencedirect.com/science/article/B9869-519FG5Y-2F/2/442dd1de20f14275af913e7d95f88c22*

Sahawneh, L. & Jarrah, M. A. (2008), Development and calibration of low cost mems imu for uav applications, *in* '2008 5th International Symposium on Mechatronics and Its Applications', pp. 1–9.

Sato, M. (2008), Dual sensor alis for humanitarian demining and its evaluation test in mine fields in croatia, *in* '2008 IEEE International Geoscience and Remote Sensing Symposium', Vol. 2, p. 184.

Schiebel (2003), *ATMID All Terrain Mine Detector Maintenance Manual MT5001/16/010E*, Schiebel Elektronische Geraete GmbH, Vienna, Austria. ID: 41.

Siegenfeld, A. (2003), *ATMID – Technologie und Schaltungsbeschreibung*, Vienna, Austria. ID: 40.

Sipos, M., Paces, P., Rohac, J. & Novacek, P. (2011), 'Analyses of triaxial accelerometer calibration algorithms', *IEEE Sensors Journal* . ID: 70.

Sipos, M., Rohac, J. & Novacek, P. (2012*a*), 'Analyses of electronic inclinometer data for tri-axial accelerometer's initial alignment', *Przeglad Elektrotechniczny* **88**(1A), 286–290.

Sipos, M., Rohac, J. & Novacek, P. (2012*b*), 'Improvement of electronic compass accuracy based on magnetometer and accelerometer calibration', *Acta Physica Polonica A* **121**(4), 945–949.

Smitha, N. & Singh, V. (2016), 'Clutter reduction techniques of Ground Penetrating Radar for detecting subsurface explosive objects'. International Conference on Information Communication and Embedded Systems (ICICES), Thruverkadu, INDIA, FEB 25-26, 2016.

Suganthi, S. R. L. & Hanumanthappa, M. (2016), Image mining using sift based object identification and tagging, *in* 'Computation System and Information Technology for Sustainable Solutions (CSITSS), International Conference on', pp. 261–266.

Svatos, J. (2015), Advanced instrumentation for polyharmonic metal detectors, *in* 'Ph.D. thesis, Faculty of Electrical Engineering Department of Measurement, Czech Technical University in Prague', p. 121.

Svatos, J., Novacek, P. & Vedral, J. (2012), 'sin(x)/x signal utilization in metal detection and discrimination', *Journal of Electrical Engineering* **63**(7 SUPPL), 110–113.

Svatos, J., Vedral, J. & Fexa, P. (2011), 'Metal detector excited by frequency-swept signal', *Metrology and Measurement Systems* **18**(1), 57–67. PT: J; NR: 9; TC: 0; J9: METROL MEAS SYST; PG: 11; GA: 749SX; UT: WOS:000289491200006.

Taylor, S., Bigl, S. & Packer, B. (2015), 'Condition of in situ unexploded ordnance', *Science of The Total Environment* **505**, 762–769.
URL: *https://www.sciencedirect.com/science/article/pii/S0048969714015046*

Theera-Umpon, N. & Auephanwiriyakul, S. (2004), Unexploded ordnance detection by measuring object symmetry via linear prediction, *in* 'TENCON 2004, IEEE Region 10 Conference', Vol. A, p. 198 Vol. 1.

Trevelyan, J. P. (1996), A suspended device for humanitarian demining, *in* 'The Detection of Abandoned Land Mines: A Humanitarian Imperative Seeking a Technical Solution, EUREL International Conference on (Conf. Publ. No. 431)', pp. 42–45. ID: 1.

Yamazaki, S., Nakane, H. & Tanaka, A. (2002), 'Basic analysis of a metal detector', *Instrumentation and Measurement, IEEE Transactions on* **51**(4), 810–814. ID: 28; M3: 10.1109/TIM.2002.803397.

Zhao, Y., Yin, W., Ktistis, C., Butterworth, D. & Peyton, A. J. (2016), 'Determining the electromagnetic polarizability tensors of metal objects during in-line scanning', *IEEE Transactions on Instrumentation and Measurement* **65**(5), 1172–1181.

Appendix B

Author's publications

B.1 Publications related to the thesis

B.1.1 Publications in Journals with Impact Factor

J1 Nováček, P., Ripka, P., Pribula, O., Fischer, J.: *"Mine Detector with Discrimination Ability,"* Journal of Electrical Engineering, 2010, 61(7/s), pp. 141-143, ISSN 1335-3632, *co-authorship: 25%.*

J2 Nováček, P., Roháč, J., Ripka, P.: *"Complex Markers for a Mine Detector,"* IEEE Transactions on Magnetics, 2012, 48(4), pp. 1489-1492, ISSN 0018-9464, *co-authorship: 50%.*

J3 Nováček, P., Roháč, J., Ripka, P.: *"Metal Detector Signal Imprints of Detected Objects,"* IEEE Transactions on Magnetics, 2013, 49(1), pp. 69-72, ISSN 0018-9464, *co-authorship: 70%.*

J4 Svatoš, J., Nováček, P., Vedral, J.: *"sin(x)/x SIGNAL UTILIZATION IN METAL DETECTION AND DISCRIMINATION,"* Journal of Electrical Engineering, 2012, 7(63), pp. 110-113, ISSN 1335-3632, *co-authorship: 45%.*

J5 Šipoš, M, Pačes, P., Roháč, J., Nováček, P.: *"Analyses of Triaxial Accelerometer Calibration Algorithms,"* IEEE Sensors Journal, 2012, 12(5), pp. 1157-1165, ISSN 1530-437X, *co-authorship: 5%.*

J6 Šipoš, M., Roháč, J., Nováček, P.: *"Improvement of Electronic Compass Accuracy Based on Magnetometer and Accelerometer Calibration,"* Acta Physica Polonica A, 2012, 121(4), pp. 945-949, ISSN 0587-4246, *co-authorship: 10%.*

B.1.2 Publications in Peer-reviewed Journals

J7 Šipoš, M., Roháč, J., Nováček, P.: *"Analyses of Electronic Inclinometer Data for Tri-axial Accelerometer's Initial Alignment,"* Przeglad Elektrotechniczny, 2012, 88(01a), pp. 286-290, ISSN 0033-2097, *co-authorship: 10%.*

B.1.3 Conference Proceedings

C1 Ripka, P., Nováček, P., Reinštein, M., Roháč, J.: *"Position Sensing System for Eddy-current Mine Imager,"* In: EUROSENSORS XXIV - Proceedings, Linz, 05.09.2010 - 08.09.2010, Elsevier BV, 2010, pp. 276-279. ISSN 1877-7058, *co-authorship: 25%.*

C2 Ripka, P., Janošek, M., Nováček, P.: *"Depth Estimation of Metal Objects,"* In: EUROSENSORS XXIV - Proceedings, Linz, 05.09.2010 - 08.09.2010, Elsevier BV, 2010, pp. 280-283, ISSN 1877-7058, *co-authorship: 33%.*

C3 Nováček, P., Svatoš, J.: *"Intelligent Metal Detector,"* In: IC-MAST - 2nd International Conference on Materials and Applications for Sensors and Transducers, Budapest, 24.05.2012 - 28.05.2012, Zürich: Transtech Publications, 2013, pp. 133-136, Advanced Materials Research, ISSN 1013-9826, *co-authorship: 50%.*

C4 Svatoš, J., Nováček, P., Vedral, J.: *"Summary of Non-traditional Methods for Metal Detection and Discrimination,"* In: Eurosensors XXVI - 2012 - The 26th European Conference on Solid-State Transducers, Kraków, 09.09.2012 - 12.09.2012, Wydawnictwo Politechniki Krakowskiej, 2012, pp. 298-301, ISSN 1877-7058, *co-authorship: 30%.*

C5 Roháč, J., Šipoš, M., Nováček, P., Pačes, P., Reinštein, M.: *"Modular System for Attitude and Position Estimation,"* In: Workshop 2011, Praha, 01.02.2011 - 04.02.2011, České vysoké učení technické v Praze, 2011, pp. 1-4, *co-authorship: 20%.*

C6 Nováček, P., Ripka, P., Roháč, J., Paroulek, L.: *"Explosive Remnants of Wars Differentiation,"* In: SPM 2011 - X Symposium of Magnetic Measurements, Czestochowa, 17.10.2011 - 19.10.2011, Polish Society of Theoretical and Applied Electrical Engineering, 2011, pp. 28, *co-authorship: 70%.*

C7 Nováček, P. and Roháč, J.: *"Využití inerciálních senzorů při humanitárním odminování,"* In: JALOVECKÝ, R. and BYSTŘICKÝ, R., eds. MDS - Měření, diagnostika, spolehlivost palubních soustav letadel 2011 - Sborník příspěvků z 11, Brno, 19.10.2011 - 20.10.2011, Univerzita obrany, Fakulta vojenských technologií, 2011, pp. 138-144, ISBN 978-80-7231-828-5, *co-authorship: 85%.*

C8 Svatoš, J., Vedral, J., Nováček, P.: *"Metal Object Detection and Discrimination Using Sinc Signal,"* In: BEC 2012 - Proceedings of the 13th Biennial Baltic Electronics Conference, Tallinn, 03.10.2012 - 05.10.2012, Tallinn Technical University, 2012, pp. 307-310, ISSN 1736-3705, ISBN 978-1-4673-2772-5, *co-authorship: 30%.*

B.1.4 Grants and Projects

G1 Roháč, J.: *"Modern Methods in Development of Inertial Navigation Systems,"* 2013-2014, Czech Technical University in Prague, Czech Republic, SGS13/144/OHK3/2T/13, member of team.

G2 Roháč, J.: *"Modular Navigation System for Attitude and Position Estimation,"* 2010-2012, Czech Technical University in Prague, Czech Republic, SGS13/144/OHK3/2T/13, member of team.

G3 Šipos, M.: *"Systems for localization and navigation in ground and aeronautical applications under non-standard conditions,"* 2015-2016, Czech Technical University in Prague, Czech Republic, SGS15/163/OHK3/2T/13, *member of team.*

G4 Ripka, P.: *"Sensors and Intelligent Sensors Systems,"* 2009-2012, Grant Agency of Czech Republic, GD102/09/H082.

B.2 Publications Not Related to the Thesis

B.2.1 Conference Proceedings

C9 Nováček, P. Roháč, J.: *"GPS Based Attitude Estimation,"* In: 2nd Conference for Unmanned Aerial Systems (UAS), Praha, 17.03.2010 - 18.03.2010, FSI ČVUT, 2010, pp. 1-8, ISBN 978-80-86059-53-2, *co-authorship: 80%.*

C10 Nováček, P.: *"The Attitude Estimation using IMU/GPS and Adaptive Filtering,"* In: AIAA-Pegasus Student Conference, Sevilla, 28.04.2010 - 30.04.2010, University of Seville, 2010, pp. 1-7, *co-authorship: 100%.*

C11 Šipoš, M., Nováček, P., Pačes, P.: *"Development of Platform for Measurement and Signal Processing of Navigation and Aerometric Data,"* In: POSTER 2011 - 15th International Student Conference on Electrical Engineering, Prague, 12.05.2011, České vysoké učení technické v Praze, Fakulta elektrotechnická, 2011, pp. 1-5, ISBN 978-80-01-04806-1, *co-authorship: 30%.*

C12 Nováček, P., Šipoš, M., Pačes, P.: *"Modular System for Attitude and Position Determination,".* In: POSTER 2011 - 15th International Student

Conference on Electrical Engineering, Praha, 12.05.2011, České vysoké učení technické v Praze, Fakulta elektrotechnická, 2011, pp. 1-5, ISBN 978-80-01-04806-1, *co-authorship: 50%.*

C13 Roháč, J., Šipoš, M., Nováček, P.: *"Azimuth Determination Based on Magnetometer Measurements,"* In: BYSTŘICKÝ, R. and JALOVECKÝ, R., eds. MDS - Měření, diagnostika, spolehlivost palubních soustav letadel 2011 - Sborník příspěvků z 11. mezinárodní vědecké konference, Brno, 19.10.2011 - 20.10.2011, Univerzita obrany, Fakulta vojenských technologií, 2011, pp. 11-17, ISBN 978-80-7231-828-5, *co-authorship: 10%.*

C14 Pačes, P., Nováček, P., Šipoš, M.: *"Laboratorní systém pro ilustraci principu stabilizace kosmických prostředků,"* In: BYSTŘICKÝ, R. and JALOVECKÝ, R., eds. MDS - Měření, diagnostika, spolehlivost palubních soustav letadel 2011 - Sborník příspěvků z 11. mezinárodní vědecké konference, Brno, 19.10.2011 - 20.10.2011, Univerzita obrany, Fakulta vojenských technologií, 2011, pp. 145-164, ISBN 978-80-7231-828-5, *co-authorship: 25%.*

C15 Nováček, P., Šipoš, M., Popelka, J., Šimánek, J., Roháč, J.: *"Modular Navigation System for Unmanned Aerial Vehicles - Flight Data Monitoring and Recording,"* In: MDS 2012 - Měření, diagnostika, spolehlivost palubních soustav letadel, Brno, 17.10.2012 - 18.10.2012, Univerzita obrany, Fakulta vojenských technologií, 2012, pp. 157-163, ISBN 978-80-7231-894-0, *co-authorship: 20%.*

C16 Šipoš, M., Šimánek, J., Nováček, P., Popelka, J., Roháč, J.: *"Modular Navigation System for Unmanned Aerial Vehicles,"* In: KŘIVÁNEK, V. and ŠTEFEK, A., eds. ICMT'13 - Proceedings of the International Conference on Military Technologies, Brno, 22.05.2013 - 23.05.2013, Univerzita obrany. 2013, pp. 1-10, ISBN 978-80-7231-917-6, *co-authorship: 20%.*

B.2.2 Utility Models

U1 Roháč, J., Nováček, P., Šimánek, J., Šipoš, M.: *"Autonomous System for Attitude Measurement,"* Utility Model, Industrial Property Office, 26785, 2014-04-14, *co-authorship: 25%.*

B.2.3 Functional Prototypes

F1 Šipoš, M., Nováček, P., Bílý, M., Šimánek, J., Roháč, J.: *"Miniature Inertial Navigation System,"* Functional Prototype, 2014, *co-authorship: 20%.*

F2 Nováček, P., Popelka, J., and Roháč, J.: *"Dual distance sensor with CANaerospace interface,"* Functional Prototype, 2011, *co-authorship: 35%.*

F3 Nováček, P., Šipoš, M., Levora, T., Roháč, J., Papaj, J.: *"Flight Data Recorder - SD logger,"* Functional Prototype, 2011, *co-authorship: 28%.*

B.3 Response to Author's Publications

J1 Nováček, P., Ripka, P., Pribula, O., Fischer, J.: *"Mine Detector with Discrimination Ability,"* Journal of Electrical Engineering, 2010, 61(7/s), pp. 141-143, ISSN 1335-3632:

1. Svatos, J., Vedral, J.: *"The Usage of Frequency Swept Signals for Metal Detection,"* IEEE TRANSACTIONS ON MAGNETICS, vol. 48, no. 4, pp. 1501 - 1504, 2012, ISSN 0018-9464.

J2 Nováček, P., Roháč, J., Ripka, P.: *"Complex Markers for a Mine Detector,"* IEEE Transactions on Magnetics, 2012, 48(4), pp. 1489-1492, ISSN 0018-9464:

1. Ambrus, D., Vasic, D., Bilas, V.: *"Robust Estimation of Metal Target Shape Using Time-Domain Electromagnetic Induction Data,"* IEEE TRANSACTIONS ON INSTRUMENTATION AND MEASUREMENT, vol. 65, no. 4, pp. 795 - 807, 2016, ISSN 0018-9456.
2. Ge, J., Dong, H., Yuan, Z., Zhao, Z., Liu, Y., Zhu, J., Zhang, H.: *"Trace metal detection technology based on background interference suppression algorithm with multi-frequency signal excitation,"* ICIC Express Letters, Part B: Applications, 2015, ISSN 2185-2766.

J3 Nováček, P., Roháč, J., Ripka, P.: *"Metal Detector Signal Imprints of Detected Objects,"* IEEE Transactions on Magnetics, 2013, 49(1), pp. 69-72, ISSN 0018-9464:

1. Ge, J., Dong, H., Yuan, Z., Zhao, Z., Liu, Y., Zhu, J., Zhang, H.: *"Trace metal detection technology based on background interference suppression algorithm with multi-frequency signal excitation,"* ICIC Express Letters, Part B: Applications, 2015, ISSN 2185-2766.

J5 Šipoš, M, Pačes, P., Roháč, J., Nováček, P.: *"Analyses of Triaxial Accelerometer Calibration Algorithms,"* IEEE Sensors Journal, 2012, 12(5), pp. 1157-1165, ISSN 1530-437X:

1. Łuczak, S.: *"Fast alignment procedure for MEMS accelerometers,"* Advances in Intelligent Systems and Computing, 2016.

2. Vaispacher, T. , Bréda, R. , Madarász, L.: *"Integration architectures of navigation systems for unmanned vehicles,"* SAMI 2015 - IEEE 13th International Symposium on Applied Machine Intelligence and Informatics, 2015.
3. Ambrozy, C., Rattay, F.: *"Alignment error compensation of an MEMS-based balance trainer measurement systém,"* International Journal of Medical Engineering and Informatics, 2015.
4. Zhao, Y., Zhang, S.-C., Hu, T.: *"A calibration and error analysis method for IMU using centrifuge,"* Transaction of Beijing Institute of Technology, 2015.
5. Li, X. , Wang, Y. , Li, Z.: *"Calibration of tri-axial magnetometer in magnetic compass using vector observations,"* Canadian Conference on Electrical and Computer Engineering, 2015.
6. Luczak, S.: *"Experimental Studies of Hysteresis in MEMS Accelerometers: A Commentary,"* IEEE SENSORS JOURNAL, vol. 15, no. 6, pp. 3492 - 3499, 2015, ISSN 1530-437X.
7. Draganova K., Lassak M., Lipovsky P., Kan V., Kliment T.: *"Gradient methodology for 3-axis accelerometer static calibration,"* 5th International Conference on Military Technologies, ICMT 2015, 2015, ISBN 978-80-7231-976-3.
8. Hsu, Y., Chu, C., Tsai, Y., Wang, J.: *"An Inertial Pen With Dynamic Time Warping Recognizer for Handwriting and Gesture Recognition,"* IEEE SENSORS JOURNAL, vol. 15, no. 1, pp. 154 - 163, 2015, ISSN 1530-437X.
9. Łuczak, S.: *"Erratum: Guidelines for tilt measurements realized by MEMS accelerometers,"* International Journal of Precision Engineering and Manufacturing, vol. 15, no. 9, pp. 2011 - 2019, 2014, ISSN 2234-7593.
10. Dong, C.-M., Chen, X.-J., Liu, Q.-B., Ren, S.-Q.: *"Calibration method for dual orthogonal accelerometers at two combinational installing positions in 1g field,"* Zhongguo Guanxing Jishu Xuebao/Journal of Chinese Inertial Technology, vol. 22, no. 5, pp. 693 - 700, 2014, ISSN 1005-6734.
11. Luczak, S.: *"Guidelines for Tilt Measurements Realized by MEMS Accelerometers(vol 15, pg 489, 2014),"* INTERNATIONAL JOURNAL OF PRECISION ENGINEERING AND MANUFACTURING, vol. 15, no. 9, pp. 2011 - 2019, 2014, ISSN 2234-7593.
12. Luczak, S.: *"DUAL-AXIS TEST RIG FOR MEMS TILT SENSORS,"* METROLOGY AND MEASUREMENT SYSTEMS, vol. 21, no. 2, pp. 351 - 362, 2014, ISSN 0860-8229.
13. Luczak, S.: *"Effects of Misalignments of MEMS Accelerometers in Tilt Measurements,"* MECHATRONICS 2013: RECENT TECHNOLOGICAL AND SCIENTIFIC ADVANCES, pp. 393 - 400, 2014, ISBN 978-3-319-02294-9.

14. Nilsson, JO., Skog, I., Handel, P.: *"Aligning the Forces-Eliminating the Misalignments in IMU Arrays,"* IEEE TRANSACTIONS ON INSTRUMENTATION AND MEASUREMENT, vol. 63, no. 10, pp. 2498 - 2500, 2014, ISSN 0018-9456.
15. Li, X.: Li, Z.: *"Vector-Aided In-Field Calibration Method for Low-End MEMS Gyros in Attitude and Heading Reference Systems,"* IEEE TRANSACTIONS ON INSTRUMENTATION AND MEASUREMENT, vol. 63, no. 11, pp. 2675 - 2681, 2014, ISSN 0018-9456.
16. Draganová K., Laššák M., Praslička D., Kán V.: *"Attitude-independent 3-axis Accelerometer Calibration Based on Adaptive Neural network,"* PROCEDIA ENGINEERING, vol. 87, pp. 1255 - 1258, 2014, ISSN 1877-7058.
17. Luczak, S.: *"Guidelines for Tilt Measurements Realized by MEMS Accelerometers,"* INTERNATIONAL JOURNAL OF PRECISION ENGINEERING AND MANUFACTURING, vol. 15, no. 3, pp. 489 - 496, 2014, ISSN 2234-7593.
18. Blasch, E.: *"Enhanced air operations using JView for an air-ground fused situation awareness udop,"* 2013 IEEE/AIAA 32nd Digital Avionics Systems Conference, DASC 2013, pp. 5A51 - 5A511, 2013, ISBN 978-1-4799-1538-5, ISSN 2155-7209.
19. Montorsi, F., Pancaldi, F., Vitetta, G.M.: *"Design and implementation of an inertial navigation system for pedestrians based on a low-cost MEMS IMU,"* 2013 IEEE International Conference on Communications Workshops, ICC 2013, pp. 57 - 61, 2013, ISBN 978-1-4673-5753-1.
20. Łuczak, S.: *"Effects of misalignments of MEMS accelerometers in tilt measurements,"* 10th International Conference on Mechatronics 2013, pp. 393 - 400, 2013, ISBN 978-3-3190-2293-2.
21. Gao, Y.: Guan, L., Wang, T., Cong, X.: *"Research on the Calibration of FOG Based on AFSA,"* 2013 IEEE INTERNATIONAL CONFERENCE ON MECHATRONICS AND AUTOMATION (ICMA), pp. 412 - 417, 2013, ISBN 978-1-4673-5560-5.
22. Song, N., Cai, Q., Yang, G., Yin, H.: *"Analysis and calibration of the mounting errors between inertial measurement unit and turntable in dual-axis rotational inertial navigation systém,"* MEASUREMENT SCIENCE & TECHNOLOGY, vol. 24, no. 11, 2013, ISSN 0957-0233.

J6 Šipoš, M., Roháč, J., Nováček, P.: *"Improvement of Electronic Compass Accuracy Based on Magnetometer and Accelerometer Calibration,"* Acta Physica Polonica A, 2012, 121(4), pp. 945-949, ISSN 0587-4246:

1. Yue, H.-B., Zhang, S.-D., Shi, Z.-R., Xi, H.-T.: *"Compass error compensation based on adaptive differential evolution and BP net-*

work," Yuhang Xuebao/Journal of Astronautics, vol. 34, no. 12, pp. 1628 - 1633, 2013, ISSN 1000-1328.

J7 Šipoš, M., Roháč, J., Nováček, P.: *"Analyses of Electronic Inclinometer Data for Tri-axial Accelerometer's Initial Alignment,"* Przeglad Elektrotechniczny, 2012, 88(01a), pp. 286-290, ISSN 0033-2097:

1. Paces, P.; Popelka, J.: *"IMU AIDING USING TWO AHRS UNITS,"* 2012 IEEE/AIAA 31ST DIGITAL AVIONICS SYSTEMS CONFERENCE (DASC), 2012, ISBN 978-1-4673-1700-9, ISSN 2155-7195.

Appendix C

List of Abbreviations

ACC Accelerometer

AP Anti-Personnel

ARS Angular Rate Sensor

AT Anti-Tank

ATMID All Terrain Mine Detector

CMM Complex Magnetic Marker

CW Continuous Wave

DC Direct Current

EM ElectroMagnetic

ERW Explosive Remnants of War

GNSS Global Navigation Satellite System

GPR Ground Penetrating Radar

IMU Inertial Measurement Unit

INS Inertial Navigation System

MATLAB MATrix LABoratory

MEMS Microelectromechanical Systems

OF Optical Flow

RX Receiving

TX Transmitting

UXO Unexploded Ordnance